NOAA Technical Memorandum ERL ARL-199

VORTEX WAKE CHARACTERISTICS OF B757-200 AND B767-200 AIRCRAFT USING THE TOWER FLY-BY TECHNIQUE

VOLUME 1

Leo J. Garodz
Kirk L. Clawson

Air Resources Laboratory
Silver Spring, Maryland
January 1993

noaa NATIONAL OCEANIC AND ATMOSPHERIC ADMINISTRATION / Environmental Research Laboratories

NOAA Technical Memorandum ERL ARL-199

VORTEX WAKE CHARACTERISTICS OF B757-200 AND B767-200 AIRCRAFT USING THE TOWER FLY-BY TECHNIQUE

VOLUME 1

Leo J. Garodz
Kirk L. Clawson

Field Research Division
Idaho Falls, Idaho

Air Resources Laboratory
Silver Spring, Maryland
January 1993

UNITED STATES DEPARTMENT OF COMMERCE

Barbara Hackman Franklin
Secretary

NATIONAL OCEANIC AND ATMOSPHERIC ADMINISTRATION

John A. Knauss
Under Secretary for Oceans and Atmosphere/Administrator

Environmental Research Laboratories

Joseph O. Fletcher
Director

DISCLAIMER

For sale by the National Technical Information Service, 5285 Port Royal Road
Springfield, VA 22061

PREFACE

This report was prepared in compliance with Military Interdepartmental Purchase Request (MIPR) DTFA03-89-A-00010, issued by the FAA Technical Center at Atlantic City, NJ. The editing co-author was K. L. Clawson. The meteorological data given herein were first summarized in Wake Vortex Research Data Packages NOAA-1 and NOAA-2, titled *NOAA Meteorological Data Summary* and *NOAA Meteorological Data Summary (Level 2 Data)*, respectively. These reports were prepared by K.L. Clawson and issued in November and December of 1990. Vortex wake characteristics presented in this report were initially summarized in a subcontractor's report to NOAA, written by L.J. Garodz and K.L. Clawson under the title *Investigation of the Vortex Wake Characteristics of Large Twin-Engine Jet Transports using the Tower Fly-by Technique (Boeing B757-200 & B767-200 Aircraft)*. It was initially issued in May 1991 with the final revision issued in May 1992. The vortex data were first presented to the public in October 1991 at the FAA International Conference on Aircraft Wake Vortices. The method of presentation was a panel discussion led by R.D. Page, and included K.L. Clawson, L.J. Garodz, and R.P. Rudis. The data presented at that time were still in draft form, and subject to further revision.

The body of this report is a compilation of the reports and the conference proceedings cited above. It draws most heavily from the report by L.J. Garodz and K.L. Clawson, issued to NOAA in 1992. However, it also contains new evaluation methods, conclusions, and recommendations not previous reported in any form, most of which originated with K.L. Clawson. It is divided into two volumes: the first contains the body of the report, while the second contains the appendices. This document completes the obligation of NOAA to the FAA specified in MIPR DTFA03-89-A-00010.

Note: present color copy technology does not permit double-sided copying. Therefore, all color copies in this report have an intentional blank page on the back side of the copy which is not indicated by the words "This page intentionally left blank."

CONTENTS

Volume 1

Volume 2
APPENDICES

TABLES

FIGURES

ACRONYMS AND SYMBOLS

A = hot film calibration coefficient (unitless), or initial vortex velocity coefficient (feet/second)

A/D = analog-to-digital

AGL = above ground level

ATC = Air Traffic Control

b = aircraft wingspan (feet)

b′ = separation of vortex pair = $\pi\frac{b}{4}$ (feet)

b_g = wingspan of leading (generating) aircraft (feet)

b_p = wingspan of following (probing) aircraft (feet)

B = hot film calibration coefficient (unitless), or vortex decay rate coefficient (unitless)

c = wing mean aerodynamic chord (feet)

C_L = airplane lift coefficient = $\frac{L}{\frac{1}{2}\rho V^2 S} = \frac{L}{qS}$ (unitless)

cs = centisecond

d = distance between aircraft and tower (feet)

E = electrical motive force (volts)

FAA = Federal Aviation Administration

fps = feet per second

FTD = Flight Test Director

g = acceleration due to gravity (feet/second^2 or meters/second^2)

G/S = glide slope of aircraft (degrees)

GW = gross weight (pounds)

h = aircraft height above ground (feet)

h_v = height of vortex intercept with the tower (feet)

h_{vge} = height of onset of vortex ground effect (feet)

I = electrical current (amperes)

IAS = indicated air speed (knots)

IFR = instrument flight rules

INEL = Idaho National Engineering Laboratory

INS = Inertial Navigation System

KIAS = knots indicated air speed

L = lift = nW (pounds)

LAN = Local Area Network

LLWSAS = Low-Level Wind Shear Alert System

MAC = Military Airlift Command

MDT = Mountain Daylight Time

MM = middle marker

MSL = mean sea level

MTOGW = maximum permissible takeoff gross weight

n = normal load factor, which equals 1 in level flight (unitless)

NAFEC = National Aviation Facilities Experimental Center

NAS = National Airspace System

NIST = National Institute of Standards and Technology

NOAA = National Oceanic and Atmospheric Administration

NRC = Nuclear Regulatory Commission

P_a = ambient air pressure (pascals)

$P_{l,m,h}$ = pressure of the low-, medium-, and high-velocity calibration ports of the hot film anemometer wind tunnel (pascals)

PAPI = Precision Approach Path Indicator

PBL = planetary boundary layer

q = dynamic pressure = $\frac{1}{2}\rho V^2$ (pounds/feet^2)

r = distance from vortex center (feet)

r^2 = coefficient of determination (unitless)

r_c = vortex core radius where V_θ is a maximum (feet)

R = electrical resistance (ohms)

Ri = Richardson Number = $\dfrac{g\left(\dfrac{d\theta}{dz}\right)}{\bar{\theta}\left(\dfrac{du}{dz}\right)^2}$ (unitless)

S = wing area (feet^2)

t = vortex age (seconds)

T = air temperature (^{o}C, ^{o}F, or K, as specified)

T_{cal} = temperature of air in wind tunnel during hot film anemometer calibration (^{o}C)

T_e = ambient air temperature influencing hot film anemometer (^{o}C)

T_s = hot film anemometer operating temperature (250 ^{o}C)

TAS = true air speed (knots)

u = ambient wind speed (knots or miles/hour or feet/second, as applicable)

UAL = United Airlines

USAF = United States Air Force

V = aircraft true air speed (knots or feet/second), or hot film-measured vortex velocity (feet/second)

V_θ = vortex tangential velocity (feet/second)

$V_{\theta max}$ = maximum vortex tangential velocity at r_c (feet/second)

VFR = visual flight rules

VNTSC = Volpe National Transportation Systems Center

W = gross weight of aircraft (pounds)

WORM = write-once/read-many

z = height above ground (feet)

$\dot{z}$ = vortex descent rate (feet/second)

α = aircraft angle-of-attack (degrees), or statistical significance level (unitless)

Γ = vortex circulation = $\frac{4}{\pi}\frac{nW}{\rho Vb}$ (feet^2/second)

Γ' = average vortex circulation at distance r (feet^2/second)

Γ_o = initial mid-span vortex circulation = $\frac{1}{2}cC_LV$ (feet^2/second)

$\Gamma_{(rc)}$ = vortex circulation at vortex core radius where V_θ is a maximum (feet^2/second)

δ_F = flap deflection (percent or degrees)

ΔT = temperature difference (°C)

Δz = height difference (feet)

$\epsilon^{1/3}$ = atmospheric turbulence dissipation rate (centimeters^2/second^3)

θ = potential temperature (°C)

Λ = wing sweep angle (degrees)

ρ = air density (slugs/foot^3 or grams/meter^3)

VORTEX WAKE CHARACTERISTICS OF B757-200 AND B767-200 AIRCRAFT USING THE TOWER FLYBY TECHNIQUE

Leo J. Garodz and Kirk L. Clawson

ABSTRACT

The number of large wing-mounted twin-engine jet transport aircraft in operation in the National Airspace System (NAS) has significantly increased over the past few years. Very little is known about the vortex wake characteristics of these aircraft, particularly in takeoff and landing configurations. Since aircraft classification and Air Traffic Control (ATC) separation criteria in terminal area flight operations are based primarily on the aircraft vortex wake hazard, the FAA undertook a flight test program in the fall of 1990 to investigate the vortex wakes of the Boeing 757-200 and 767-200. The tests were conducted at the NOAA vortex test facility near Idaho Falls, Idaho. This report presents the results of the flight tests using the tower flyby technique. Included are characterizations of vortex wakes as a function of aircraft configuration and performance, and ambient atmospheric conditions. Very high vortex tangential velocities were created by the B757 aircraft, with the most intense vortex measured at 326 feet per second (fps). Vortex velocities generated by the B757 were approximately 50% higher than those of the B767 at similar vortex ages younger than 60 seconds. The oldest vortices generated by the B757 were much younger than those generated by the B767, and were 84 and 135 s, respectively. The most intense vortices were generated under stable or near-neutral atmospheric conditions. Richardson Number, air temperature gradient, and wind speed were good general indicators of the $V_{\theta max}$-vortex age envelope. The 3° glide slope did not produce vortices that were statistically significantly greater in intensity. The Hoffman-Joubert logarithmic model adequately predicted vortex velocity profiles in which $V_{\theta max}$ was $\geq$ 50 fps. Further flight testing of the B757 was recommended as a basis upon which to review present ATC separation standards for this aircraft.

INTRODUCTION

This report documents the most recent Federal Aviation Administration (FAA) study of the aircraft vortex wake phenomenon through controlled flight tests. The effort was multifaceted, and several institutions participated. Page et al. (1992) described the test effort and its various participants, which included the FAA Technical Center, the Volpe National Transportation Systems Center (VNTSC), and the National Oceanic and Atmospheric Administration (NOAA). Although the study encompassed several major objectives, e.g., in-flight aircraft probing of the vortex system and cross comparison of two vortex sensing systems based on remote sensing techniques with tower data, only those objectives that pertain to tower data are reported herein. The other major participants have issued, or will issue their own reports.

CURRENT VORTEX WAKE PROGRAM

The FAA is currently conducting a high-priority aircraft vortex wake program. The primary objective of the program is to safely increase airport capacity. This is to be accomplished by reducing the restraining effects of the aircraft trailing vortex hazard on efficient air traffic flow in the terminal airspace, including both arrivals and departures. For example, if vortex wakes were not a problem, aircraft separations for arriving traffic would be based only on aircraft runway occupancy times, resulting in increased traffic flow, since a much closer aircraft spacing on final approach would be permitted than is currently authorized. However, because vortex wakes are the major reason for the current aircraft separation standards, the goal of increasing airport capacity by decreasing aircraft separations cannot be safely accomplished until the vortex phenomenon is understood in greater detail.

The current program is separate and distinct from the programs that the FAA initiated and pursued for en route operations in the mid-1960's and for terminal-area flight operations in the early 1970's. Those programs were effectively terminated in late 1979. The current program plan calls for studies on vortex detection and avoidance, vortex characterization, atmospheric characterization for vortex behavior correlation, and the reexamination and possible modification of aircraft classification criteria and Air Traffic Control (ATC) separation standards based on the vortex hazard.

PREVIOUS VORTEX WAKE PROGRAMS

The planned introduction in early 1970 of the Lockheed C5A and Boeing 747-100 aircraft into the National Airspace System (NAS) caused considerable apprehension among several foreign and domestic aviation-oriented organizations. Concern was raised about the vortex wake hazard of these so-called "jumbo" or "wide-bodied" jet transports on following aircraft. Other large transport aircraft with maximum permissible takeoff gross weights of greater than 300,000 lb, e.g., the Boeing 707-300 and the Douglas DC-8-63, were also of concern. It subsequently became imperative to investigate the safety aspects of the vortex wakes of these large and heavy aircraft. Wake vortex characteristics were needed to evaluate the potential effects on other

aircraft encountering the trailing vortices. A safe separation criterion for ATC use was needed for arrivals and departures in terminal-area flight operations.

The FAA took the lead among several U.S. government agencies in a program to evaluate the vortex wake phenomenon. The program primarily involved full-scale flight testing. Although the testing was costly, it was assumed that the results from this approach would be more readily accepted by the aviation community. The flight tests and analyses were performed by various government agencies and private industry. The results helped to determine and establish the present ATC separation standards.

The current ATC separation standards were initially discussed with the aviation community at an FAA symposium on turbulence (FAA, 1971). The standards are a categorization of the vortex wake hazard based on aircraft maximum permissible gross takeoff weight. This scheme was not necessarily agreeable to all participants; some recommended using the wing span ratio (b_p/b_g) of the following (probing)/leading (generating) aircraft. Other schemes have been developed and are still being advocated. A reevaluation of the applicability of the current standards is needed, particularly regarding the new-generation aircraft now in operation in the NAS.

The many full-scale flight tests conducted in the last two decades are well documented in numerous reports. NOAA was a major participant in several of those flight tests. Start and Dickson (1970), Bailey et al. (1979), and Clawson (1988) provided specific details of flight tests conducted at the NOAA test facility since the early 1970's. Of particular note is the recent reexamination by NOAA of the vortex wake characteristics of three U.S. Air Force (USAF) Military Airlift Command (MAC) aircraft (Garodz and Clawson, 1991). The work was requested by the FAA with the goal of applying the results to the FAA's vortex wake program elements. The vortex flight test data were acquired by NOAA on the Lockheed C5A/B Galaxy, C141B Starlifter, and C130E Hercules aircraft in the spring of 1987 using the tower flyby technique. All three aircraft are built with a high wing; two are T-tail aircraft, and one is a turbo-prop. Garodz and Clawson (1991) recommended that the C5A/B be placed in a new weight category called superheavy. They also reported that the trailing vortex systems differed greatly between aircraft, depending on engine and tail configurations.

STUDY OBJECTIVES

This study reported here was designed to assist the FAA in its plan to increase airport capacity. The focus of the study was on new-generation aircraft in the large and heavy weight categories as currently defined by the FAA. Controlled flight test vortex characterizations of these aircraft are nonexistent. If airport capacity is to be increased by safely decreasing ATC aircraft separation standards, it follows that vortex characteristics of the new aircraft must be known. The vortex hazard to following aircraft must also be known. Hence, the main objective of this study was to examine the vortex wake characteristics of the relatively large, twin-engine Boeing 757 and 767 (B757 and B767). It is left to the FAA to determine the hazards associated with the vortex characteristics reported herein. The original plan also called for testing the

B737-300 and an Airbus A-300 series aircraft, since these are also new-generation aircraft. Testing of a B747-400 was also included in the program plan, in view of its higher gross weight and different wing geometry (including winglets) compared with earlier B747 series. Federal budget constraints, however, forced the FAA to fund only the evaluation of the B757 and B767.

The FAA has established the B727 aircraft as the baseline model against which all other aircraft vortex characteristics (particularly vortex intensity) are to be evaluated. Accordingly, new flight test data were to be acquired on the B727 and combined with older vortex flight test data for comparisons. Vortex characteristics from all aircraft were to be determined as a function of aircraft model, configuration (takeoff and landing), flight performance, and ambient atmospheric conditions.

Another objective of the study was to correlate vortex persistence and movement as a function of the character of the ambient atmosphere in which the vortex system is generated and transported. An attempt was to be made to determine a reliable correlation parameter (or parameters) descriptive of the atmosphere, other than ambient wind velocity, to be used with vortex characterization. Such a parameter was to describe vortex persistence and decay mode in the planetary boundary layer (PBL).

Yet another objective of the study was to determine the effect, if any, of level versus descending glide-slope (G/S) flight on the intensity and persistence of the vortex wake. Previous vortex study reports indicated that jet engine thrust settings had an effect on vortex wake characteristics, particularly intensity.

No attempt has been made in this report to define the wake vortex hazard of the B757-200 or the B767-200. The definition of what constitutes a hazardous vortex is a very important one. It seems as if there are as many definitions as there are researchers in the wake vortex discipline. Current ATC separation standards (FAA, 1972) are based upon its definition, which was established on a ***no*** vortex encounter premise. Recent activity in the FAA indicates that the definition may be altered to permit aircraft to encounter a "benign" vortex (Michael Harrison, personal communication). Therefore, it has been left to the discretion of the FAA to determine the wake vortex hazards of these two aircraft. However, if the hazard definition is to be changed, then the type and the degree of the vortex hazard should be defined and subsequently validated or modified by actual flight testing involving vortex probing. Factors such as aircraft dynamic response parameters (primarily pitch, roll, and yaw and associated rates and accelerations), jet engine performance degradation due to a vortex ingestion, phase of flight, pilot experience level (average pilot), among other things, must be considered.

REPORT STRUCTURE

The format of the report is structured around the study objectives. The following chapter contains a description of the test site, the instrumentation, the data acquisition techniques, the aircraft used in the study, and data processing and analysis procedures. The third chapter contains the results of the flight tests, which are presented in numerous graphs and tables. In

addition, some effort was devoted to existing vortex model validation including the determination of vortex tangential velocity distributions and the onset of ground effect. The fourth chapter contains the data analysis conclusions. The fifth chapter contains the study recommendations. Appendices give details on aircraft specifications, graphs of ambient wind speed, wind direction, and air temperature profiles, and data listings with accompanying graphs of vortex tangential velocity profiles.

EXPERIMENTAL DESIGN

The study was conducted on 20 and 21 June 1990 and from 21 through 30 September 1990. The following details are included in this section: (1) a description of the flyby technique, which was the method used to measure the vortex strengths of the test aircraft; (2) a description of the test site; (3) instrumentation and calibration details of the data acquisition systems; (4) a summary of the test aircraft used for the flight tests; (5) other flight test details; and (6) data processing and analysis procedures.

TOWER FLYBY TECHNIQUE

The tower flyby technique has been used several times in the last two decades for aircraft vortex wake characterizations. Start and Dickson (1970), Garodz (1971b), and Clawson (1988), for example, described and utilized the tower flyby technique in their studies of vortex wakes. The technique was again employed in this study to acquire vortex data on the test aircraft. The technique is depicted schematically in Figure 1. It consists of flying a test aircraft both

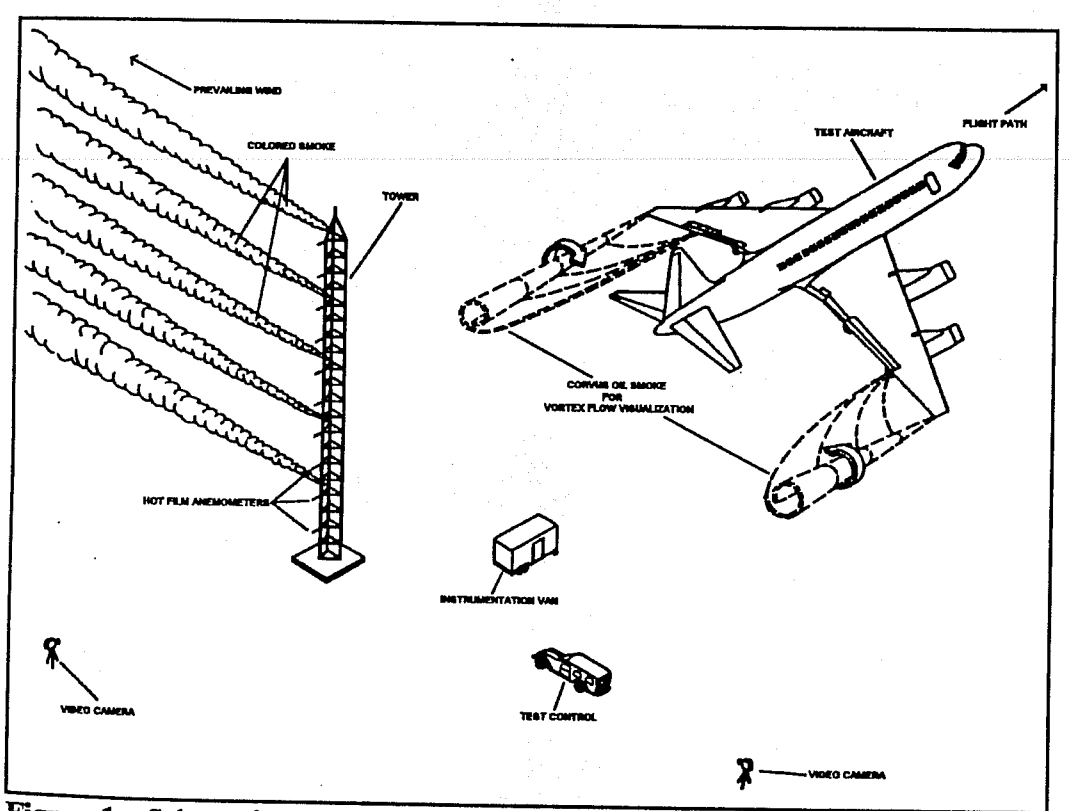

Figure 1. Schematic representation of the tower flyby technique for aircraft wake vortex characterizations.

crosswind and upwind of a tall tower instrumented with fast-response anemometers. As the test aircraft flies past the tower, the vortices generated by the aircraft are advected by the prevailing ambient wind into the instrumentation mounted on the tower. The instrumentation and accompanying data acquisition equipment in the instrument van record the strengths of the vortices. The vortices, as they pass through the tower, become visible through incorporation of colored smoke emanating from point sources on the tower. Video and still cameras photographically record the decaying vortex wake. The flight test director, located at the test control vehicle, communicates with the test aircraft pilot and requests the pilot to fly the aircraft at specific altitudes and distances upwind from the tower. This is done to vary the ages of the vortices measured at the tower. Whenever possible, wing-tip smoke generators are attached to the test aircraft to aid in vortex movement and decay measurements.

TEST SITE

The flight tests were conducted at the Idaho National Engineering Laboratory (INEL) in southeastern Idaho (Figure 2). INEL is approximately 45 miles west of Idaho Falls, Idaho, on the western edge of the Eastern Snake River Plain. It covers an area of roughly 10,000 acres. A portion of the Salt Lake City Sectional Aeronautical Chart that includes the INEL complex is shown in Figure 3. An expanded view of the INEL complex in the vicinity of the test site, and the NOAA test site known as Grid 3, is shown in Figure 4. The floor of the Snake River Plain is broad and rolling, having an average elevation of 5,000 ft above mean sea level (MSL). Major landmarks that are used by test flight pilots for flight pattern orientation are Big Southern Butte, Middle Butte, and East Butte on the south end of the INEL complex. The Lost River and Lemhi Mountain Ranges, which border the INEL complex on the west (approximately 10-12 miles away), rise to approximately 11,000 ft MSL.

The terrain is fairly level at and near the test site, as shown in Figure 5. Because annual precipitation is less than 10 inches, vegetation consists primarily of sagebrush. The area around the test site is free of trees and other tall vegetation. In addition, there are no other protuberances or structures to generate undesirable atmospheric turbulence in the vicinity of the flight test area. The small number of days with inclement weather make the site ideal for flight testing of aircraft with limited availability. The test site is a high-security area and is free of transient aircraft. The test site is also fairly unpopulated, particularly with regard to the projected surface area of the aircraft's flight path over the ground. This helps to minimize any unwanted outside test interference, including low-flying aircraft and aircraft noise.

INSTRUMENTATION

The 200-ft-tall vortex test tower was the focal point for the flight tests. The tower and nearby ground-based equipment are shown in Figure 6. The base of the tower is at 4905 ft MSL. The tower is restrained laterally by guy-wires extending from four levels at all four corners of the tower to the ground. The wires from the top attachment points at 200 ft form an angle of about 45° with the vertical tower. The wires are marked with high-visibility orange balls.

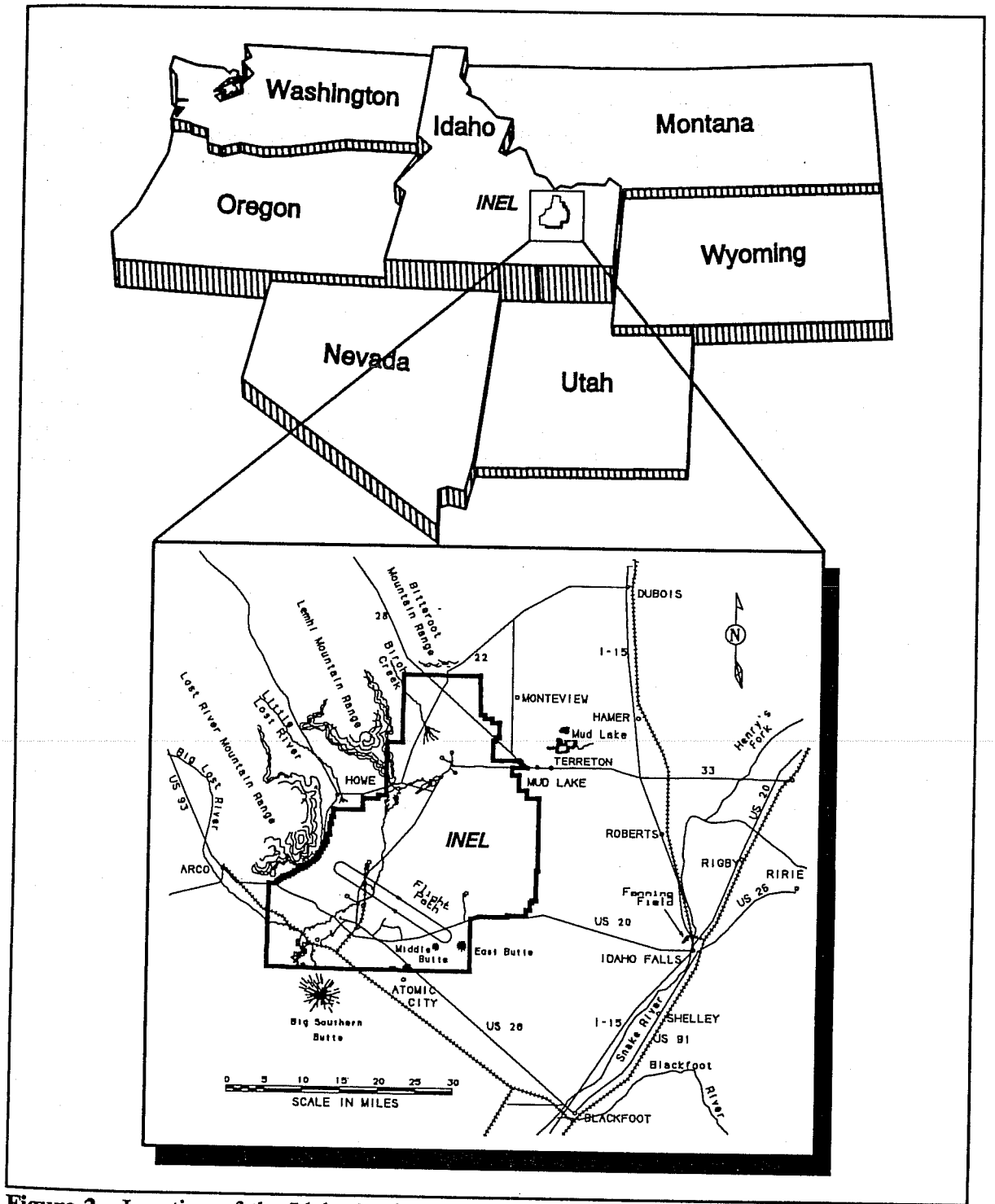

Figure 2. Location of the Idaho National Engineering Laboratory (INEL) in relation to the Pacific Northwest portion of the United States. Major regional landmarks and the test flight path are also indicated.

The tower was outfitted with vortex measurement sensors (Figure 7), standard meteorological sensors, and a vortex flow visualization system. It also had a flash-bulb-type event marker installed at 10 ft above ground level (AGL) for the benefit of the video and photo crews. Other sensors were also deployed to measure vortex characteristics in ground effect at some extended distance from the tower and to measure various meteorological characteristics of the atmosphere above the top of the tower.

Tower Hot Film Anemometers

The vortex velocity measurement sensors consisted of platinum hot film anemometers, as shown in Figure 8. They were manufactured by TSI, Inc. (Model 1210-60), and have a frequency response of about 200 kHz. The controlling circuitry was custom designed and built by NOAA. The total system response of the sensor and circuitry were certified independently by EG&G engineers to be sufficient to meet the design criteria for this study. The anemometers were used to measure vortex tangential velocities as the vortex pair were advected into the tower by the ambient wind.

The anemometers were spaced at 2-ft intervals along the vertical span of the tower, which is depicted schematically in Figure 9. The anemometers were each mounted in a holding arm that extended out approximately 2 ft from the tower. The sensing rod of each anemometer was oriented horizontally. A total of 198 sensors were situated on opposite sides of the tower (99 each side) and oriented into the two prevailing wind directions. This permitted flight testing to continue uninterrupted and without vortex wake flow distortion as the ambient wind shifted from the prevailing northeast direction in the early morning hours to southwest at midday.

The vertical sensor spacing provided fairly good resolution compared with a 6-ft vertical spacing interval for the Air Force tower flyby tests (Clawson, 1988). The chance of measuring the true peak velocity of a vortex was thereby increased. The 2-ft spacing probably represents the density limit for this tower without introducing serious errors due to aerodynamic interference between the sensors and the adjacent mounting hardware.

Theory of Measurement

The speed and temperature of the air flowing around a hot film anemometer influence the heat transfer between the heated sensor and the cooler environment surrounding it. The hot film anemometer then responds to convective heat transfer. A "King's Law" relationship between convective heat transfer and wind speed is therefore the theoretical basis of thermal anemometry. Fortunately, the effect of air temperature and wind speed on the sensor voltage can be deconvoluted.

The convective heat transfer of the hot film anemometer to the environment is measured in terms of the electrical power (E^2/R) dissipated by the anemometer, where E is the voltage required to maintain the anemometer sensing wire at a constant temperature (in this case 250 °C)

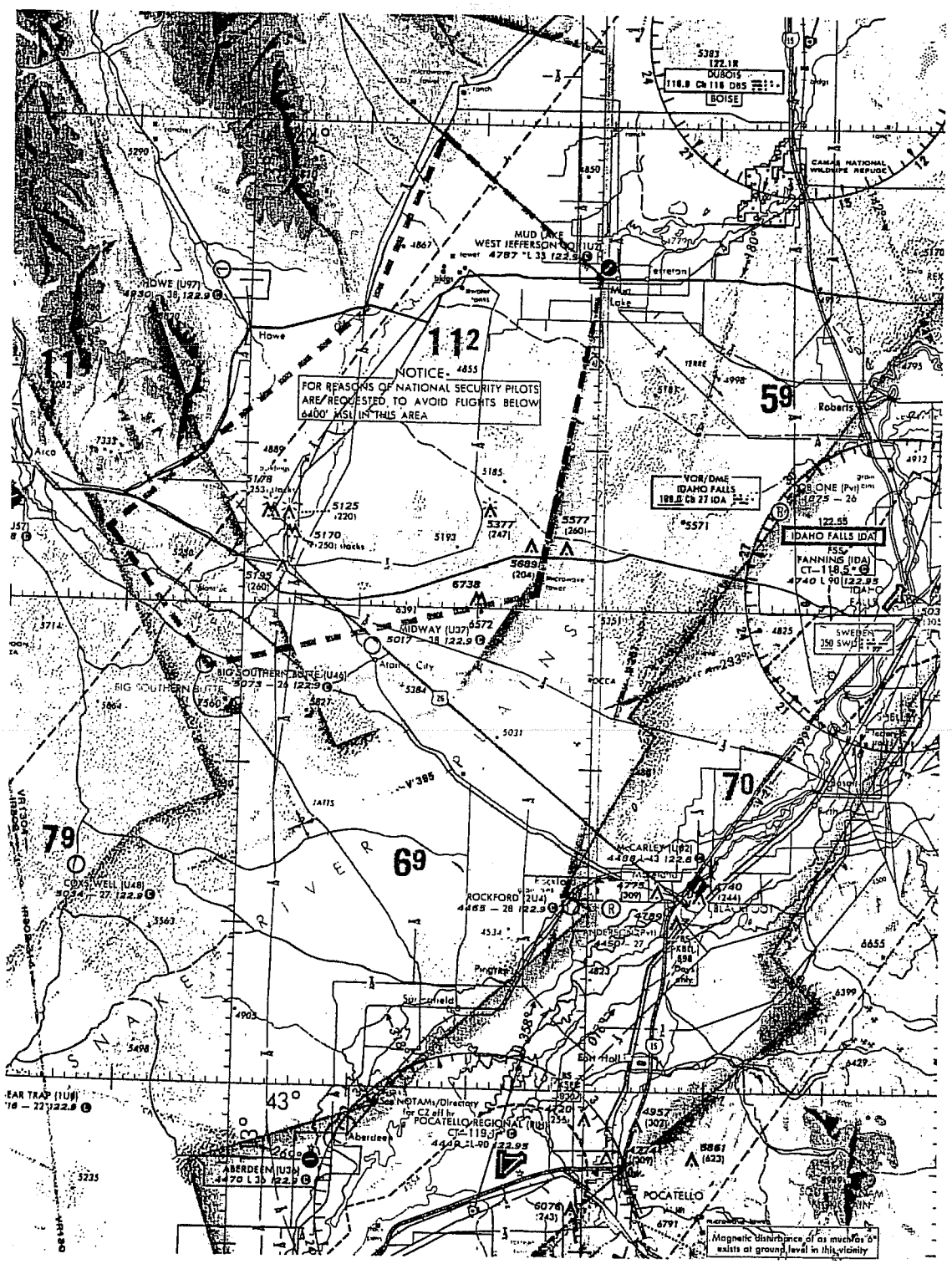

Figure 3. The Idaho National Engineering Laboratory (INEL) and vicinity as illustrated in the Salt Lake City Sectional Aeronautical Chart.

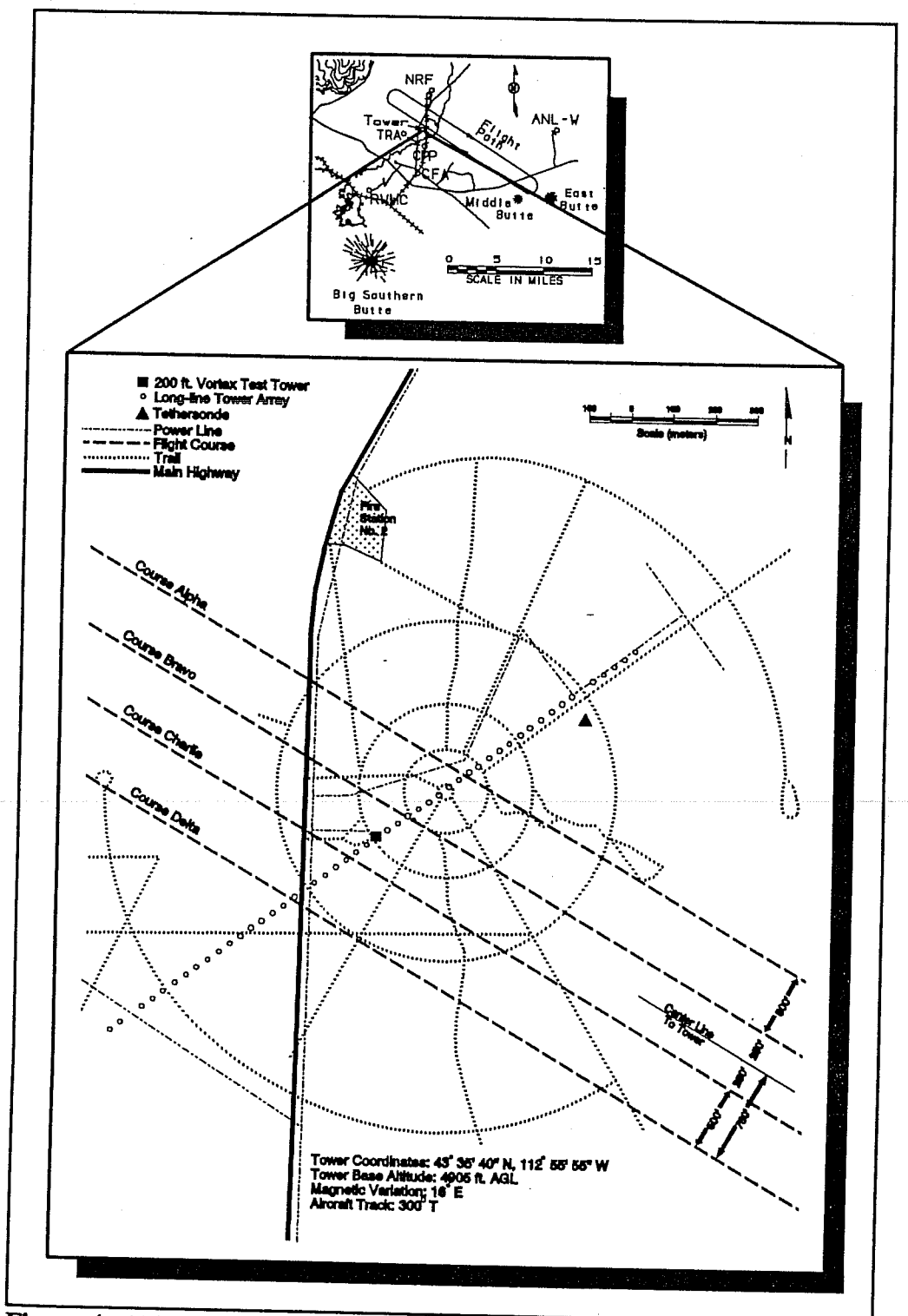

Figure 4. NOAA wake vortex test site and associated aircraft flight path in relation to various local landmarks on and near the INEL complex.

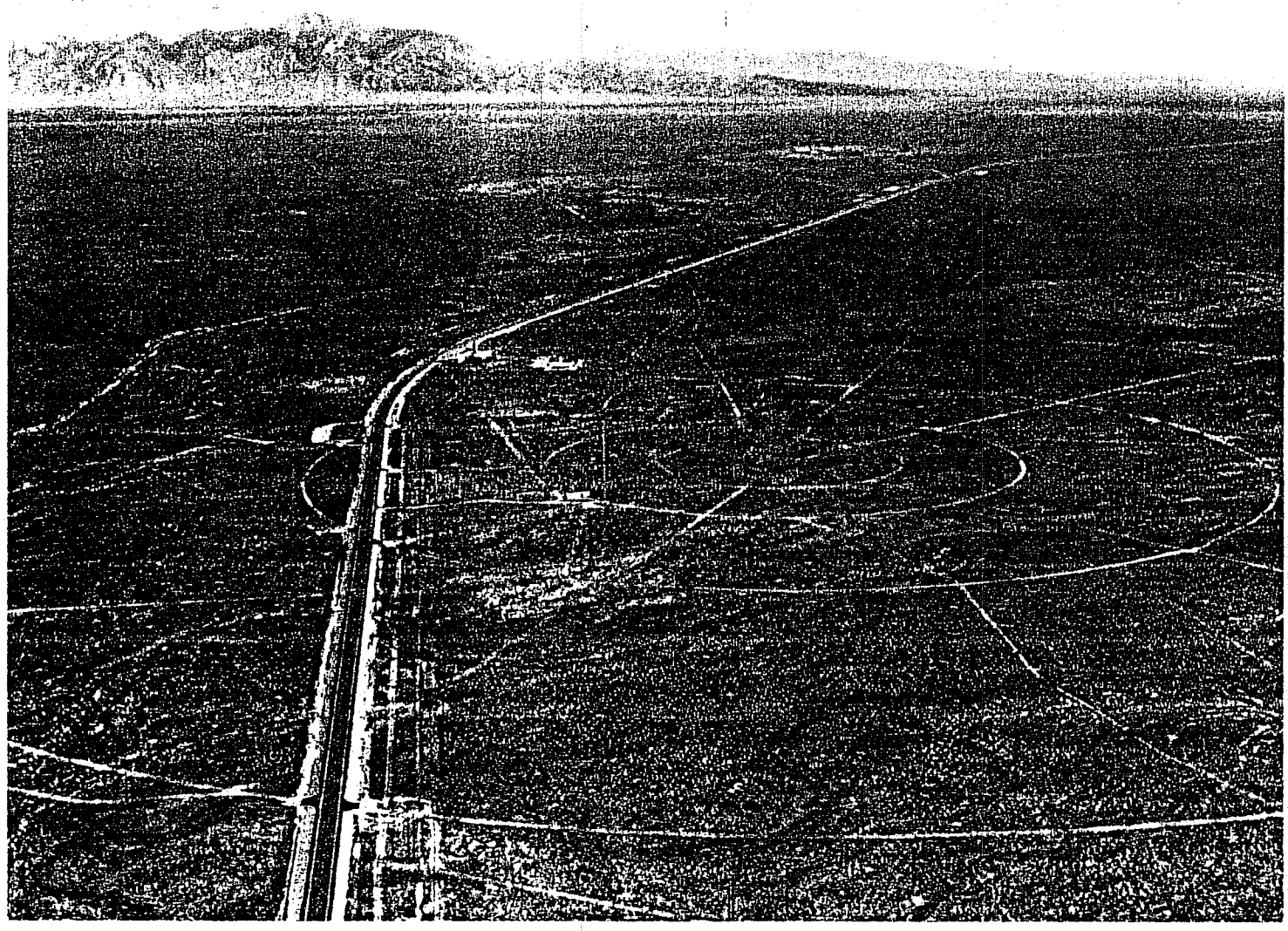

Figure 5. NOAA wake vortex test site as seen from a test aircraft, with a view to the north.

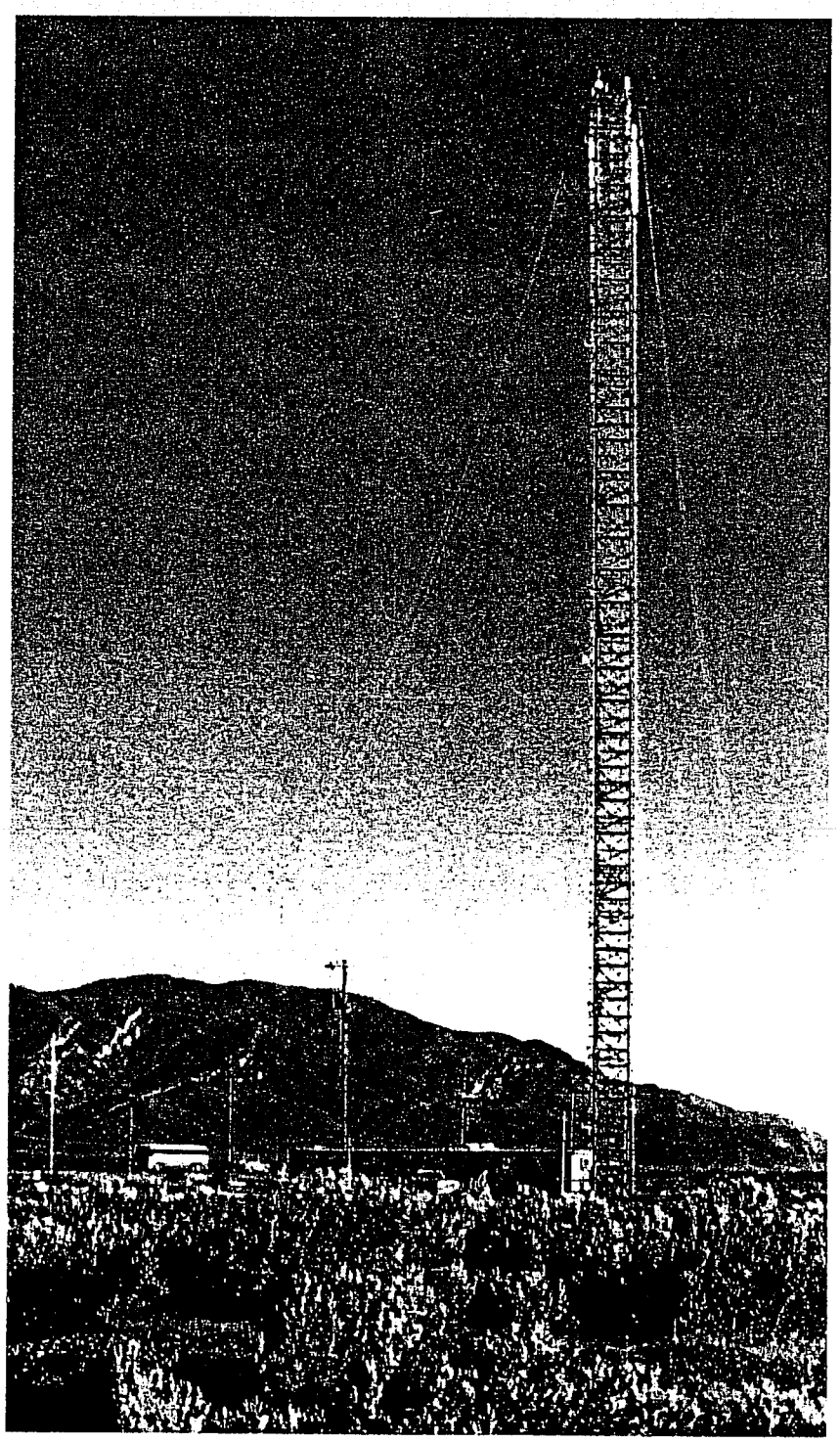

Figure 6. NOAA 200-ft aircraft wake vortex test tower.

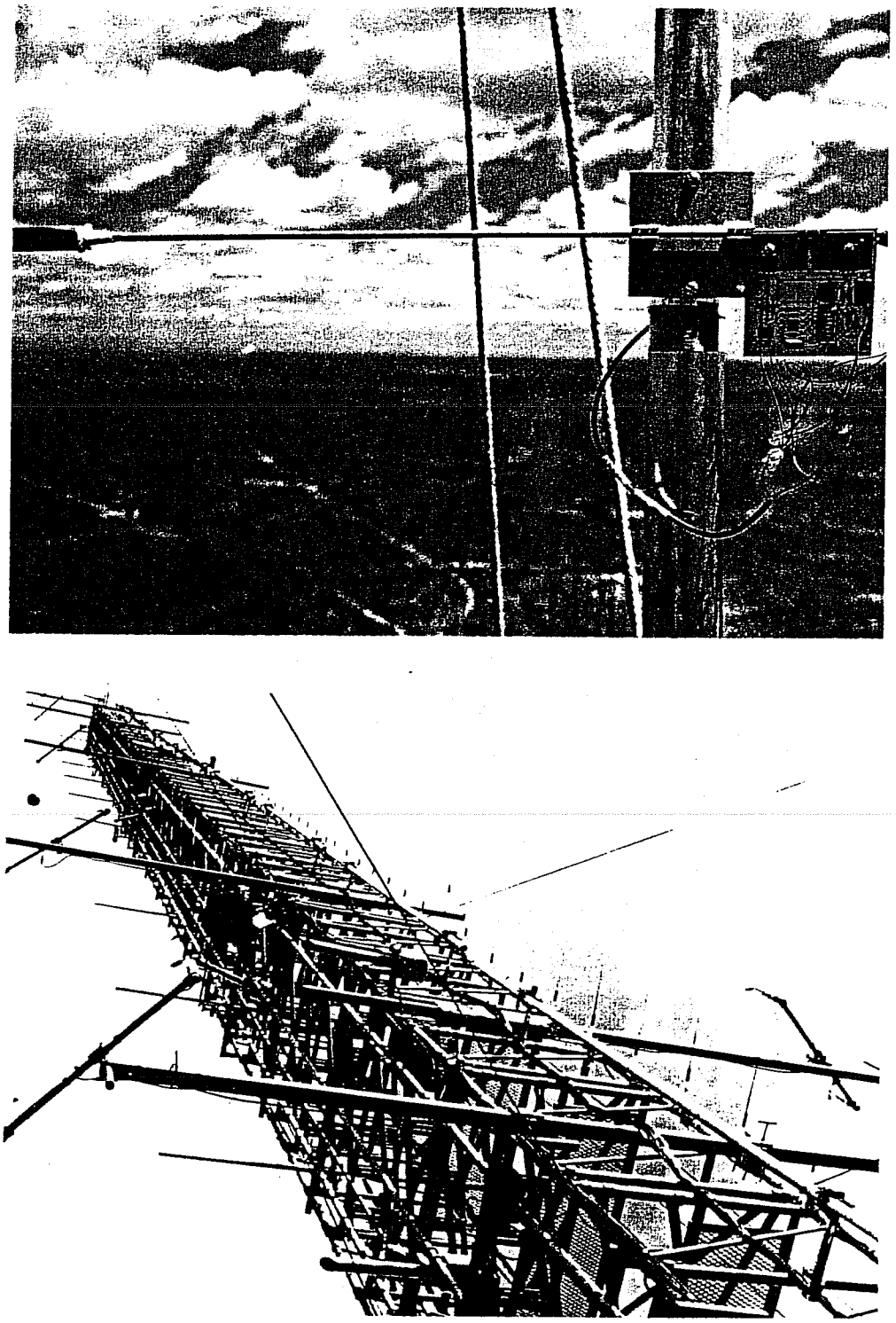

Figure 7. Hot film anemometer electronics, mounting arm, and cover (top), and hot film anemometers mounted at 2-ft intervals on the 200-ft tower.

and R is the electrical resistance of the anemometer sensing wire itself. The equation used to compute wind speed from the sensor voltage, according to TSI, Inc. (no date, Tech. Bull. 16 and 18) is

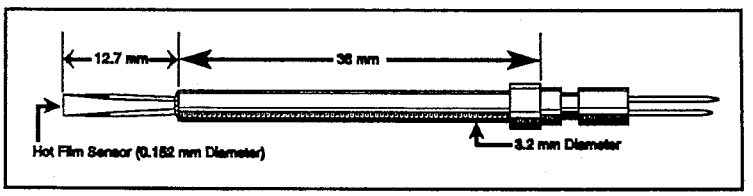

Figure 8. Schematic of the TSI, Inc., Model 1210-60 platinum hot film anemometer.

$$V^{0.45} = A + B\,\frac{E^2(T_s - T_{cal})}{(T_s - T_e)} \qquad (1)$$

where V is the air velocity, A and B are calibration coefficients, E is sensor voltage, T_s is the sensor temperature (always 250 °C), T_{cal} is the laboratory air temperature during calibration, and T_e is the ambient air temperature during field use. The ratio $(T_s - T_{cal}) / (T_s - T_e)$ is the

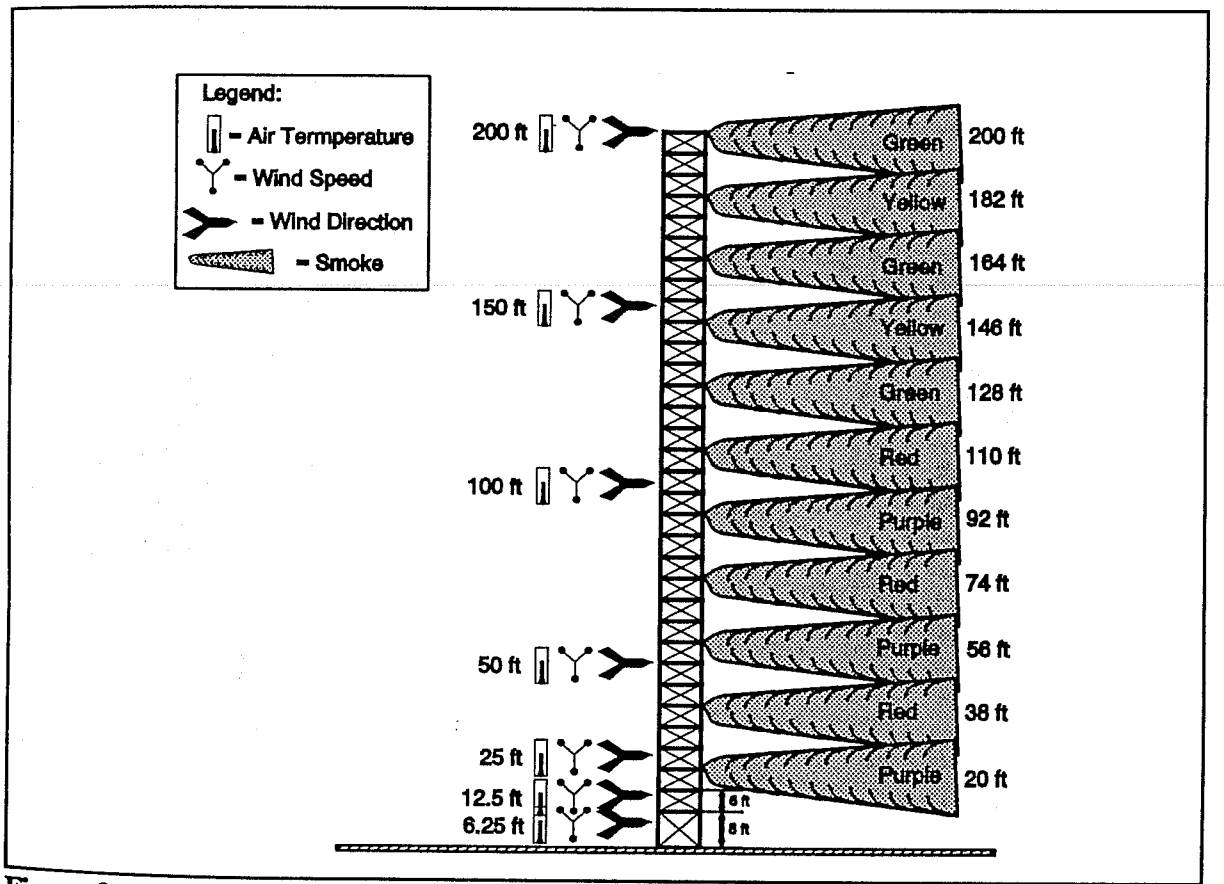

Figure 9. Schematic of the primary test tower, illustrating the location of conventional meteorological sensors (air temperature, wind speed, and wind direction) and tower smoke generators.

correction necessary to account for any sensor heat transfer due to field temperatures different from those observed during sensor calibration in the laboratory. The value for T_e was determined from tower temperature sensors that are described later in this chapter.

Current (I) can be substituted for E using Ohm's Law in Equation (1), since the resistance of the hot film is constant. Current through the hot film, rather than E across the hot film was measured by the data acquisition system because the NOAA electronics package used a two-wire design in its circuit board.

Calibration

All hot film sensors with matched NOAA electronics were calibrated for wind speeds from 2 to 330 ft/s (fps) in a Flow Corporation Probe Velocity Calibrator (wind tunnel) shown in Figure 10. Before the calibration of the hot film sensors was undertaken, the wind tunnel was first calibrated with two National Institute of Standards and Technology (NIST)-traceable hot film anemometers. The medium-velocity (0.5 to 45 fps) and the high-velocity (10 fps to Mach 1) chambers of the wind tunnel were calibrated. The calibrations relate wind velocity measured by the NIST-traceable hot film anemometers in either chamber with the differential pressure of

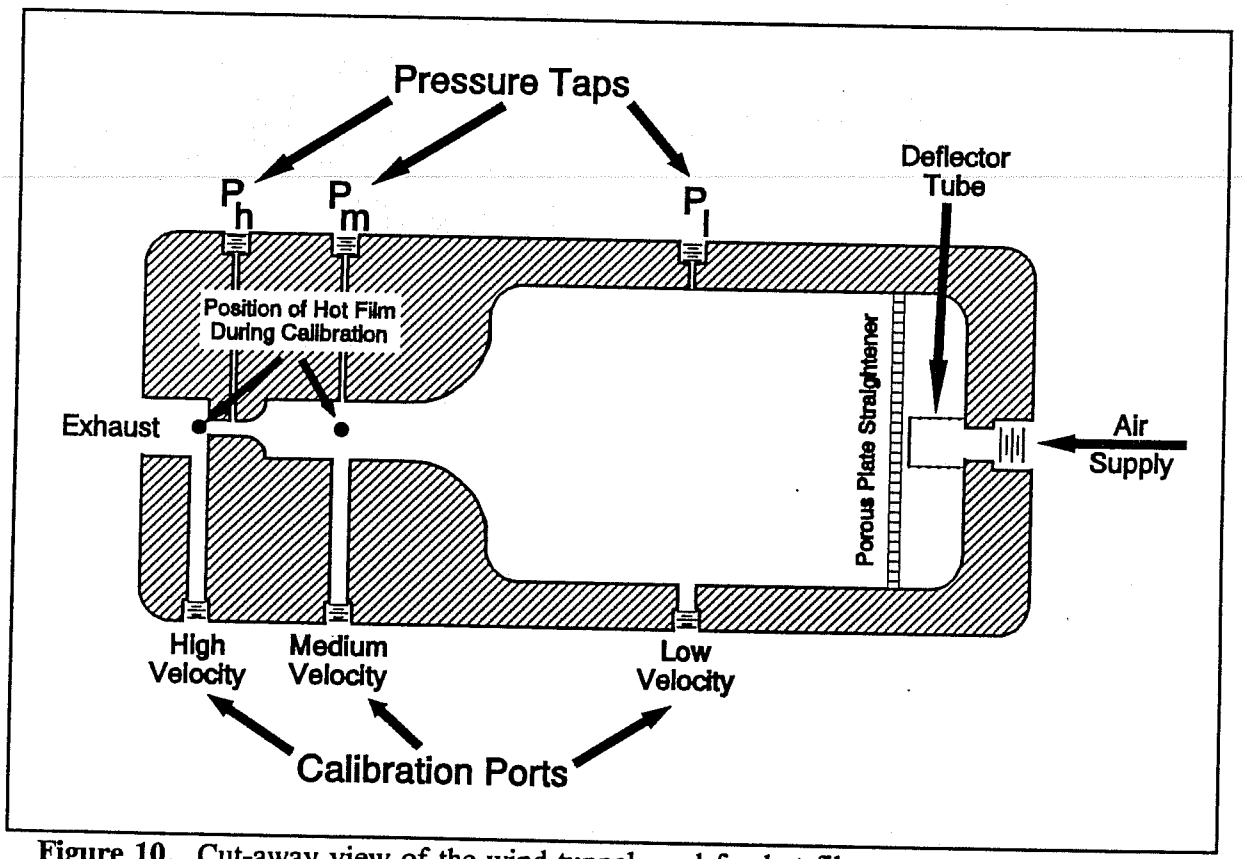

Figure 10. Cut-away view of the wind tunnel used for hot film anemometer calibration.

wind tunnel port P_l to ambient pressure P_a. The calibration curves for both velocity chambers are shown in Figure 11. Coefficients of determination (r^2) for both of the linearized curves were greater that 0.99.

Following calibration of the wind tunnel with NIST-related standards, each field hot film anemometer was subsequently calibrated in both the medium- and high-velocity chambers of the wind tunnel. The hot film anemometer calibration consisted of simultaneously recording air temperature measured with a copper-constantan thermocouple inserted into the low-velocity calibration port (T_{cal}), the pressure differential (P_l - P_a), and the current response of a given anemometer at three speeds in the medium-velocity chamber and four speeds in the high-velocity chamber. Figure 12 illustrates a typical anemometer calibration curve. The correlation between velocity and current using the transformation expressed by Equation (1) was typically greater than 0.99.

Tower Standard Meteorological Sensors

For ambient atmospheric measurements, precision meteorological instrumentation was installed at seven logarithmically spaced levels along the vertical span of the tower (Figure 9). Cup anemometers and wind vanes from Climatronics Corp. (model 100075 and 100076, respectively) were used to monitor wind speed and direction, respectively. A typical wind speed/wind direction instrument installation is shown in Figure 13. Aspirated copper-constantan thermocouples were used to measure air temperature.

A calibration of each piece of tower meteorological equipment was completed, as appropriate, to ensure accurate data collection. Each cup anemometer was calibrated in a wind tunnel prior to installation on the tower and again after the field research program was completed. Comparison of the before and after anemometer calibrations were within the manufacturer's sensitivity and accuracy specifications. Each wind vane was calibrated before the test series to ensure proper readout of the positioning potentiometer. Orientation of each wind vane (after field installation) was checked twice during the study. NIST calibration equations were used for the thermocouples. Each aspirator was also checked for proper operation prior to installation and again after the study and found to be in good working order.

Tower Vortex Flow Visualization System

Tower-mounted, colored-smoke generators were used for vortex flow visualization. Each smoke generator was a specially modified standard-issue hand-held smoke grenade (Type M18). The modification consisted of replacing the factory-installed igniter with an electric match to permit remote ignition of the grenade. The system consisted of four different colors mounted at 11 levels spaced 18 ft apart (Figure 9). The colors provided good visual contrast and resolution of the vortex system. Eighteen smoke generators were installed at each level, as shown in Figure 14, thereby permitting 18 consecutive data runs to be flown with smoke during a scheduled test period.

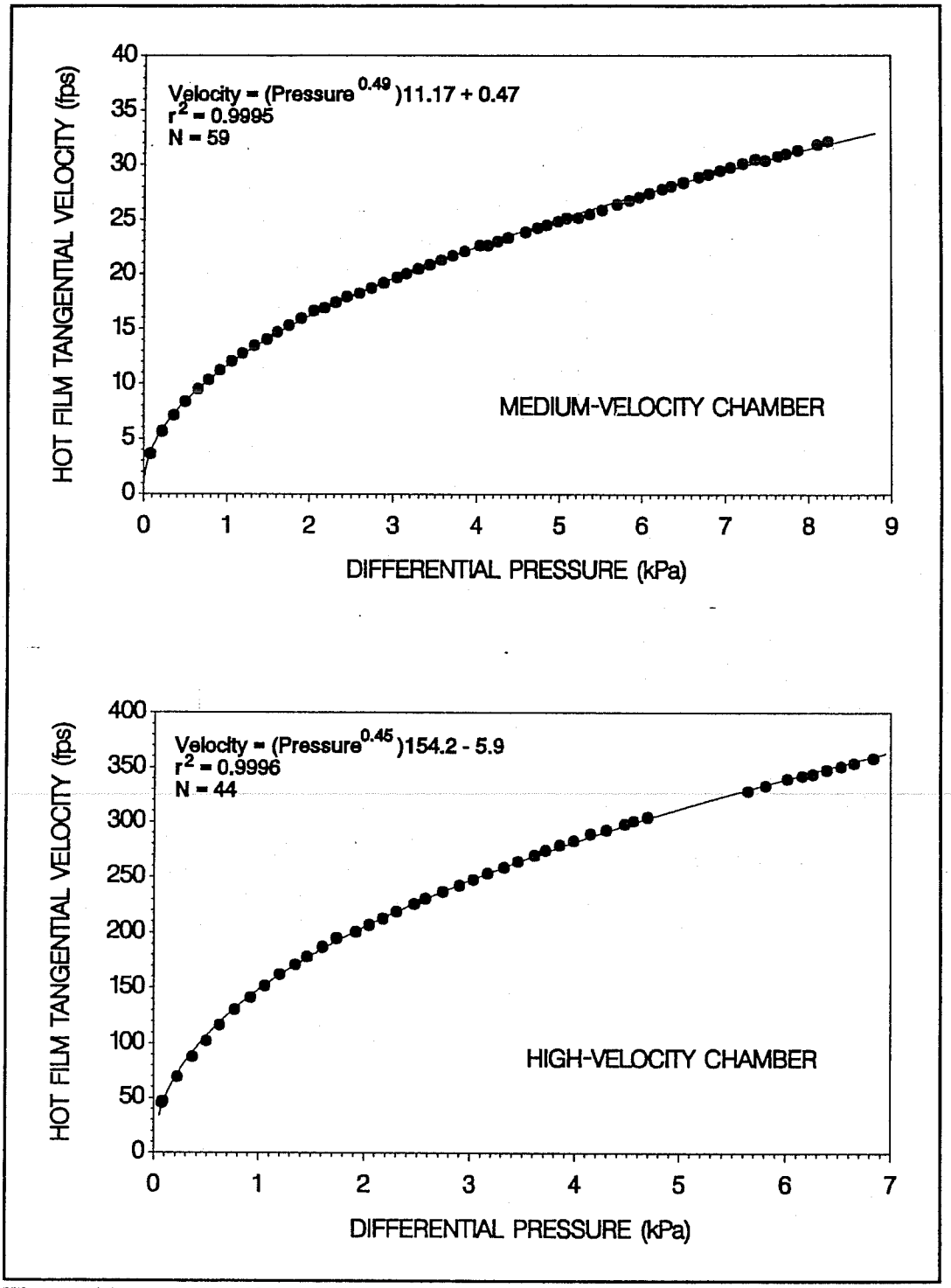

Figure 11. Results of the NIST-traceable hot film anemometer calibration of the medium (top) and high (bottom) velocity chambers of the hot film anemometer wind tunnel.

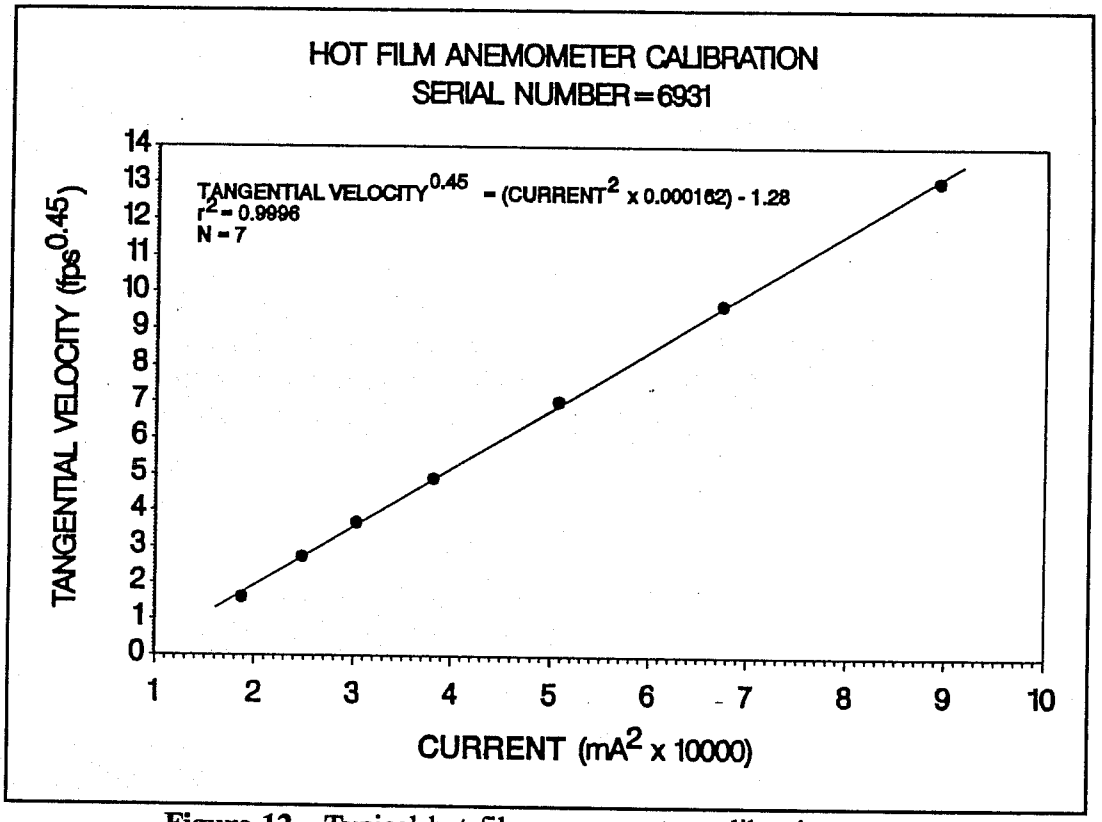

Figure 12. Typical hot film anemometer calibration curve.

The smoke generators had a burn time of about 60 s. The initial ignition time of the smoke-generating system had to be judiciously determined by the Flight Test Director (FTD) for each flyby, depending on the arrival time of the vortex to be marked. The smoke showed if and when one or both vortices passed through the tower, at what height AGL, and the visual characteristics of the vortex flow field during and after tower passage. Interpretation of the flow field required careful analysis to ensure that what was seen downwind of the tower was the basic vortex structure and not a distorted flow field induced by tower passage.

At various times when the tower smoke system was not available, a backup vortex flow visualization system was used. In these cases, vortex age and height of tower penetration were determined by viewing the motion of short, plastic, orange-colored tape streamers mounted on a line extending from the surface to the top of the tower. The backup system is shown in Figure 15. This quick field fix worked remarkably well.

Ground-based Hot Film Anemometers

A ground-based vortex-sensing system was installed at the base of the 200-ft tower. It consisted of an array of approximately fifty 30-ft-tall towers spaced at 100-ft intervals, as shown schematically in Figures 4 and 16. The array extended outward radially for 2500 ft to the

northeast and the southwest, as shown in Figures 16 and 17. Thus, the total length of the array was 5000 ft. Each ground-array tower had one hot film anemometer mounted horizontally on top. Every fifth tower had an additional vertically oriented anemometer. Each hot film anemometer installed in the ground-based system was calibrated in the same manner as the tower-based hot film anemometers.

The ground-based sensors were installed to measure the tangential velocities of vortices that descended into ground effect. It was understood *a priori* that when this occurred, only the bottom part of the vortex would be measured most of the time. The size of the vortex flow field would normally prevent the core tangential velocity from being measured. Only occasional vortex penetrations into ground effect were expected. With these limitations fully understood, the array was nevertheless installed at the request of the FAA to record vortex lateral movement velocity and distance in ground effect.

Upper-Air Meteorological Instrumentation

Characteristics of the atmosphere above the top of the 200-ft tower were measured by a tethersonde. The balloon and sonde are shown in Figure 18. The balloon was a 3-m^3 kitoon that was raised and lowered continuously during each test period. The sonde, manufactured by A.I.R. Inc. (Model TS-3A-SP), measured wind speed, wind direction, air temperature, wet bulb temperature, and air pressure. The sonde was calibrated at the factory before use in the field. The tethersonde was deployed at approximately 200 ft AGL (tower top level) up to an altitude of approximately 1000 ft AGL. It was positioned approximately 2000 ft northeast of the 200-ft tower in the vicinity of the ground-based vortex sensors. This was a sufficient distance away from the tower so as not to be a hazard to test aircraft.

DATA ACQUISITION SYSTEMS

Three distinct data acquisition systems were employed to automatically measure and record data from the hot film anemometers, the standard meteorological sensors, and the tethersonde. Two of the three acquisition systems were connected to a local area network (LAN) using Ethernet protocols, as shown in Figure 19. The LAN connected both the hot film anemometer and standard meteorological sensor data acquisition systems.

Hot Film Anemometers

The hot film data acquisition system consisted of two identical units designated System #1 and System #2. Only one system was operational for a given flyby, with the second providing redundancy. The 80386 16-MHz-based PC's contained a fast 12-bit analog-to-digital (A/D) converter from National Instruments Corp. (Model AT-MIO-16). Current output from all the hot film anemometers was multiplexed into the A/D converter through a 64-channel multiplexer also from National Instruments Corp. (Model AMUX-64T). Scan rate was 100 Hz per channel. Although the scan rate could have been faster, experience had shown that 100 Hz was fast enough in most instances to measure vortex core velocities. However, the selected sampling rate

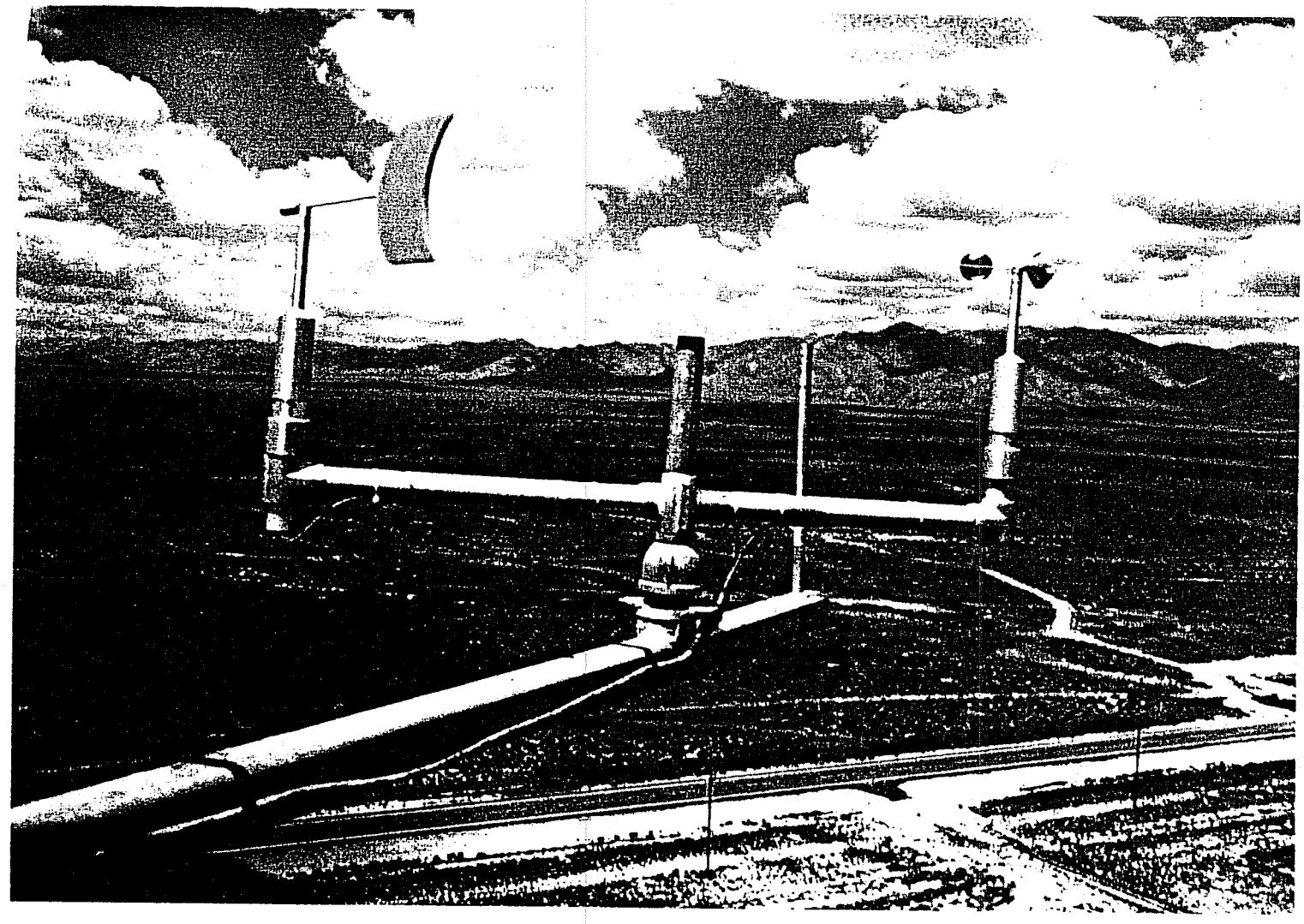

Figure 13. Wind speed and direction equipment mounted at the 200-ft level on the NOAA vortex test tower.

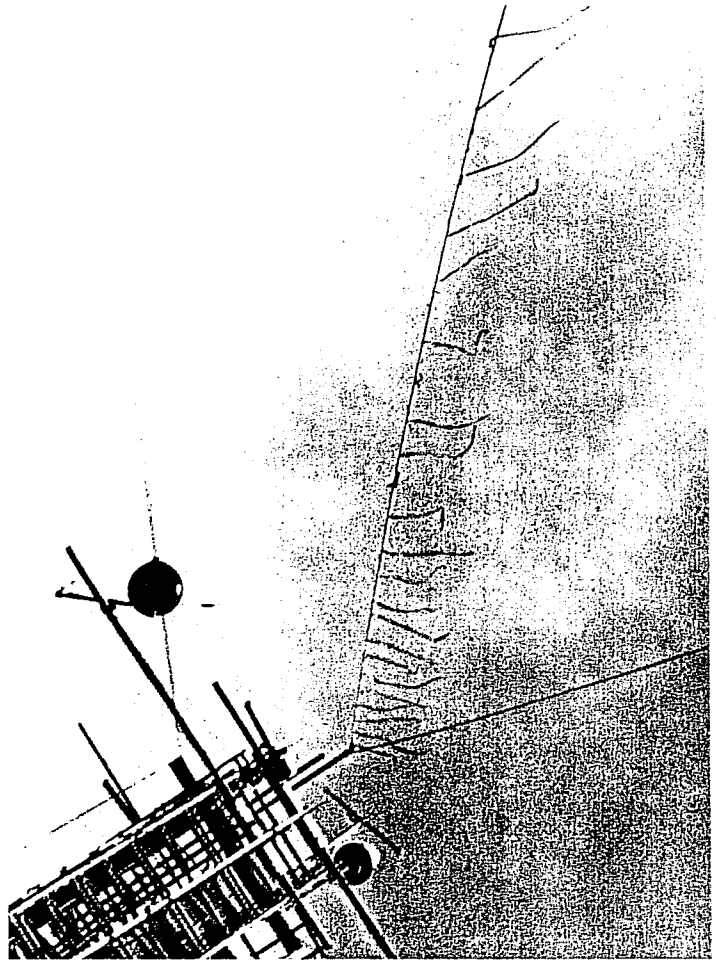

Figure 15. Streamers mounted on the vortex test tower hoist rope as an alternate method of vortex age and tower intercept height determination.

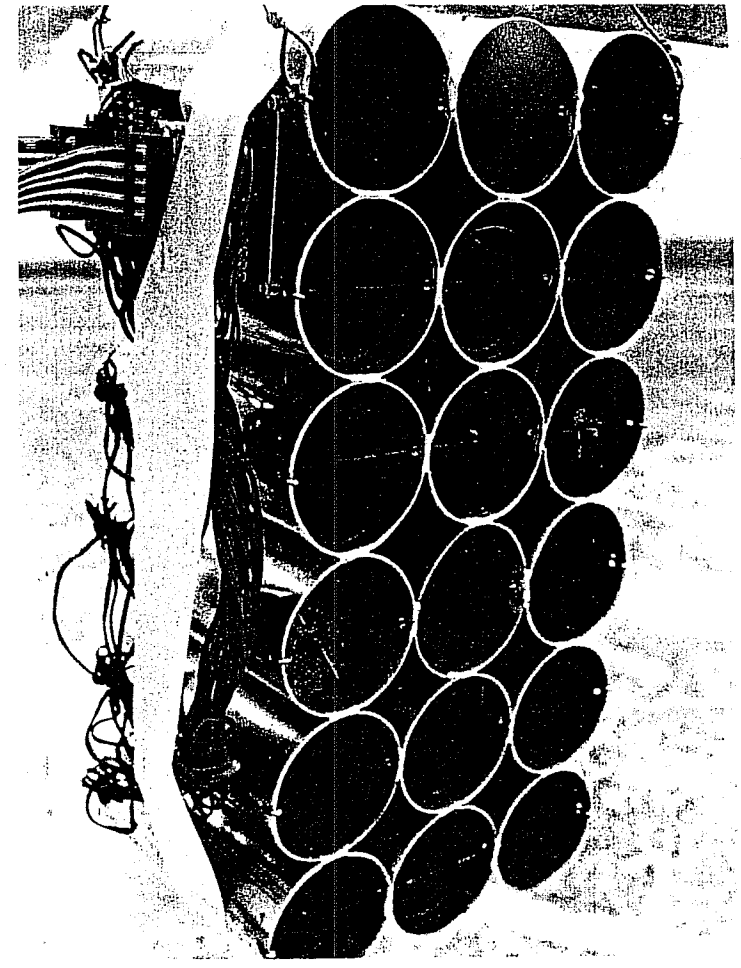

Figure 14. Tower-mounted smoke generator canisters for vortex flow visualization.

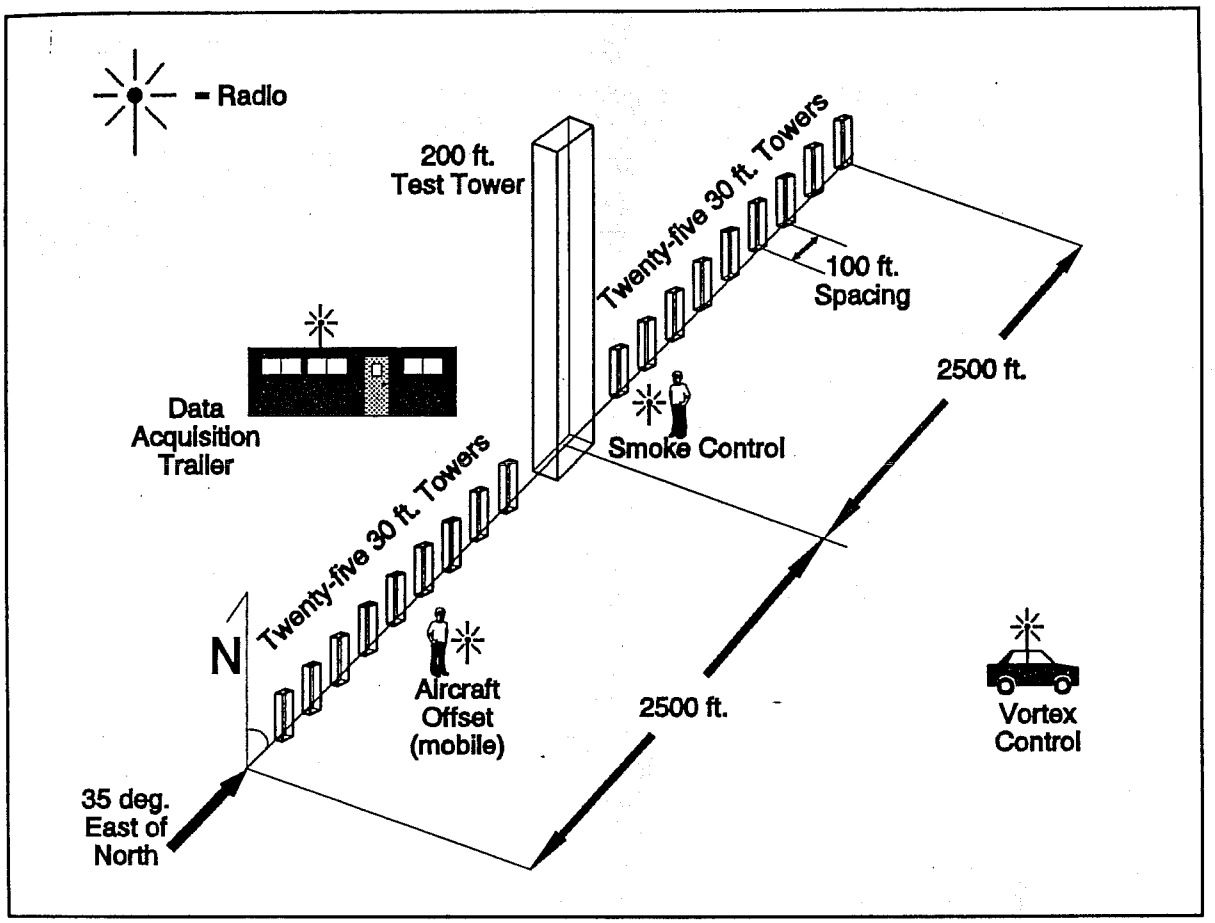

Figure 16. Schematic of the ground array of hot film anemometers in relation to the 200-ft tower. Approximate locations of various other control and support facilities are also shown.

could result in two deficiencies in the data: (1) missing peak vortex tangential velocities generated during high-speed lateral transport of the vortex through the tower as a result of high ambient crosswinds, and (2) missing velocity signatures of high-frequency turbulent eddies embedded in the vortex, e.g., "satellite" vortices or wing-tip vortices rotating around the predominant wing-flap vortex when the aircraft is in the landing configuration. Wind speeds were only moderate during the flight tests, which permitted measurement of the core of nearly all vortices advected through the tower. The latter deficiency was not an important consideration, since measurement of small eddies was outside the scope of the study.

The data acquisition sequence consisted of many steps. When the aircraft was on final approach and about 30 s from arrival at the tower, the computer operator initiated hot film anemometer data collection by the computer system. When the aircraft was precisely above the line of ground-based hot film anemometer towers, an electronic signal under the control of the tower smoke operator was recorded in the hot film data. This "abeam time" was considered to be time zero; the time of birth of the vortex, which was later measured at the 200-ft tower.

Vortex ages were calculated from this time. The computer continued to collect data for 5 min. Approximately 10 Mbytes of data were acquired during each 5-min scan cycle. After completion of the scanning sequence, the data from the computer were then transferred over the LAN to the file server for initial processing and data archiving. After completion of the data transfer, the computer was placed in a standby mode awaiting another final approach of the aircraft. During data transfer to the file server, the other acquisition system was placed into service and used to acquire vortex data during the next tower flyby. Thus, the two hot film data acquisition units were used in a "leap-frog" fashion.

Once the data were transferred to the file server, they were subjected to numerous quality assurance processes. The data were converted from current to engineering units on the data processing computer using the coefficients and conversion routines obtained during wind tunnel calibration. The conversion process also contained a battery of statistical routines. The data were further averaged into 1-s blocks to permit a quick-look check on the graphic display computer. A sample graphical image is shown in Figure 20. The data were observed for outliers and "reasonability." Any suspicious data were immediately investigated. Hot film anemometers suspected as being defective through this process were replaced as quickly as circumstances permitted.

The final repository of the hot film anemometer data was on two different media. The primary storage device was a write-once/read-many (WORM) drive. The secondary storage device was a 150-Mbyte streaming tape. The redundancy provided a means to recover critical data, should one device fail.

Standard Meteorological Sensors

The tower meteorological data collection began approximately 45 min before the first flyby was scheduled and continued until approximately 15 min after the last flyby was completed for a given test period. All the output from the standard meteorological sensors was measured by a Campbell Scientific datalogger (Model CR-10). Each sensor was scanned at a rate of 1 Hz with the exception of the cup anemometers. The pulse output of the light chopper in each anemometer was continuously monitored and the counting period was 1 s.

The data obtained by the datalogger were continuously monitored and recorded on a 80386 PC using a proprietary OS/2 program from Campbell Scientific, which was still under development. The graphical output of this program provided a real-time display of the temperature gradient, wind speed gradient, and wind direction shear over the entire height of the tower. A photograph of the CRT display is shown in Figure 21. The data displayed in this manner were of great help to both the on-site FTD and the NOAA forecaster for establishing flight test schedules and flight patterns. The FTD communicated this information to the flight test crew before commencing tower flybys. Key on-site test equipment and support personnel were positioned to best observe and record the flight test data. The NOAA forecaster utilized the data in forecasting wind direction shifts primarily from the northeast to the southwest as the day progressed. Final repository for the meteorological data was on 40-Mbyte streaming tape and on a WORM disk.

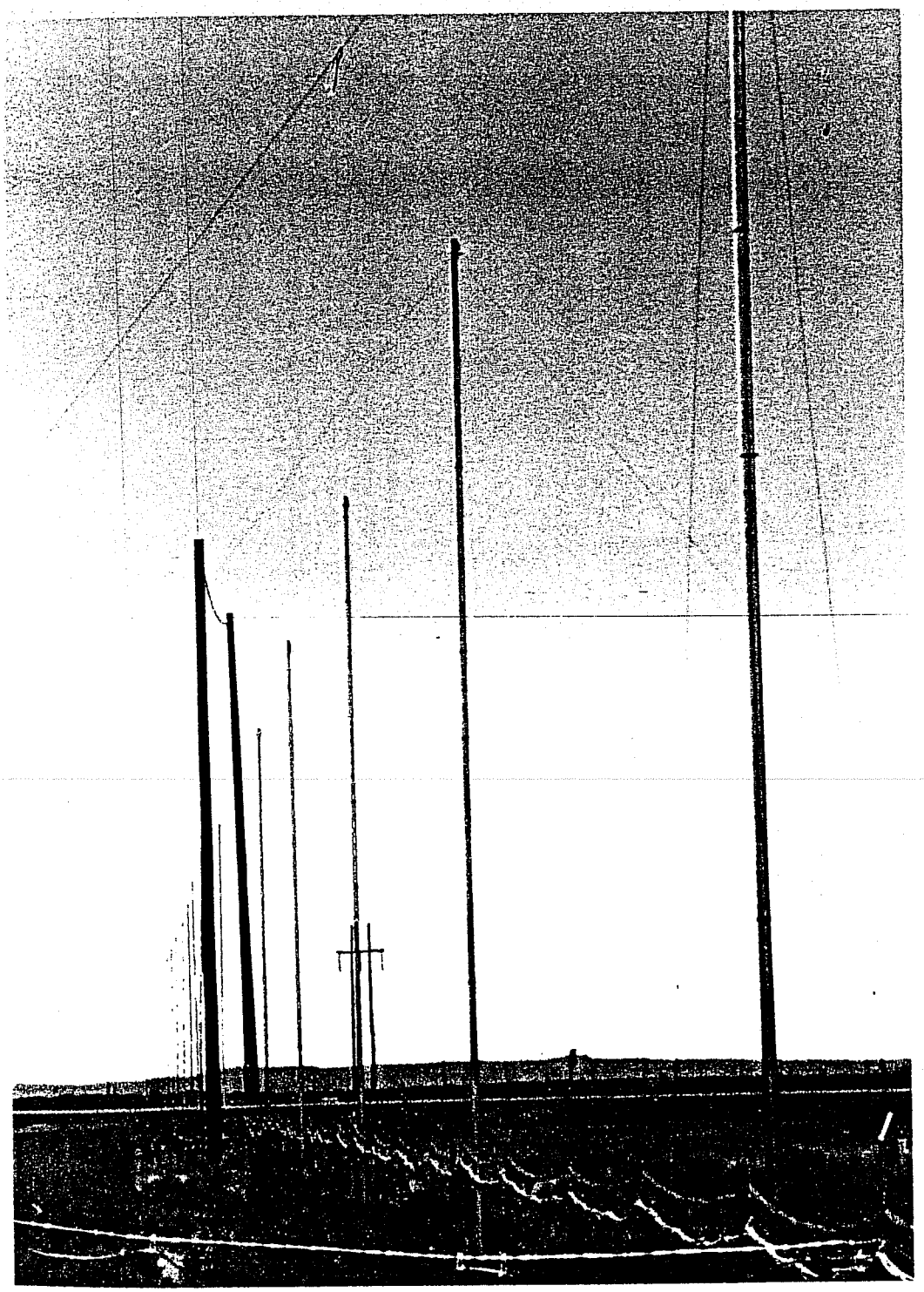

Figure 17. Horizontal ground array of hot film anemometers and associated towers extending radially outward from the base of the 200-ft tower toward the northeast and southwest.

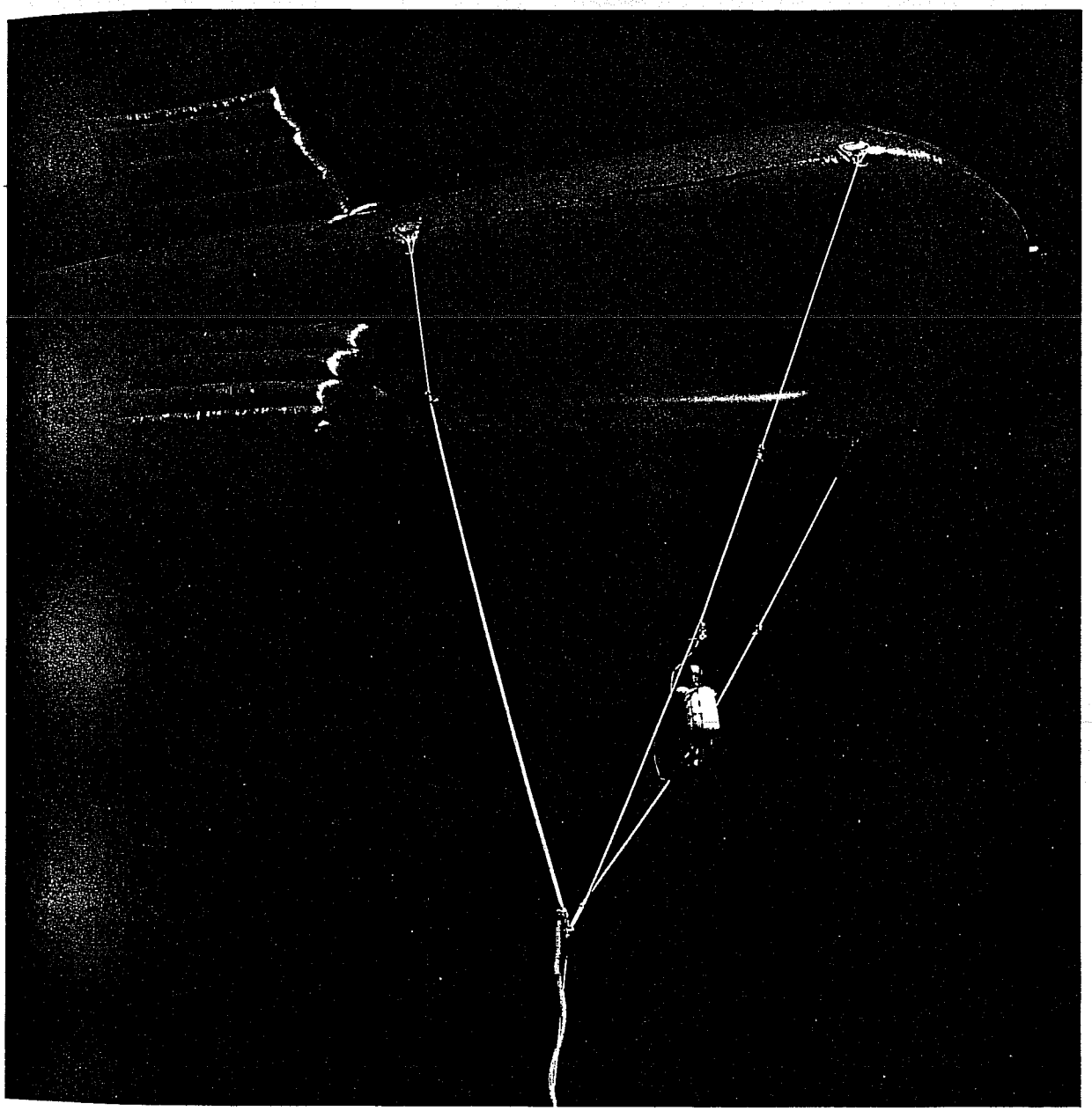

Figure 18. NOAA tethersonde showing the kitoon and meteorological sensor package used to measure wind speed, wind direction, air temperature, relative humidity, and air pressure at altitudes between 200 and 1000 ft AGL.

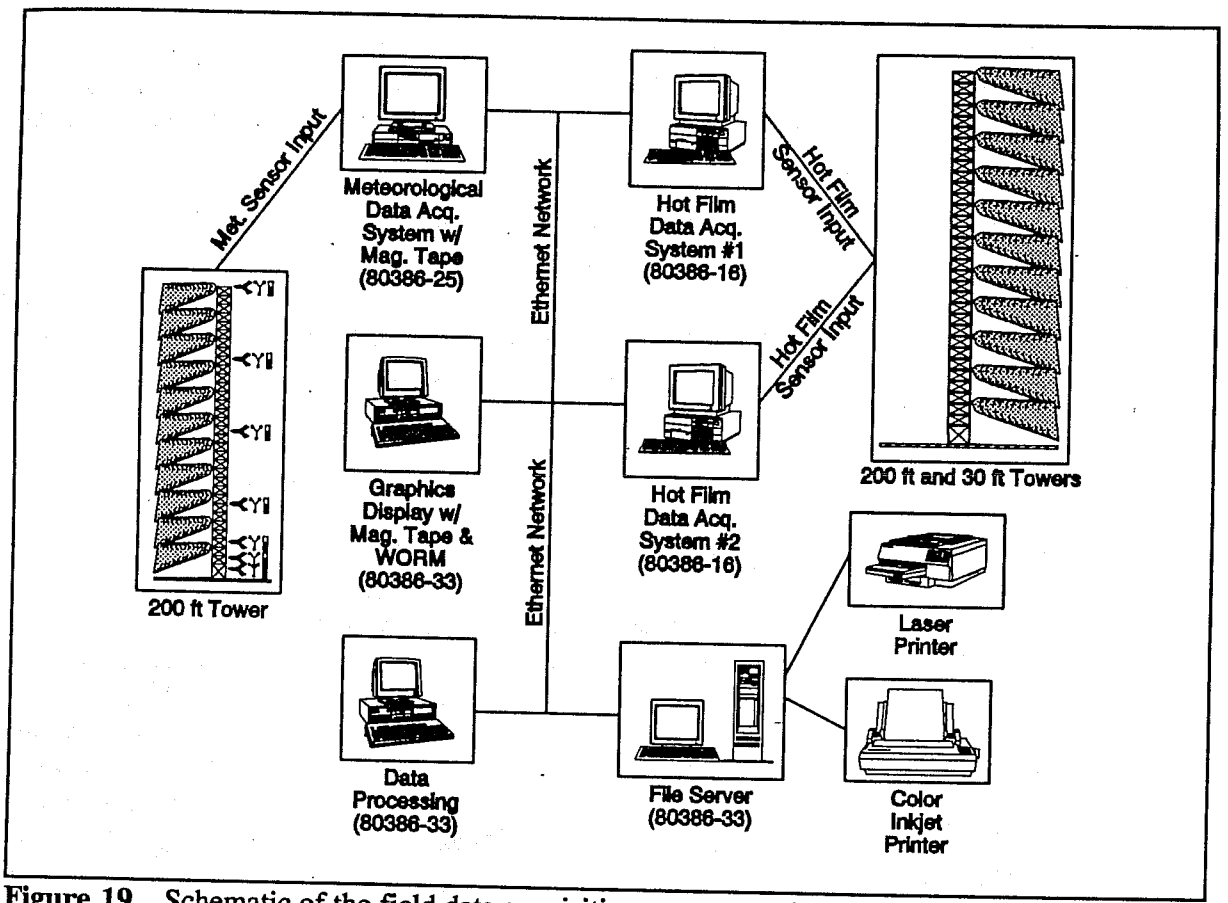

Figure 19. Schematic of the field data acquisition system used at the NOAA vortex test facility for the collection of hot film anemometer and standard meteorological sensor data. Numbers in parentheses are the processor type-speed (MHz).

Tethersonde

The tethersonde data were collected with the Atmospheric Data Acquisition System from A.I.R. Inc. (Model AIR-3A). These data were recorded only during the September test period on an 80386-SX laptop computer connected to the acquisition system via an RS-232 link. This computer and associated data acquisition unit were not a part of the LAN described above. However, the data were verbally transmitted, as needed, to the FTD and onsite forecaster via a radio link. Final repositories for these data were floppy disk and WORM disk.

AIRCRAFT

Three commercial jet transport aircraft were used for the flight tests: the Boeing B727-222, the B757-200, and the B767-200. Three view drawings of each of these aircraft are shown in Figures 22, 23, and 24, respectively. The aircraft were leased by NOAA from United Air Lines (UAL) and flown by UAL flight crews. A B727-100 owned by the FAA was also used for data

acquisition systems shakedown as well as for some limited vortex data. A drawing of the B727-100 is shown in Figure 22 along with its -222 counterpart. The B727-222 differs from the -100 only in the length of the fuselage, which is 20 ft longer. Relevant design specifications of the four aircraft are detailed in Appendix A.

Each UAL test aircraft was provided with an Inertial Navigation System (INS). This greatly aided the aircraft flight crew in locating the remote NOAA test site. It also aided in final aircraft alignment on the desired approach course at the test site. In addition, the INS provided supplementary data on winds aloft to the on-site FTD for calculating the desired offset position of the aircraft when it was abeam of the tower. These data also assisted the on-site NOAA meteorologist in forecasting the site wind conditions during the course of a test period.

No special data recording instrumentation was required or installed onboard the test aircraft. Aircraft performance data were recorded by hand ("knee-pad data") by an onboard observer. Knee-pad data were sufficient for aircraft performance and configuration determination because the test aircraft were flown under steady-state conditions, i.e., straight and level flight [or a 3° glide slope (G/S)] at constant air speed. Knee-pad data were recorded at the time the aircraft was abeam of the tower. These data included the following: (1) time the aircraft was abeam of the tower, (2) aircraft configuration, i.e., flap setting, leading-edge slat position, landing gear position, (3) gross weight, (4) indicated air speed, (5) radar altitude above the ground, (6) pressure altitude, (7) magnetic track, (8) estimated lateral distance from the tower (actual distance was obtained from ground personnel), (9) engine performance, and (10) pilot opinion of test altitude atmospheric turbulence [none, light, moderate, or severe, according to Garodz and Miller (1975)].

A vortex flow visualization system was installed only on the wing tips of the B727-222 (Figure 25). It was desirable to attach the system on all of the aircraft used in the flight test effort, but the installation would have been too costly and would have required considerable aircraft down-time. Installation of the system on the B727-222 was possible because this particular airplane had been previously modified by UAL for a vortex flow visualization system and had been used in previous vortex flight test programs conducted by both the FAA and NASA (Kurkowski et al., 1976). The vortex marking system consisted of two self-contained smoke generator pods manufactured specifically for these types of flight tests by Frank Sanders Aircraft. The smoke was generated by vaporizing Corvus oil in a heated chamber inside the pod.

The original test plan called for the test aircraft to fly as close as possible to maximum permissible takeoff gross weight (MTOGW) in an attempt to achieve the highest lift distributions (W/b) and vortex intensities (Γ) possible. This would have required placing ballast onboard the aircraft, since the aircraft were to be flown without cargo and passengers. However, this was not possible because each UAL aircraft was available for only 2 days of flight tests. The aircraft were loaded instead with the maximum permissible fuel load, taking into consideration aircraft performance limits for the ambient temperatures and flight altitudes associated with a particular daily test flight operation.

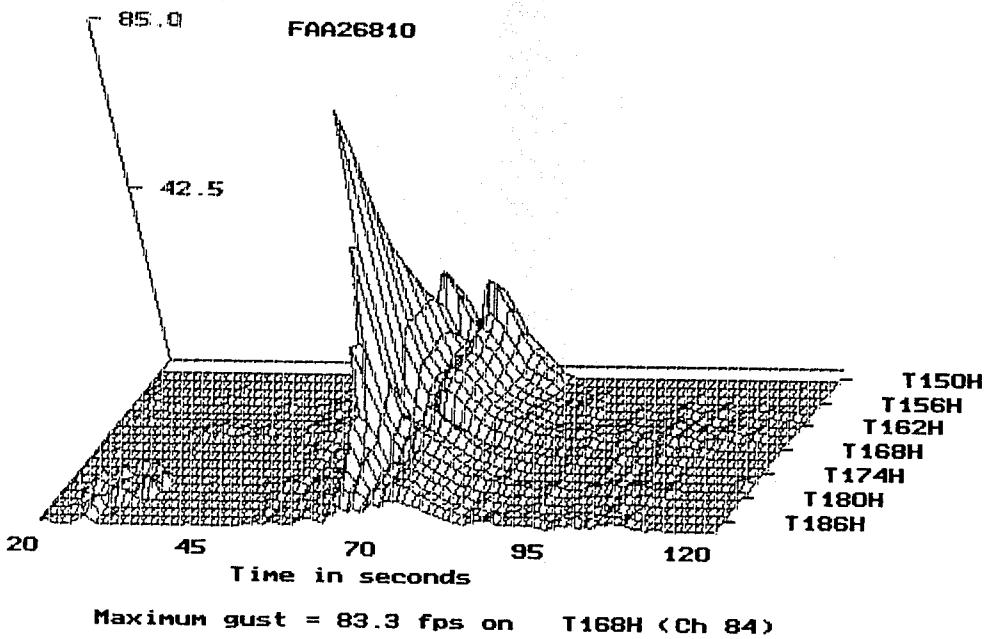

Figure 20. Typical pseudo-three-dimensional image of hot film anemometer data from the 200-ft tower used in the field for data quality control purposes. The data are from flyby 10 of the B757-200 and show the majority of the downwind vortex.

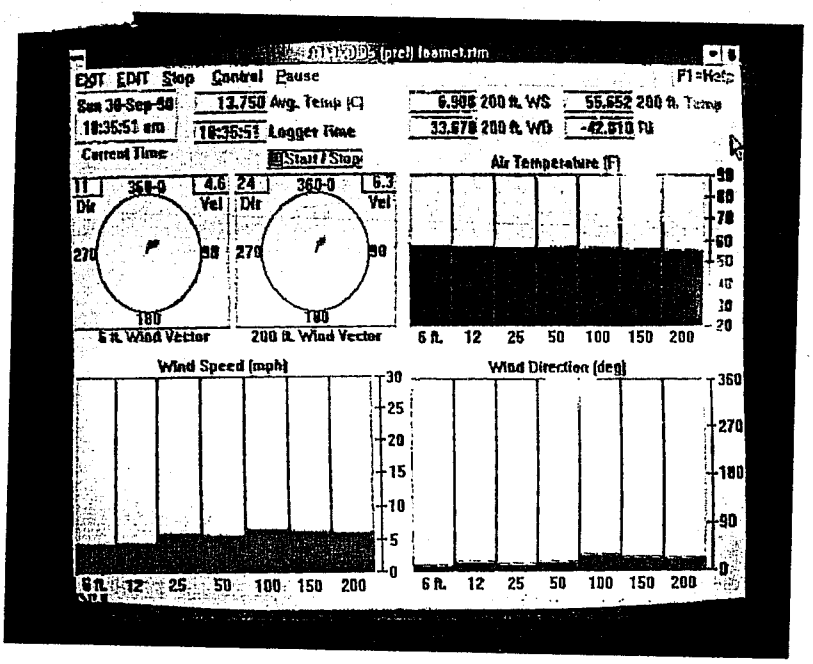

Figure 21. CRT display of real-time meteorological conditions at the NOAA vortex test facility.

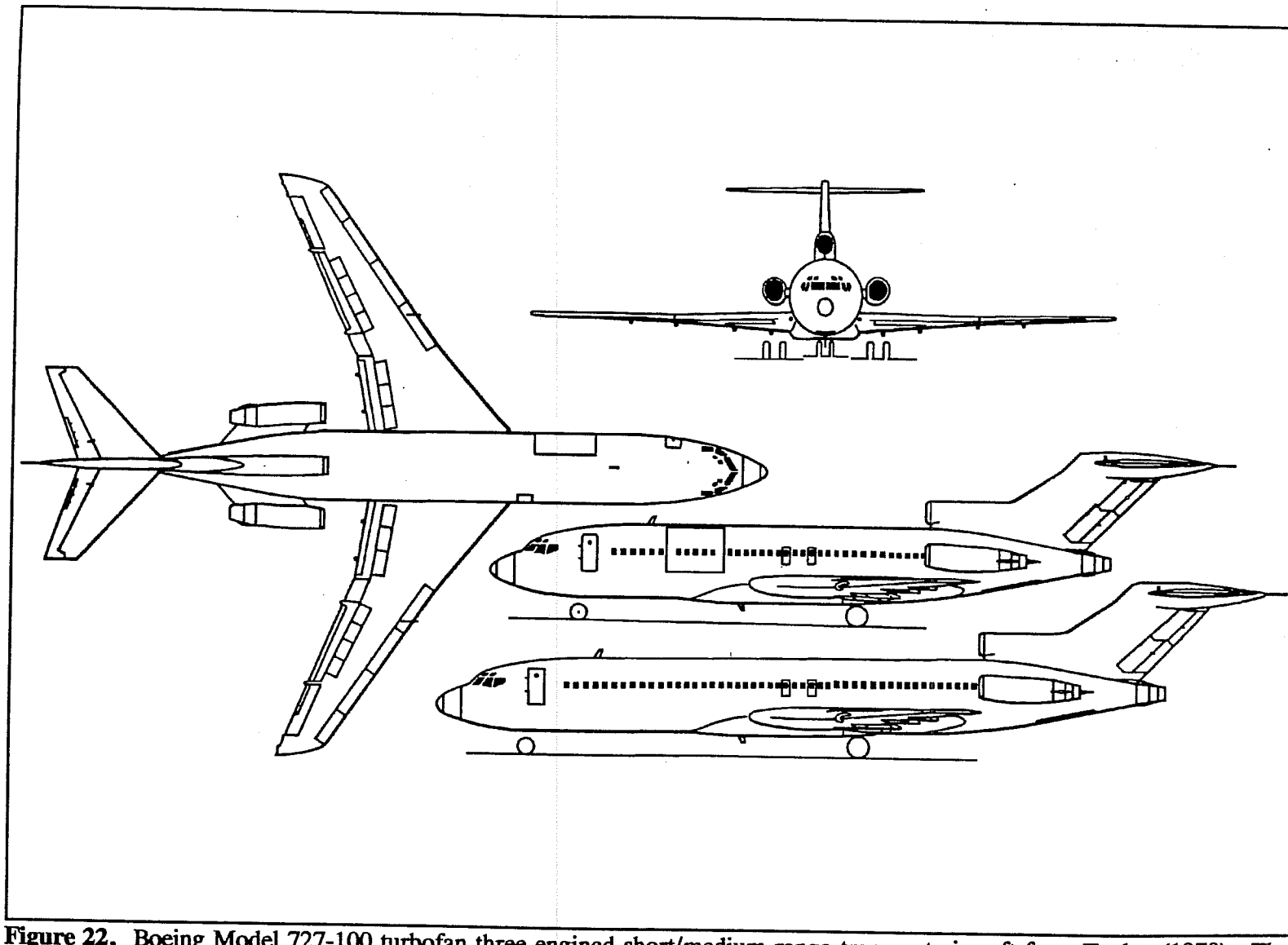

Figure 22. Boeing Model 727-100 turbofan three-engined short/medium-range transport aircraft from Taylor (1970). The longer side view is the larger 727-222.

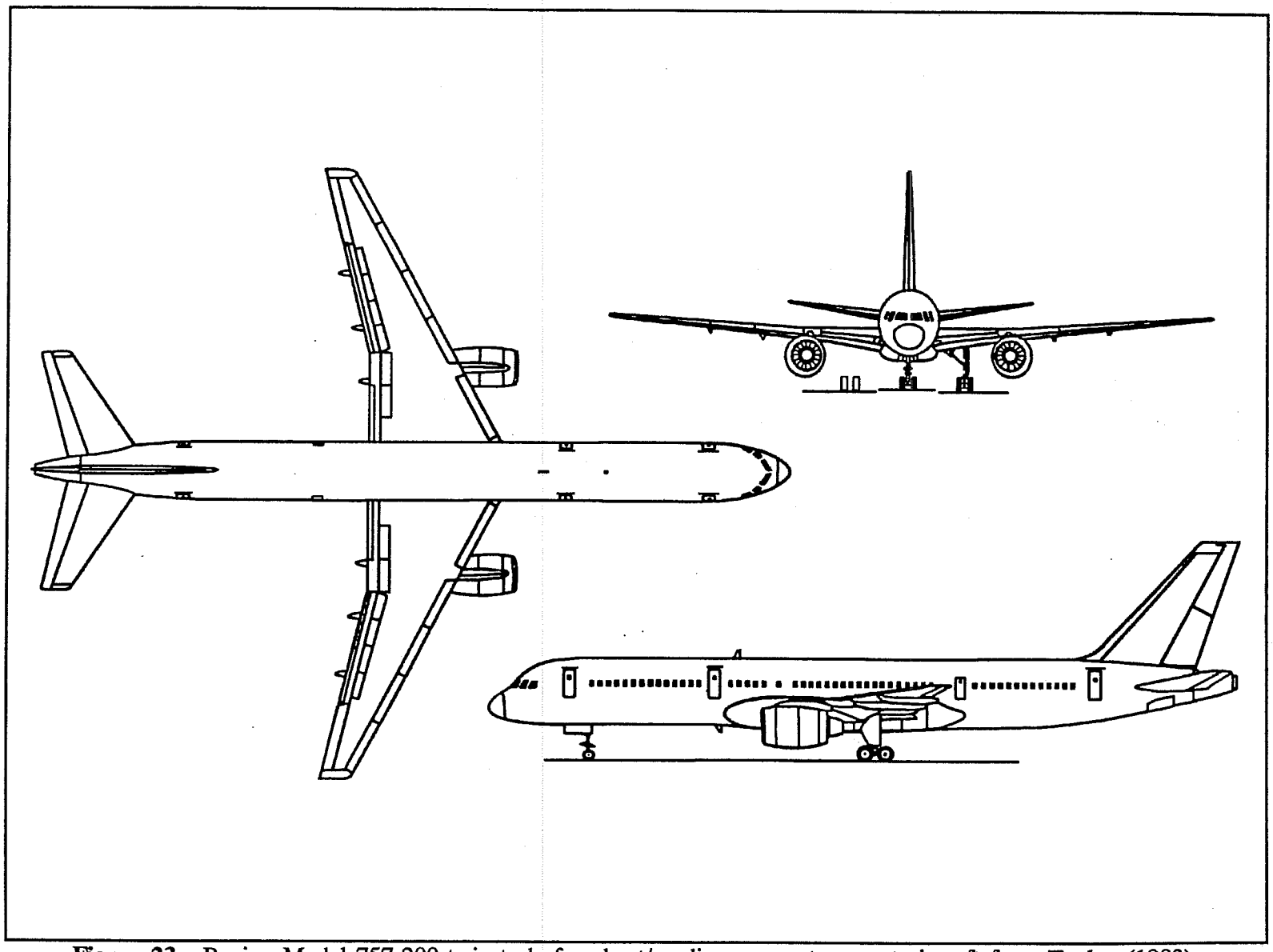

Figure 23. Boeing Model 757-200 twin-turbofan short/medium-range transport aircraft from Taylor (1983).

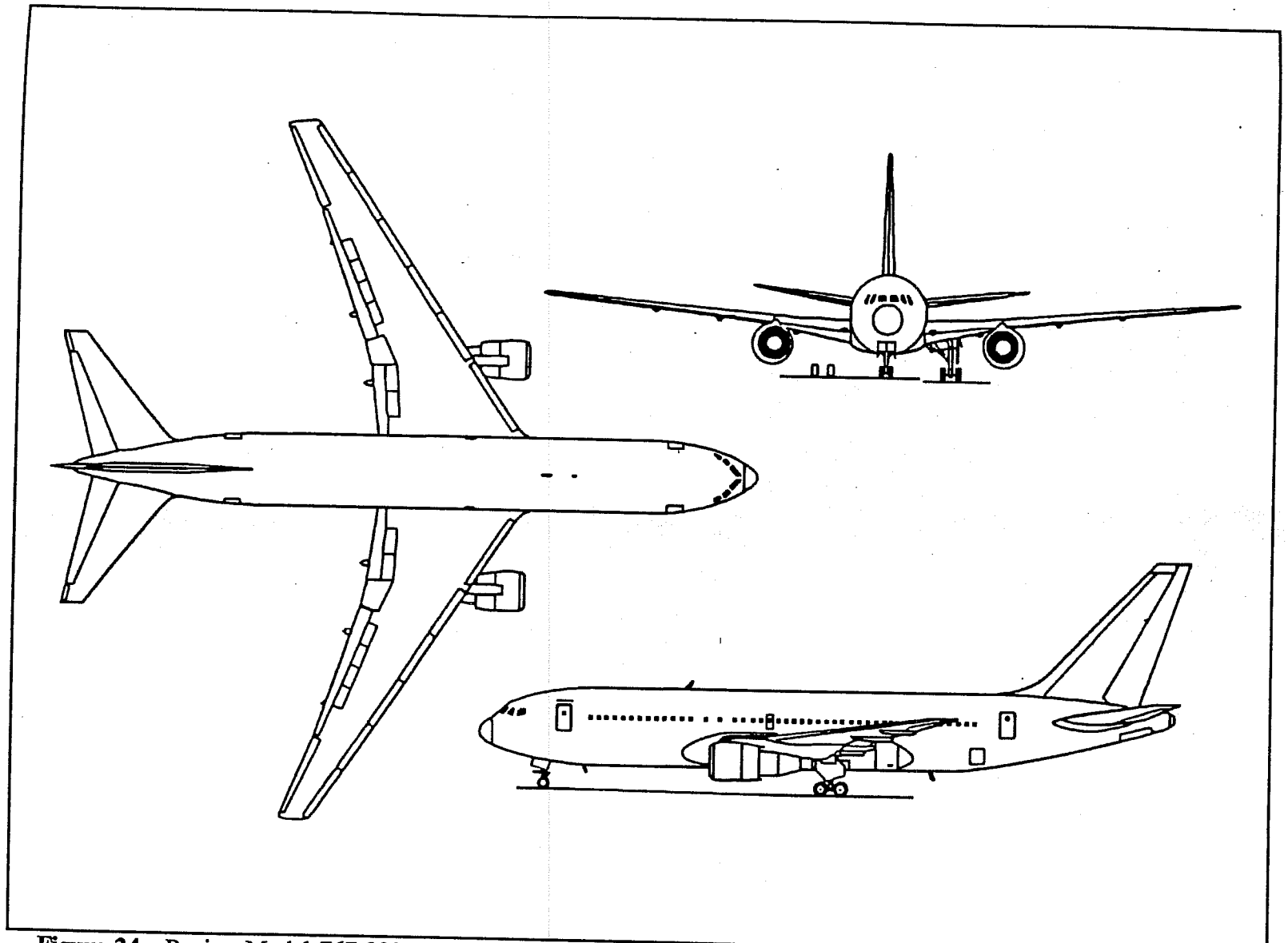

Figure 24. Boeing Model 767-200 twin-turbofan wide-bodied medium-range transport aircraft from Taylor (1983).

The test aircraft were flown in four different flight modes or configurations: (1) landing, (2) takeoff, (3) holding, and (4) clean. These configurations are used in routine flight operations. Table 1 gives specific flap settings and gear positions used for takeoff and landing configurations. The leading-edge slats on the wing were always extended when the landing flaps were lowered to any degree of flap setting. For the holding and clean configurations, the landing gear was always up and leading-edge slats were retracted.

FLIGHT TEST DETAILS

Fifty-four flybys were planned for each UAL airplane using tower-mounted smoke generators to visually mark the wake vortex. Additional flybys were also planned without tower smoke, most of them with the UAL B727-222 at about 300 to 600 ft AGL. These flybys were flown to support other Wake Vortex Program requirements, which are not reported here. Each UAL test aircraft was available for only two consecutive days. The Flight Test Plan called for using each aircraft for two test periods during the first day and one test period during the second day. Further breakout called for 18 tower flybys with a duration of about three hours for each test period. The test periods were limited to 18 flybys, since the tower-mounted vortex flow visualization system could provide smoke only 18 times before restocking. Three hours with 18 flybys approached effectiveness limits because both flight and ground personnel felt the fatiguing effects of demanding flight operations and accurate and coordinated data acquisition.

The first test period of each day commenced with the first flyby at or slightly before sunrise (approximately 0700 MDT). The tower flyby pattern was established so that the pilot would be flying away from the sun on the final leg of a tower flyby at sunrise rather than toward the sun, for visibility and safety purposes.

Pilot Aids

The flight crews were subjected to very precise flying requirements. These requirements included: (1) flying at a very low altitude AGL, (2) flying both 0° and 3° G/S approaches, (3) flying continuously under crosswind conditions, (4) flying, at times, with light-to-moderate atmospheric turbulence, and (5) flying a required track over the ground to ensure proper lateral distance abeam of the tower. The several measures taken to assure aircraft safety are described below.

All flight test crews were thoroughly briefed on flight test details by the FTD at the NOAA facility in Idaho Falls prior to beginning any project work at the vortex test site. The briefings covered operational flight procedures, communications, weather limitations, flight safety, and emergency procedures. Written documentation on these various aspects was included along with a video presentation.

Ground-based pilot aids were installed for pilot guidance, because of the requirement to fly a precision track and G/S. For flight track and lateral offset guidance, high-intensity course alignment lights were installed along the four major flight paths (Figure 4). The lights installed

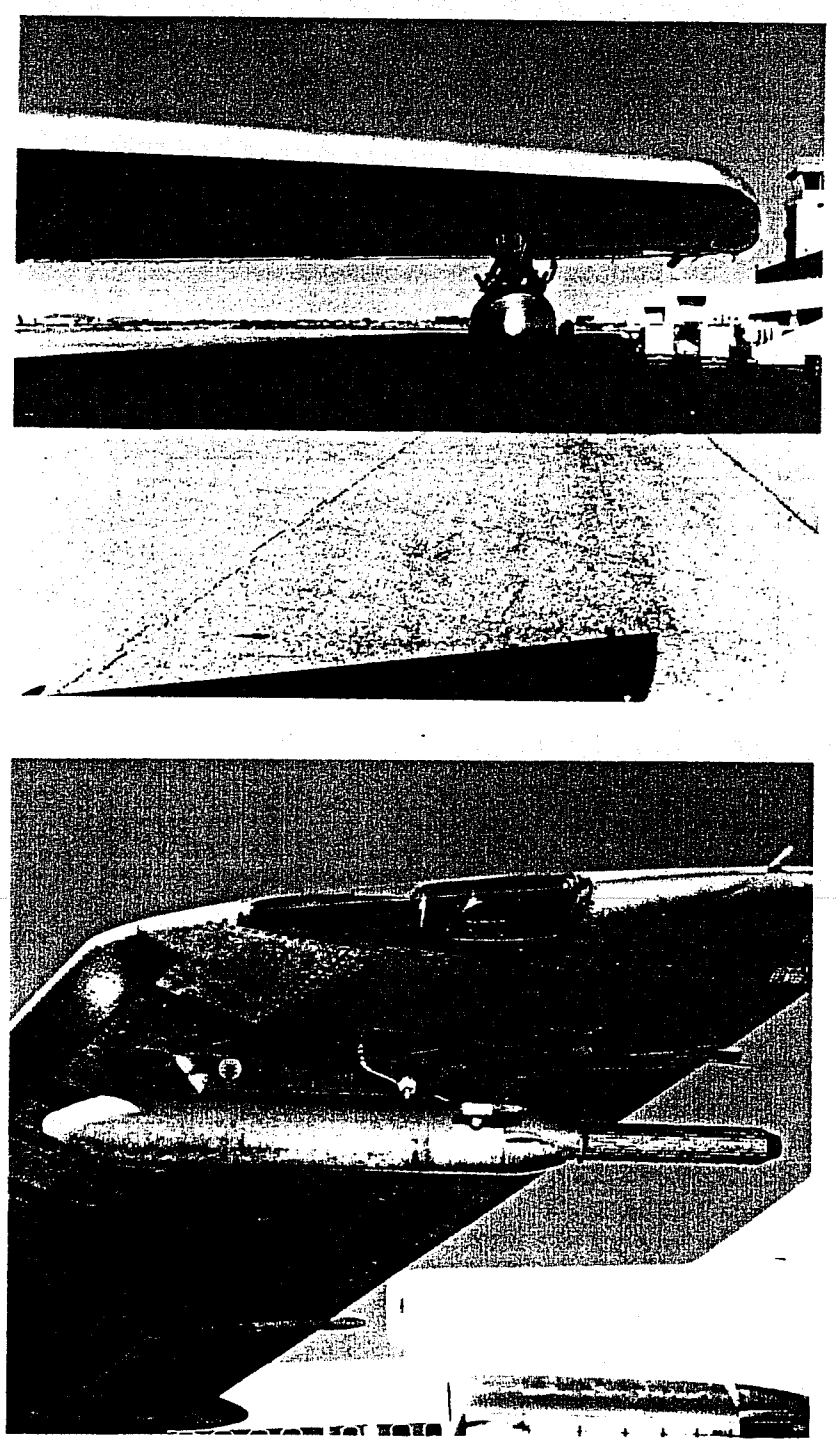

Figure 25. Front and side views (top and bottom, respectively) of the Frank Sanders aircraft Corvus oil smoke generators mounted under the wingtip of the UAL B727-222 airplane.

Table 1. Test aircraft flap settings and gear positions for landing and takeoff configurations.

Aircraft	Takeoff Configuration		Landing Configuration	
	Flaps (Degrees)	Landing Gear (Position)	Flaps (Degrees)	Landing Gear (Position)
B727-100 and B727-222	5	up	30	down
	15	up	40	down
B757-200	1	up	25	down
	5	up	30	down
	15	up		
	20	up		
B767-200	1	up	25	down
	5	up	30	down
	15	up		
	20	up		

along courses Bravo and Charlie were placed to mark the innermost course the pilot could safely fly. The test aircraft was flown between courses Alpha and Bravo when the ambient wind direction was from the northeast. The test aircraft was conversely flown between courses Charlie and Delta when the ambient wind direction was from the southwest. The area between courses Bravo and Charlie was off limits because of the proximity of the tower. The Bravo and Charlie courses were 250 ft away from the centerline of the tower, providing a margin of safety that was at least 1.5 times the wingspan of the B767-200.

G/S guidance was provided by a Precision Approach Path Indicator (PAPI) system. A PAPI is shown in Figure 26. The system was used to provide 3° G/S guidance for the pilot when such was required. The system was portable and could be accurately repositioned to change the desired aircraft height when the aircraft was abeam of the tower. Repositioning required about 15 min because of the somewhat rugged terrain along the northwest end of the flight path.

For obstruction clearance recognition and pilot alert, a high-visibility strobe light was mounted on top of the 200-ft tower. The tower height was approximately 85%, 60%, and 28% greater than the wingspan of the B727-222, B757-200, and B767-200 test aircraft, respectively.

Communications

All activities at the test site were coordinated through the FTD. Verbal communication between the FTD and ground crews was provided by NOAA through a radio link between all parties. Figure 16 illustrates some of those entities. Two-way radios were provided to the FTD at Vortex Control and to personnel in the Data Acquisition Trailer, to Smoke Control, to Aircraft Offset, to the video and still camera operators, and to personnel operating the tethersonde. A ground-to-air radio was also provided to the FTD for communication with the test aircraft.

Aircraft Positioning

Determination of the decay rate of wake vortices requires the measurement of vortices of various ages. Different-aged vortices are measured in the tower flyby technique by varying the distance (d) between the aircraft and the tower. The age of the vortex is also affected by the ambient wind speed, which governs the rate of advection of the wake vortex into the instruments mounted on the tower. Whenever the aircraft distance to the tower at aircraft abeam time is adjusted, the height of the aircraft above the ground (h) must also be adjusted in order to advect the vortices into the tower at an appropriate altitude above the ground.

When positioning the test aircraft in space abeam of the tower for a flyby, the FTD is confronted with several possible vortex trajectories, some of which are illustrated in Figure 27. Position A represents a test aircraft position high and close to the tower. In this position, on e or both of the vortices usually pass over the top of the tower. Similar trajectories can be obtained when the aircraft is flown at a higher altitude, but farther away from the tower. Positioning the aircraft as in Position B results in both vortices passing through the tower. However, one vortex is in ground effect. This pair of trajectories occurs most often during flight testing. Positioning the aircraft too far out or too low, as in Position C, can result in both vortices being in ground effect. The FTD attempts to position the aircraft to maximize vortex data recovery. The director attempts to prevent a vortex from passing over the top of the tower and at the same time tries to prevent a vortex from descending into ground effect. However, even ground effect data are useful for vortex characterizations.

The height above the ground at which the trailing vortex system becomes affected by ground effect can be calculated assuming an elliptical lift distribution over the wing by

$$\Gamma_o = \frac{4}{\pi}\frac{nW}{\rho V b} \qquad (2)$$

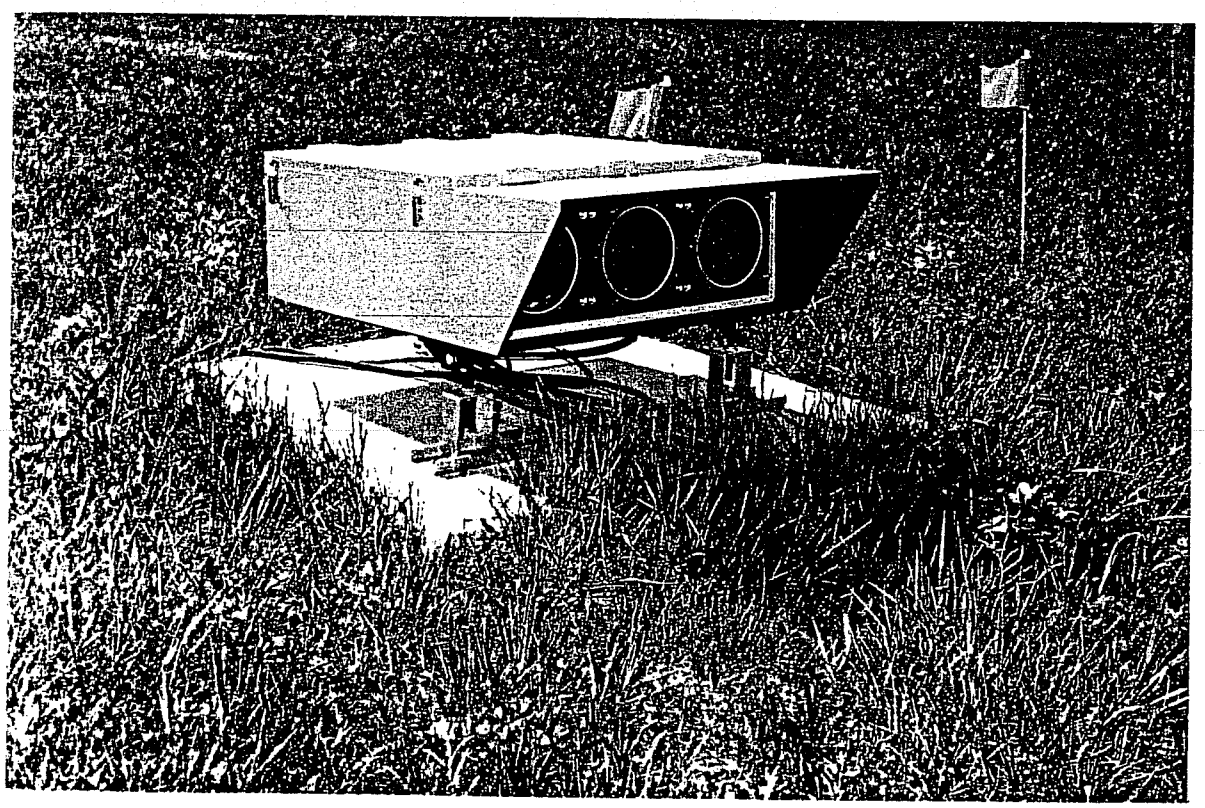

Figure 26. Precision Approach Path Indicator (PAPI) system for pilot glide-slope guidance, which was installed at the NOAA wake vortex test facility.

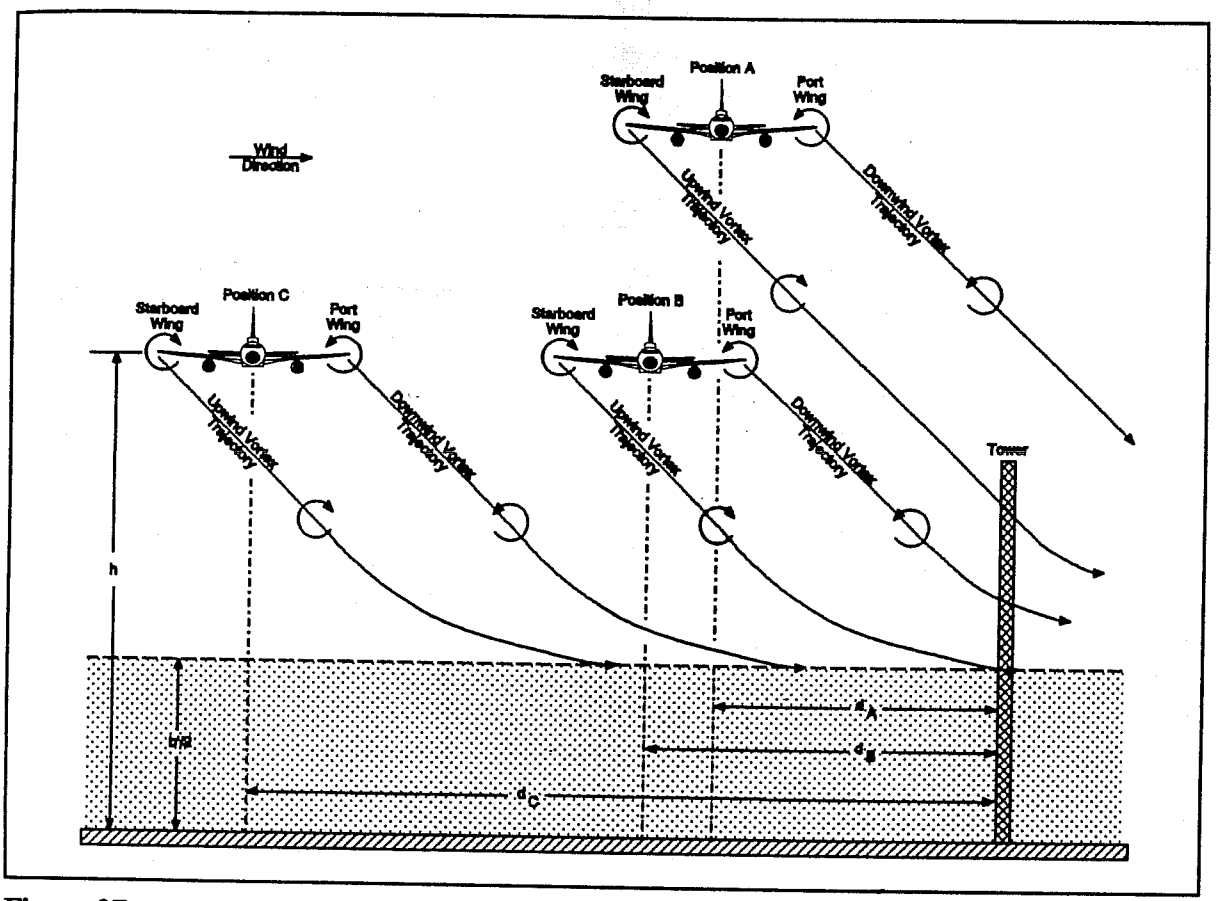

Figure 27. Potential vortex trajectories as a function of aircraft distance from the tower (d) and height AGL (h). The shaded area represents the height above ground in which ground effect is predominant (b′/2, where b′ is separation of the vortex pair).

where Γ_o is the mid-span circulation, n is the normal load factor, W is the aircraft gross weight, ρ is air density, V is the aircraft's true air speed (TAS), and b is the aircraft wingspan. If this assumption is used, a first approximation of ground effect in relation to vortex movement through space initially begins at an altitude (h_{vge}) of

$$h_{vge} = \frac{\pi}{8} b \approx \frac{1}{2} b' \tag{3}$$

where b′ is separation of the vortex pair. Two values of b′ can be used to calculate h_{vge}: one for a clean wing and one for a wing with extended flaps. The latter assumes that the flap vortex is the predominant vortex. The term $h_{vge\ clean}$ is used to denote the ground effect altitude of a vortex generated by a clean wing, while the term $h_{vge\ dirty}$ is used to denote the ground effect altitude of a vortex generated by a wing with extended flaps. Table 2 contains the initial clean and dirty h_{vge} calculated from Equation (3).

The FTD must also take into account vortex descent rates to estimate the proper aircraft altitude for the best vortex advection into the tower. An initial vortex descent velocity ($\dot{z}_v$) can be calculated by again assuming an elliptical lift distribution such that

$$\dot{z}_v = \frac{\Gamma}{2\pi r} \tag{4}$$

where $r = b' = \frac{\pi}{4}b$. As with h_{vge}, two different $\dot{z}_v$ values can be calculated, based on the position of the wing flaps. The term $\dot{z}_{v\ clean}$ is used to denote the descent rate of a vortex generated by a clean wing, while the term $\dot{z}_{v\ dirty}$ is used to denote the descent rate of a vortex generated by a wing with extended flaps. The calculated descent velocity values are summarized in Table 2.

The data in Table 2 served as a "first cut" approximation of expected vortex sink speeds. The FTD adjusted these speeds as the flight tests progressed inasmuch as the vortex sink speeds were dependent on aircraft configuration, atmospheric convection, and aircraft/vortex proximity to the ground when abeam of the tower. Aircraft positions were subsequently adjusted accordingly.

Although it is preferable to conduct the flight tests during relatively low ambient wind speed and atmospheric turbulence conditions, such is not always possible, particularly when test aircraft availability is limited. Light and variable winds and low-altitude wind shears are not desired. When any of these atmospheric conditions are present, it is difficult, if not impossible, to obtain vortex lateral transport through the instrumented tower. The exception to this rule is an occasional downwind vortex that rolls in ground effect into the tower.

The quasi-unpredictable nature of the trailing vortex system adds to the difficulty of exactly positioning the aircraft. This can be a perplexing problem for the FTD, particularly when the vortex system undergoes a Crow-instability type of oscillation (Crow, 1970), as shown schematically in Figure 28. The oscillation may cause a vortex to pass over the top of the

Table 2. Aircraft wingspans (b), estimated separations of vortex pairs (b′), estimated height of vortex ground effect (h_{vge}), and estimated initial vortex descent velocities ($\dot{z}_v$) for a clean (flaps retracted) and a dirty (flaps extended) wing.

Aircraft	b (ft)	b'_{clean} (ft)	b'_{dirty} (ft)	$h_{vge\ clean}$ (ft AGL)	$h_{vge\ dirty}$ (ft AGL)	$\dot{z}_{v\ clean}$ (fps)	$\dot{z}_{v\ dirty}$ (fps)
B727-100/-222	108.0	85	65	42	33	8.2	10.7
B757-200	124.8	98	74	49	37	7.4	9.9
B767-200	156.0	123	82	61	41	6.2	9.3

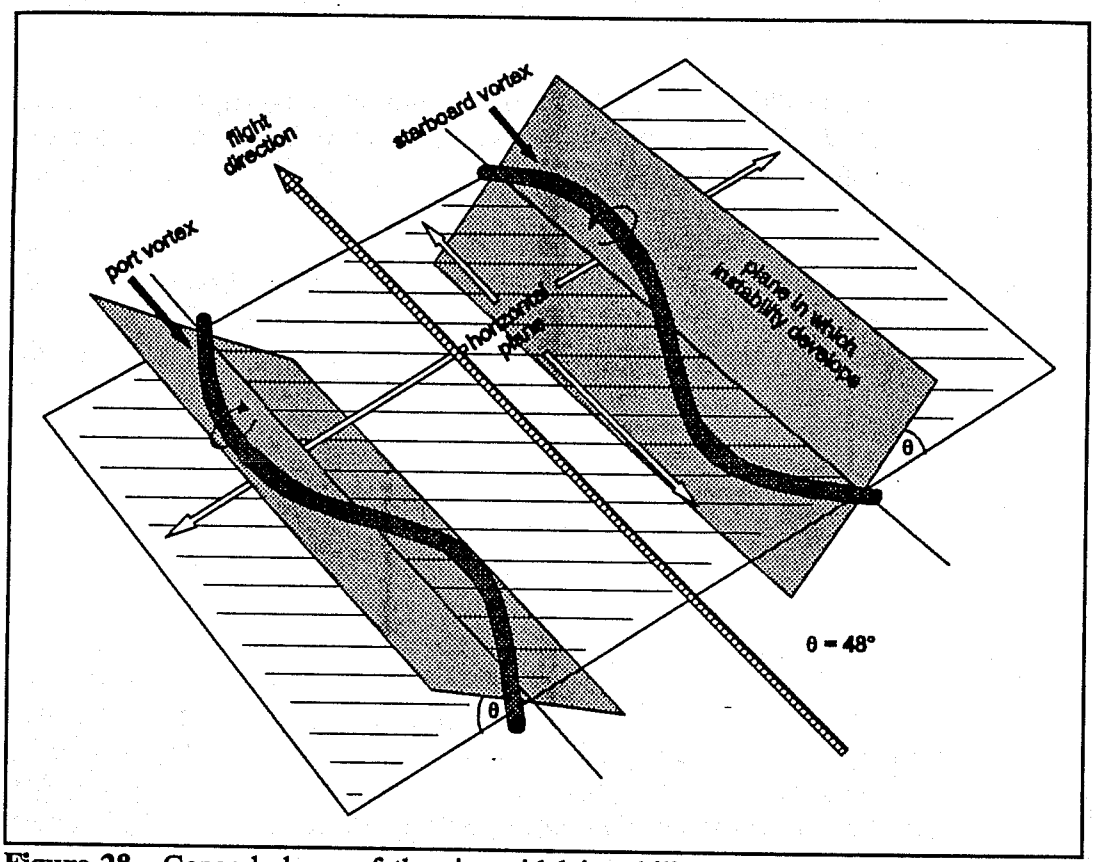

Figure 28. General shape of the sinusoidal instability of vortices in the symmetric mode (Crow, 1970). The vortices are viewed from above, and the generating airplane lies beyond the upper left-hand corner of the figure.

tower, even though the vortex was assumed to be on an intercept trajectory with the tower. In addition, the trailing vortices may dissipate by "bursting" even in the absence of linking before ever arriving at the vortex test tower.

Last, but not least, the test pilot can inadvertently fly the aircraft either too high or too distant from the tower, or both, particularly when crosswinds are relatively high or in the presence of strong atmospheric turbulence. The pilot may also perform some last second-course corrections, causing the plane to "waggle." Every reasonable effort was made on preplanning each flyby to ensure a safe flight and a high probability of one or preferably both vortices passing through the instrumented tower.

DATA PROCESSING

Initial data processing was performed in the field to support quality assurance procedures, as discussed above. Most data processing was performed in the laboratory offices after the conclusion of the flight tests.

Standard Meteorological Data

Postprocessing of the standard meteorological data consisted of averaging the 1-s data for 3 min prior to the aircraft abeam time. This was done to ensure that the influence of the aircraft vortex was not included in the averaged data. A summary of tower meteorology was produced for each tower flyby.

In addition to wind speed, wind direction, and air temperature, Richardson Number (Ri) and vertical air temperature gradient were calculated for the 3-min average. Ri is a ratio of the buoyant forces to Reynold's stresses of the atmosphere and is defined mathematically as follows:

$$Ri = \frac{g\left(\frac{d\theta}{dz}\right)}{\bar{\theta}\left(\frac{du}{dz}\right)^2} \tag{5}$$

where θ is potential temperature, z is height, u is wind speed, and g is the acceleration due to gravity. Air temperature (T) was substituted for θ, which is an appropriate replacement at the low altitudes AGL. Ri was calculated using the 6.25- and 200-ft levels of air temperature and wind speed. A negative Ri indicates an unstable atmosphere whereas a positive Ri indicates a stable atmosphere. A value near zero indicates near-neutral conditions. It can be seen that the Ri value may become unstable when the wind speed gradient approaches 0. Large negative or positive values indicate a relatively large contribution of buoyant forces to the turbulence parameter. Values near 0 indicate a relatively large contribution of Reynold's stresses to the turbulence parameter.

The vertical air temperature gradient ($\Delta T/\Delta z$) is defined as the change in air temperature across a vertical 100-m span. The temperature difference between 6.25 and 200 ft AGL was linearized and extrapolated to 100 m in order to calculate $\Delta T/\Delta z$. A positive number indicates an inversion, whereas a negative number indicates a lapse temperature profile. A stability class was assigned to $\Delta T/\Delta z$ according to U.S. Nuclear Regulatory Commission regulations (U.S. NRC, 1980) as follows:

stable:	$\Delta T/\Delta z > -0.5$ °C/100 m
neutral:	-0.5 °C/100 m $\geq \Delta T/\Delta z \geq -1.5$ °C/100 m
unstable:	$\Delta T/\Delta z < -1.5$ °C/100 m.

Under normal meteorological practice, Ri, $\Delta T/\Delta z$, and stability class are usually calculated from at least 15-min averages of wind speed and air temperature. The reported data, which were derived from 3-min averages, are expected to exhibit a wider range and larger standard deviation than data obtained from a longer averaging period.

Tethersonde Data

Postprocessing of the tethersonde data consisted of calculating the height of the sonde above ground level based on temperature-pressure relationships, and calculating dew point temperature and relative humidity. These calculated values were summarized together with the measured values discussed previously. An attempt to establish a one-to-one correspondence of each tethersonde sounding to each flyby was not undertaken. A given tethersonde sounding must currently be used to describe the atmosphere for several flyby runs at altitudes above 200 ft.

Hot Film Anemometer Data

The two types of hot film anemometer data, i.e., tower- and ground-based, were processed separately. The data was processed in a different manner because of the distinct and separate design purposes of the two types of data. Each process is described below.

Tower-mounted Anemometers

The tower-mounted hot film anemometer data were processed according to protocols used previously (Clawson, 1988) and revised for this particular study. Initially, the recorded current value from each anemometer was converted to velocity using Equation (1). The environmental temperature (T_e) required for the conversion was a linearly interpolated value from the two temperature sensors immediately above and below the hot film anemometer of interest. Data quality control was of primary importance in this phase of data processing. The first step of the quality control process consisted of an automated screening of the 1-s-average velocity data used for initial quality control checks in the field. The screening process located the characteristic velocity peaks in the recorded 200-ft-tower data both in time and vertical space. The time and sensor location of the velocity peaks were all manually verified through visual checks of the printed graphs.

Hot film data from a typical flyby used in the automated screening process are shown in Figure 29. The graph contains the first 5-185 s of tower vortex data from run (flyby) 10 of the B757-200. Averaged data from the first second of the 300-s-long data block were used as an initial estimate of ambient wind speed. The ambient wind velocity value thus obtained from each sensor was subtracted from the remaining data of the identical sensor to exclude the ambient wind effect from the vortex tangential velocity profile. The figure also illustrates the point at which the electronic signal was recorded in the data, indicating the precise abeam time. The elapsed time from that moment until the vortex velocity peak was recorded is the age of the vortex.

After determining the time of each vortex peak within a data file, a 5-s time slice surrounding each peak was extracted for further analysis. Figure 30 illustrates hot film anemometer data obtained from both the downwind and upwind vortices of flyby (run) 10 of the B757-200. The graphs are a pseudo-three-dimensional representation of the vortex velocity flow field in time and space. The time resolution is centiseconds (cs), which is the A/D scan rate.

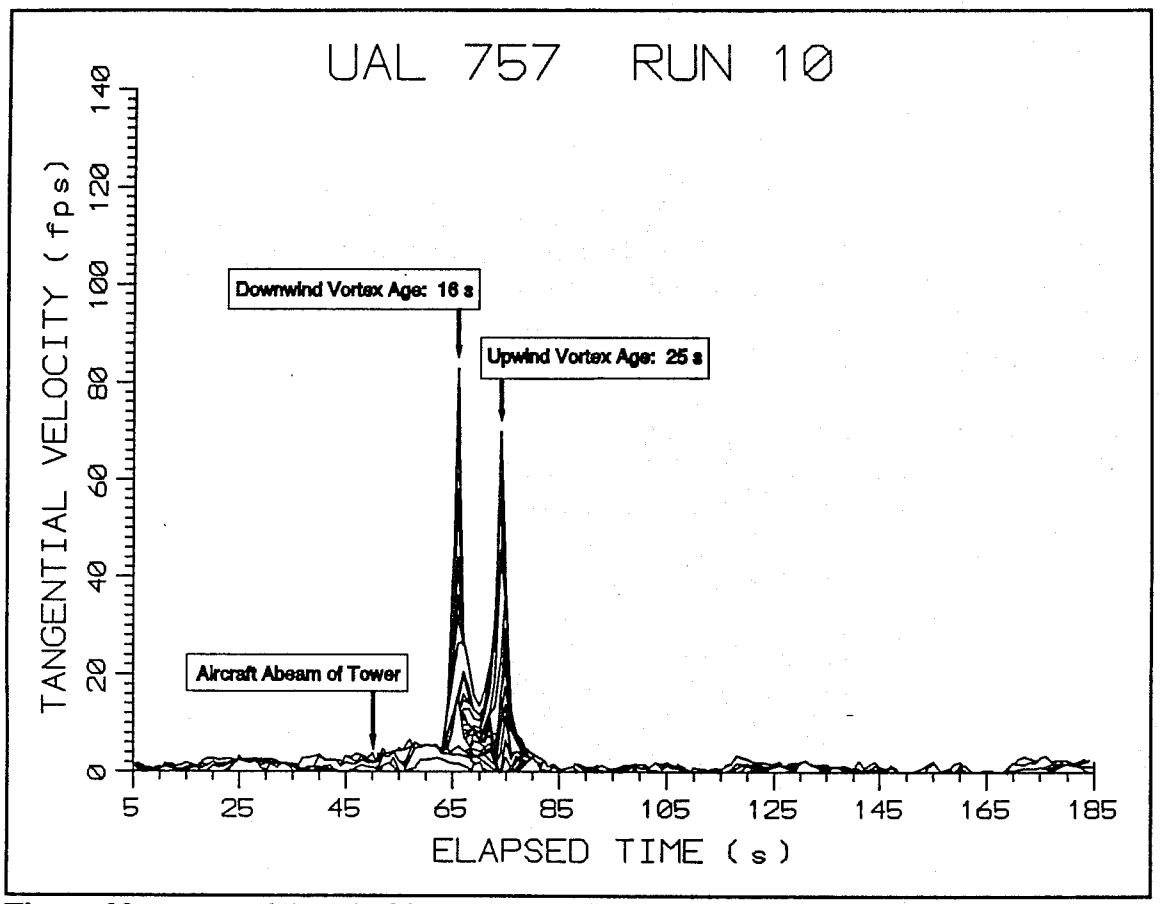

Figure 29. Tangential velocities averaged for 1 s from tower-mounted hot film anemometers versus elapsed time from near the beginning of a scan period. Each trace represents a single anemometer. Abeam time and vortex ages are also denoted.

The space resolution is 2 ft, which is the vertical separation between hot film anemometers. Each trace represents velocity data from a different anemometer. The graphs include data from the sensor that recorded the maximum tangential velocity bracketed by data from five neighboring sensors mounted immediately above and below that sensor. The data were not adjusted at that time for ambient wind velocity.

These graphs showed distinctly the vortex peak and associated flow field. For the downwind vortex from run 10, the height at which the maximum velocity was recorded was 168 ft, and for the upwind vortex, it was 132 ft. The second step of the quality control process involved visual checks of these graphs; this ensured that a false vortex peak was not determined as a result of noise in the data. The graphs also served other quality control purposes. For example, the velocity output from the anemometer located at 132 ft AGL fell to 0 after passage of the upwind vortex. The written field log indicated that the electronics package was ripped from the tower as the vortex passed through the tower. The package was recovered on the ground after this flyby.

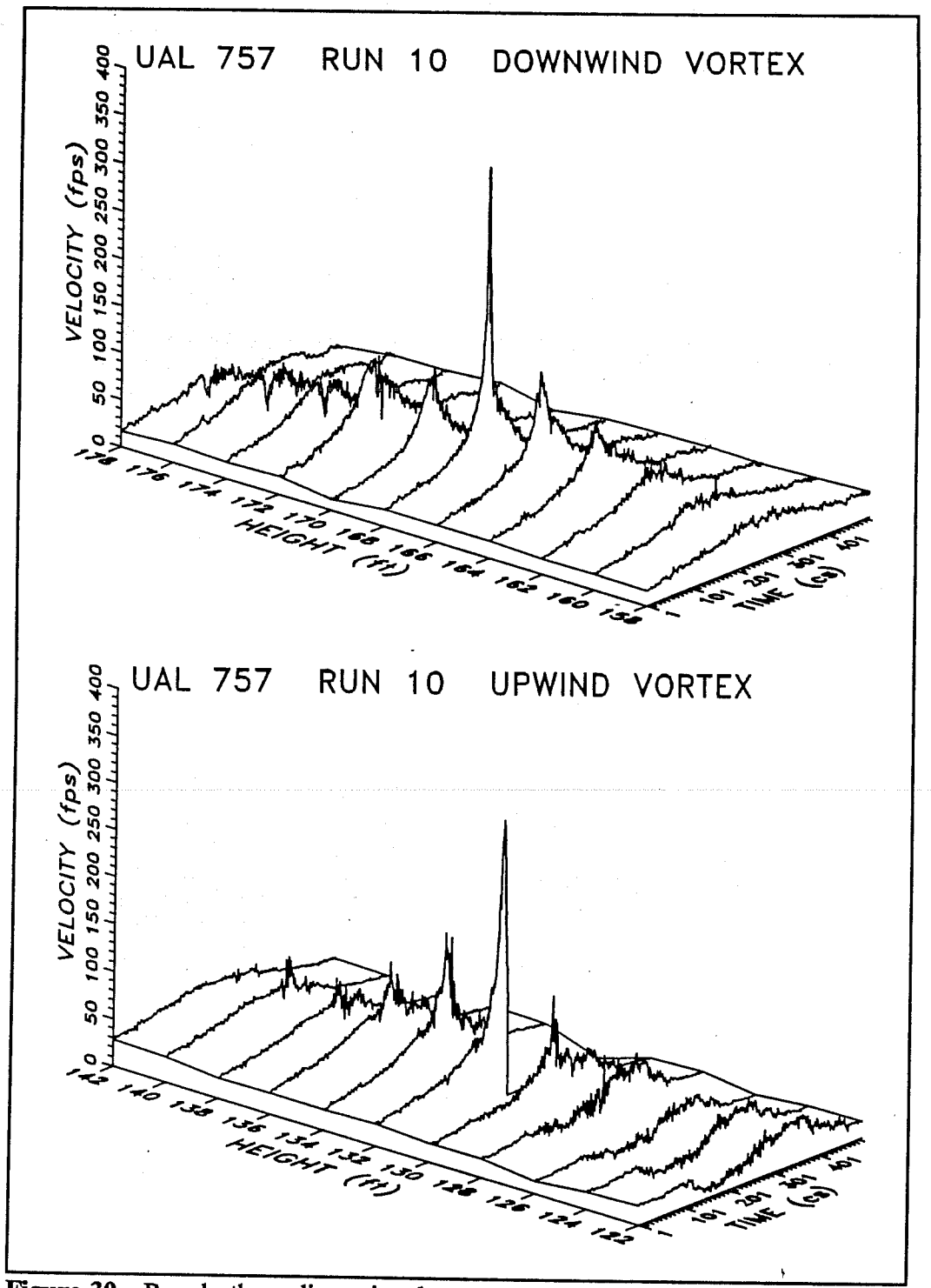

Figure 30. Pseudo-three-dimensional representation in time and space of tangential velocities for the downwind (top) and upwind (bottom) vortices from flyby 10 of the B757-200.

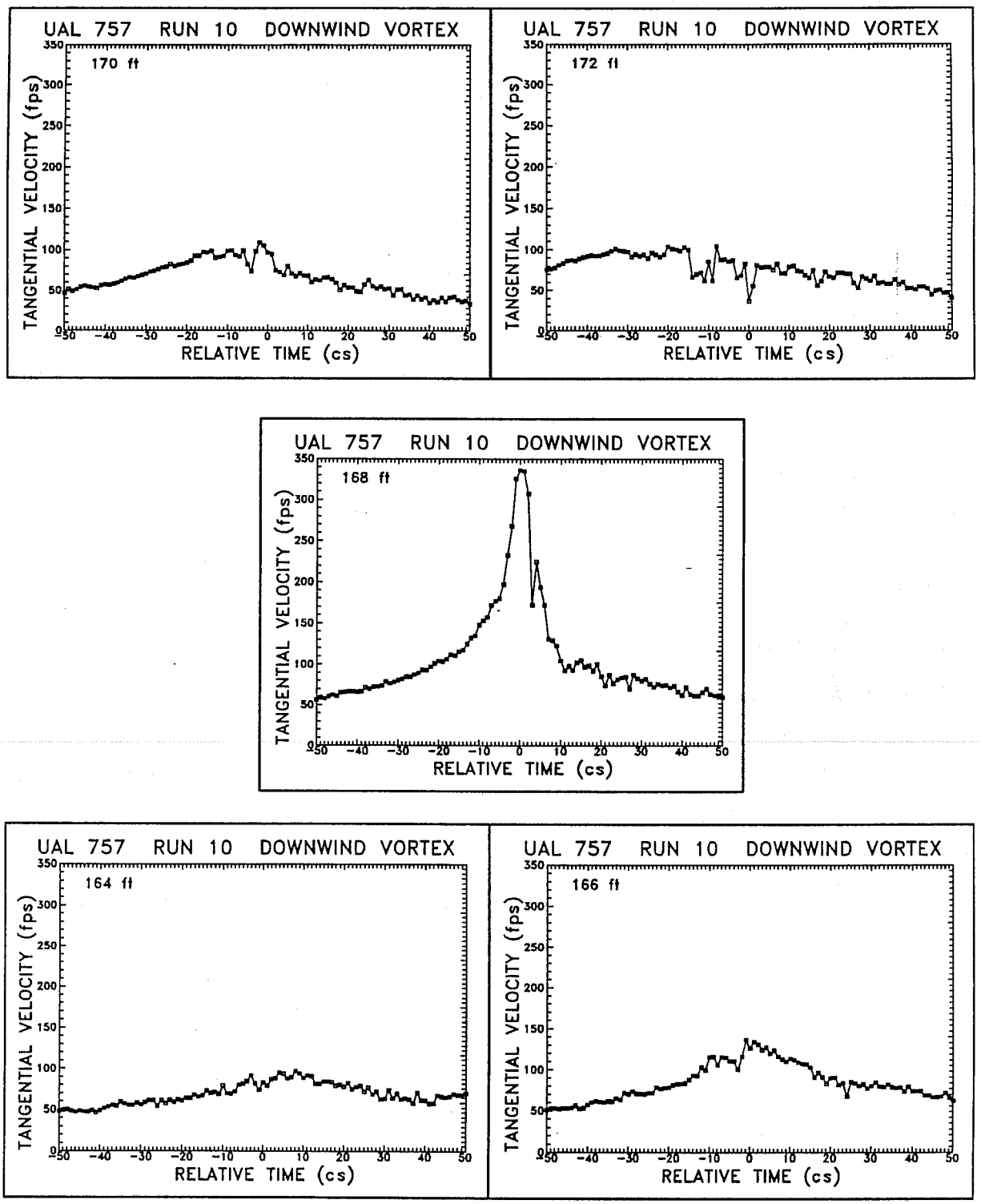

Figure 31. Graphs of individual hot film sensor velocity time histories for the downwind vortex of the B757-200 from flyby 10. The center graph contains $V_{\theta max}$ for this vortex.

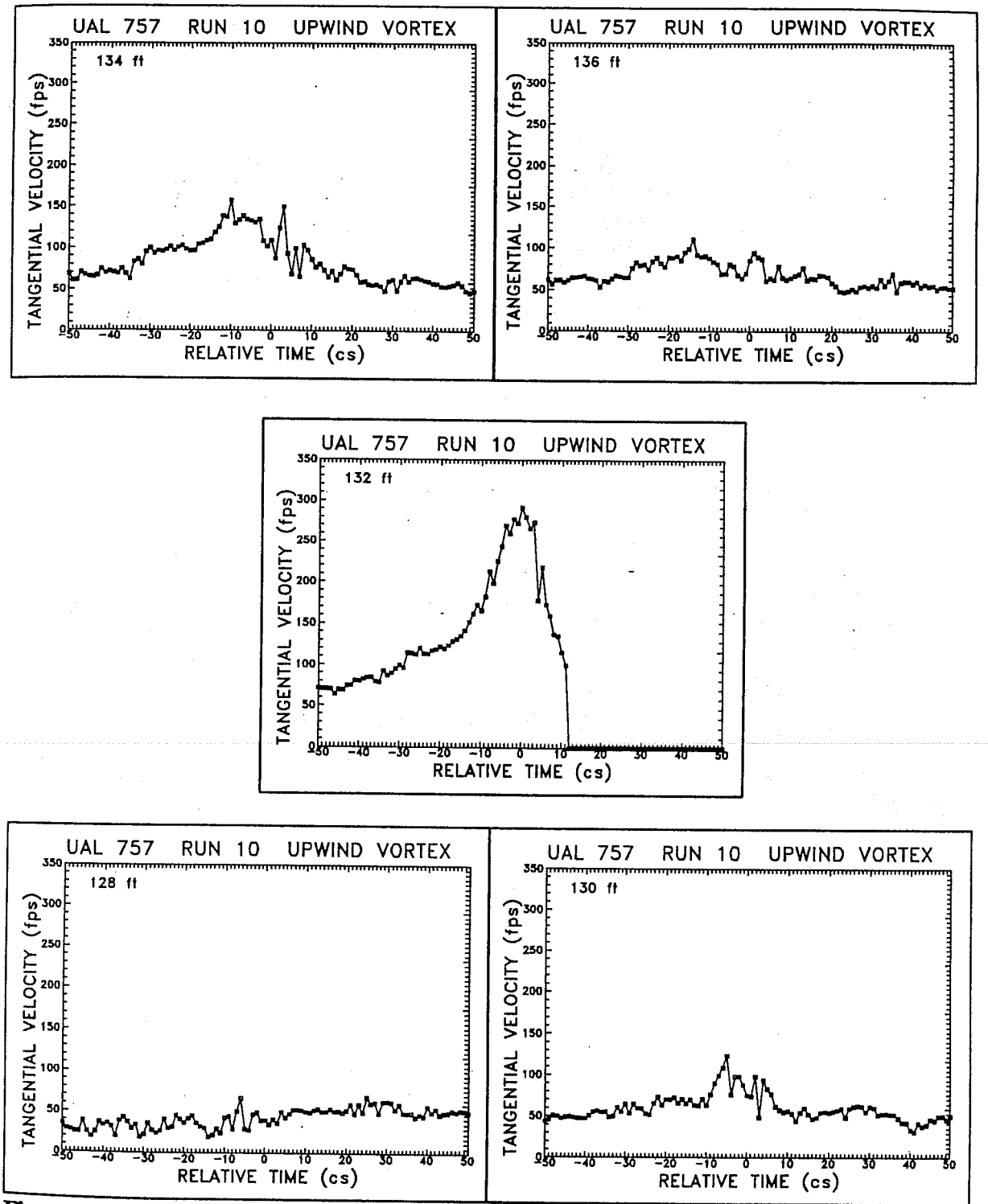

Figure 32. Graphs of individual hot film sensor velocity time histories for the upwind vortex of the B757-200 from flyby 10. The center graph contains $V_{\theta max}$ for this vortex.

The third step of the quality control process involved careful scrutiny of each vortex peak. Each downwind and upwind peak was plotted individually in a 1-s time window centered on each peak, as illustrated in Figures 31 and 32, respectively. The graphs were again scrutinized for noise and for false vortex peaks.

When it was certain that all vortex peaks had been properly identified, the ambient wind velocity was calculated for each sensor for each flyby. The ambient wind for each anemometer was calculated as the average response of the anemometer up to aircraft abeam time. A "snapshot" of the velocity from each hot film anemometer (V_θ) was made at the precise instant in time at which the maximum velocity of the entire vortex ($V_{\theta max}$) was measured. This yielded a single unique velocity value from each anemometer. These values were adjusted to account for the additive or subtractive effect of ambient wind on the measured velocities.

The effect of the ambient wind on measured vortex tangential velocities is illustrated schematically in Figure 33. As can be seen, downwind vortex velocities measured at and below the vortex core are affected by the additive component of the ambient wind. The downwind vortex is always the vortex closest to the tower, regardless of the generating wing, i.e., starboard or port. Downwind vortex velocities measured above the vortex core are affected by the subtractive component of the ambient wind. The opposite is true for the upwind vortex. Hence, the addition or subtraction of the ambient wind velocity from the measured vortex velocities depended on the known direction of rotation about the vortex core and the height at which the maximum vortex tangential velocity was measured. In order to account for the ambient wind speed effect on vortex tangential velocities, the ambient wind component was added to the hot film-measured tangential velocities in zones 1 and 4. In zones 2 and 3, the ambient wind component was subtracted from the measured tangential velocities.

Individual V_θ values were also adjusted for the direction of flow around the vortex core. This adjustment was performed because the hot film anemometers used in the study do not distinguish the flow direction. Referring again to Figure 33, the signs of all V_θ obtained in zones 1_N, 4_N, 2_S, and 3_S were positive, conforming to established convention (Donaldson et al., 1973). Conversely, the sign of all V_θ obtained in zones 2_N, 3_N, 1_S, and 4_S were made to be negative.

Ground-based Anemometers

The ground-based hot film anemometer data were subjected to different data processing and quality control procedures as compared with data from the tall tower. The ground-based array was not designed to obtain vortex core data, but rather to measure vortex transport as the wake vortex envelope descended into ground effect and was advected by the ambient wind. Hence, the data required unique processing techniques. These are documented in Clawson (1988).

First, the current value recorded from each hot film anemometer was converted to velocity using Equation (1). The environmental temperature (T_e) required by Equation (1) was linearly interpolated from the temperatures measured from the 25- and 50-ft sensor levels. The data

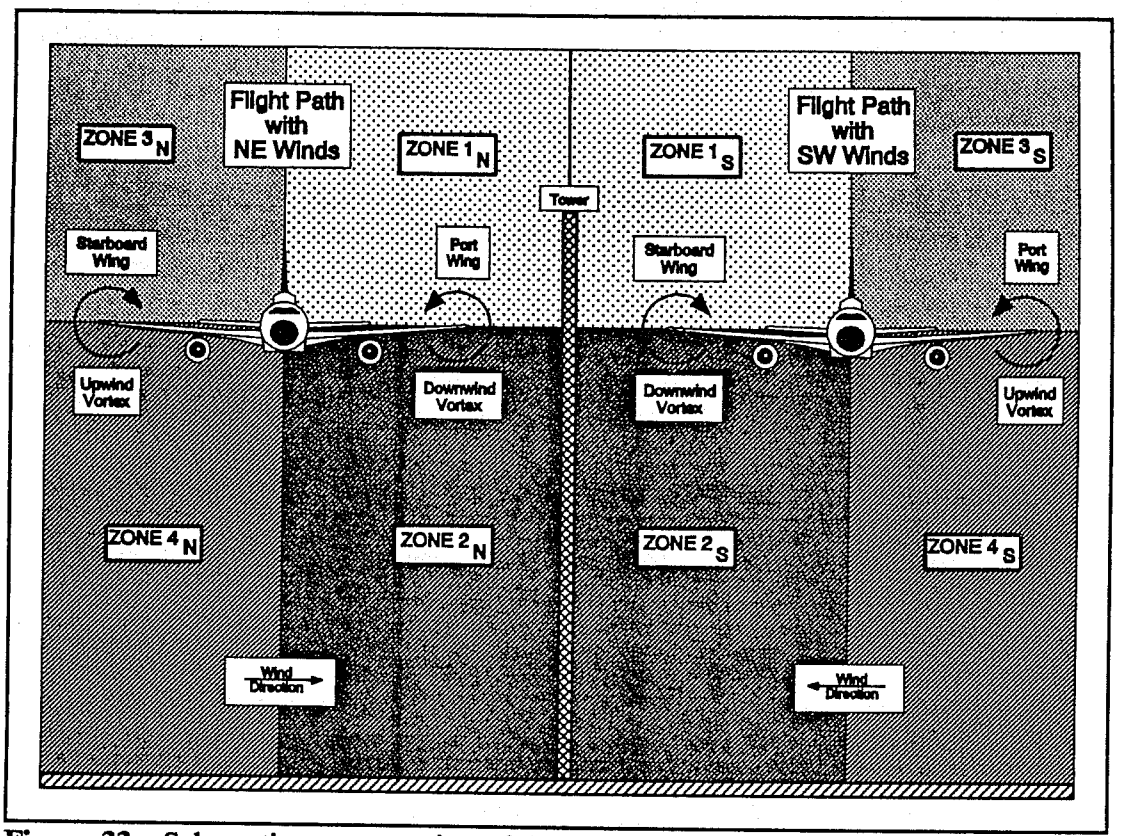

Figure 33. Schematic representation of the various zones of ambient wind influence on measured vortex tangential velocities. In zones 2 and 3, the ambient wind is additive. In zones 1 and 4, the ambient wind is subtractive.

were then averaged for 1-s time periods. The first second of the entire scan period was used to initially represent the ambient wind speed. This wind speed value was subtracted from the data to yield a wind speed-corrected velocity value. These data were then plotted in a three-dimensional manner similar to that shown in Figure 30. These graphs provided the basis for the data analysis phase.

DATA ANALYSIS

Analysis of the hot film anemometer data proceeded along two distinct avenues. Different analysis procedures were performed on the tower-mounted and ground-based hot film anemometer data.

Tower-mounted Anemometer Data

Once the data processing and quality control procedures were complete, the data were subjected to several comparisons and analyses. Many analysis procedures have been used previously and are described in numerous reports (Garodz et al., 1974a,b; Garodz, 1976). The

comparisons usually involved the maximum tangential velocity from each vortex ($V_{\theta max}$) and the age of the vortex at which $V_{\theta max}$ was determined. The use of symbols in the graphs follows those of previous reports. This was done to permit rapid comparison of previous data with new data presented in this report.

The first analysis performed on the data was an intercomparison of the FAA B727-100 with the UAL B727-222, and these two aircraft with previous B727-100 data obtained near sea level at the FAA's Technical Center (previously known as the National Aviation Facilities Experimental Center or NAFEC) and reported by Garodz et al (1974a). The intercomparison was performed to determine vortex characteristic differences, if any, between the two B727 aircraft models, and to verify the consistency of the new data with old data. Data collection methods varied only slightly between this and the previous study. Newer acquisition equipment and a new hot film anemometer controller were used in this study. Garodz et al. (1974a) characterized the vortices of the FAA B727-100 using a vertical hot film separation of 1 ft at an altitude near sea level. A 2-ft spacing was used for the current study, which was conducted at an altitude of near 4900 ft MSL. In addition, vortices of two models of the B727 were measured during the current study. The B727-100 and -222 differ slightly in fuselage length and MTOGW.

The intercomparison consisted of contrasting $V_{\theta max}$/vortex age relationship of the new data to that of the old data. This was accomplished by observing the envelope of new data plotted on top of old data and by using a vortex decay function previously developed for the B727-100. Garodz et al. (1974a) defined a $V_{\theta max}$-age envelope with an exponential equation that encompassed all of the previous B727-100 data. The equation related $V_{\theta max}$ to vortex age. The equation is expressed as

$$V_{\theta max} = Ae^{-Bt} \tag{6}$$

where A and B are coefficients indicating initial $V_{\theta max}$ at time zero and the exponential decay rate, respectively.

Similar comparisons were made by plotting $V_{\theta max}$ as a function of vortex age for each test aircraft. The data envelopes were observed for unique aircraft features. The exponential decay equation (6) was fitted to the outer envelope of the entire data set as well as to the outer envelope of each aircraft data set. The equation coefficients were used to compare the initial $V_{\theta max}$ of the test aircraft.

Statistical significance tests and least-squares regression tests were applied to $V_{\theta max}$ and to vortex age relationships with various atmospheric turbulence indicators. These indicators included Ri, $\Delta T/\Delta z$, and ambient wind speed measured at the top of the 200-ft tower.

Paired t-tests were performed on the $V_{\theta max}$ and age data obtained in the landing configuration during both level flight and during a 3° G/S approach. Two types of data pairs

were constructed. First, since most 3° G/S approaches were flown immediately following the level flight approach, the combination of both flybys constituted a data pair. Thirty-six data pairs were subjected to the t-test. However, some of the paired $V_{\theta max}$ data were not in similar age brackets. Age differences as large as 35 and 79 s were observed for the paired downwind and upwind vortices, respectively. Therefore, a second pairing of the data was performed by averaging $V_{\theta max}$ in 5-s age brackets. Two values for each bracket were obtained in this manner: one for level flight and one for 3° G/S. Seven data pairs were prepared from 125 separate data points and subjected to the statistical test.

The Hoffman-Joubert vortex velocity profile model was applied to each vortex (Hoffman and Joubert, 1963). This model was used with success on full-scale flight test data as reported by Eisenhuth et al. (1971), Nelson (1974), Garodz (1976), and Garodz and Clawson (1991), among others. It is applied to the radial distribution of the vortex velocity flow field outside of the vortex core (r_c). The theory stipulates a logarithmic distribution of circulation (Γ) as a function of radial distance, vortex core radius, and circulation at the vortex core ($\Gamma_{(r_c)}$) such that

$$\Gamma = \Gamma_{(r_c)} \left[1 + \ln \left(\frac{r}{r_c} \right) \right]. \tag{7}$$

The theory also specifies a logarithmic distribution of vortex tangential velocity (V_θ) as a function of radial distance, vortex core radius, and tangential velocity at the vortex core ($V_{\theta max}$) as follows:

$$V_\theta = V_{\theta max} \left[\frac{1 + \ln \left(\frac{r}{r_c} \right)}{\left(\frac{r}{r_c} \right)} \right]. \tag{8}$$

The modeling effort was centered around Equation (8), since the hot film anemometers measure vortex tangential velocities. Equation (8) is valid only for velocity distributions outside of the vortex core. For velocity distributions inside of the vortex core, where solid-body rotation is assumed, the function is

$$V_\theta = V_{\theta max} \frac{r}{r_c}. \tag{9}$$

Equations (8) and (9) require a specified value of r_c. However, this parameter was not measured directly by the hot film anemometers. Two schemes are possible for determining r_c. The first approach was used by Start and Dickson (1970) and Garodz and Clawson (1991). It consists of using time-dependent velocities of the hot film anemometer that recorded the $V_{\theta max}$

of a given vortex. The data set so obtained is assumed to contain the vortex core, which is characterized by a velocity peak which contains an inverted "W". The time delay measured across the inverted "W" is combined with the vortex advection rate to yield the diameter of the vortex core. The data set did not readily lend itself to this analysis because only a few inverted W's were observed in the data. Thus, the size of the vortex core could not be determined in this manner for every vortex.

The second approach for calculating r_c, and the approach used in this study, consisted of using Equation (8) with the so-called "snap-shot" vortex velocity profile data in an iterative fashion to solve for r_c. This was accomplished by substituting values for r_c into Equation (8) and solving for V_θ at each corresponding level of measured V_θ. The iteration selected r_c when the difference between the sum of the actual and calculated values along the profile was at a minimum. Only profile data from the first 30 ft of radial distance from the center of the vortex were used in the iteration. This procedure maximized the iteration process by concentrating on vortex velocities near the vortex core. In addition, only vortex profile data below the vortex core were used in the iterative process for downwind vortices, and above the vortex core for upwind vortices. This avoided the area of the vortex velocity profile where the ambient wind speed was added to the vortex velocity, which occasionally resulted in partial velocity profiles that were not logarithmically shaped.

Equations (8) and (9) were further employed in calculating circulation for each vortex. Vortex circulation is generally considered to be related to the rolling moment imposed on an aircraft that encounters the vortex. However, the utility of this parameter is still under debate. The circulation calculation technique provided only initial estimates for discussion purposes internal to this report. The calculated values were not intended for comparison purposes with data from other experiments. In addition, the circulation values calculated in this manner assume that the Hoffman-Joubert model accurately describes the vortex profile, which may not always be valid. Hence, Γ' calculated in this manner should only be used for comparison and discussion purposes with Γ' values obtained in a similar manner. More robust techniques could be employed in a future examination of the data for a more accurate determination of circulation for comparison with data from other studies.

To begin with, the circulation at a given distance r from the center of the vortex is

$$\Gamma_{(r)} = 2\pi r V_{\theta(r)}. \tag{10}$$

It is obvious from this equation that small errors in $V_{\theta(r)}$ result in large $\Gamma_{(r)}$ errors. However, average circulation (Γ') can be used to overcome this limitation. Γ' at r is

$$\Gamma'_{(r)} = \frac{1}{r} \int_0^r \Gamma_{(r)} dr. \tag{11}$$

An appropriate substitution of Equations (8), (9), and (10) into Equation (11) yields

$$\Gamma'_{(r)} = \frac{1}{r} \left[\int_0^{r_c} 2\pi r V_{\theta max} \left(\frac{r}{r_c} \right) dr + \int_{r_c}^{r} 2\pi r V_{\theta max} \left[\frac{1+\ln\left(\frac{r}{r_c}\right)}{\left(\frac{r}{r_c}\right)} \right] dr \right]. \tag{12}$$

Thus, the Hoffman-Joubert model and the iterated vortex core radius can be used to calculate Γ'. Three values of Γ' were calculated for each vortex at radii of 15, 30, and 45 ft. These distances are related to the vortex-induced rolling moment of aircraft with wingspans of 30, 60, and 90 ft. The three radii values were also chosen to limit the calculation of Γ' to within 50 to 60% of b′. Interaction of the vortices within the wake envelope of the B727-100/-222 (wingspan of 108 ft) probably becomes significant at distances greater than 45 ft. Comparisons of average vortex strength (Γ') as a function of vortex age and aircraft type were subsequently performed.

Ground-based Anemometer Data

Most of the analysis effort was focused on the tower-mounted anemometers, which supported the main purpose of the study. Additional effort supported the analysis of the ground-based anemometer data. Three-dimensional graphs obtained from the data processing phase of the tower anemometer data formed the basis for analysis of the ground-based hot film anemometer data. Visual inspections verified the difficulty in distinguishing between ambient wind-induced gusts and vortex-induced gusts, as indicated by velocity peaks in the hot film data. A much larger effort would have been required to investigate this problem and obtain a suitable solution. Therefore, that investigation was closed with only a cursory examination of the ground-based anemometer data.

This page intentionally left blank.

RESULTS AND DISCUSSION

A total of 241 data acquisition flybys were made during the test program. Figures 34, 35, and 36 picture the UAL B727-222, UAL B757-200, and UAL B767-200, respectively, on vortex characterization flybys at the NOAA test site. Figure 34 also shows the wing tip smoke generators in operation on the UAL B727-222. Table 3 summarizes the flybys as a function of aircraft model and configuration. The FAA B727-100 made 34 flybys during the June test period and an additional 18 during the September test period; the UAL B727-222 made 60; the UAL B757-200 made 70; and the UAL B767-200 made 59. Approximately 59% of all flybys were made in the landing configuration, and approximately 28% were in the takeoff configuration.

Of the 241 flybys, approximately 55 were for the benefit of other agencies that were gathering data with their own unique data acquisition systems. The majority of the 55 flights were flown with the B727-222. For those flights, the altitude and/or lateral offset of the aircraft from the tower were such that they usually precluded the advection of the wake vortex system into the tower. In all but four of the flybys, the tower data acquisition system was operated in tandem with the other acquisition systems. This provided an opportunity, under the appropriate atmospheric conditions, for the unexpected advection of one or both vortices into the tower instrumentation. These events were recorded by the data acquisition system and subsequently used in the data analysis. Twenty or so flybys were flown in addition to the 241 recorded under the flyby accounting scheme. In these cases, the tower data acquisition system was not activated, precluding the measurement of vortices of opportunity.

Data on either or both of the vortices (downwind or upwind) were recorded by the hot film anemometers on 60% of all numbered flybys. Of the numbered flybys that resulted in no data, 17% produced vortices that either dissipated upwind of the tower or passed over the top of the tower. The recovery percentage was good, considering the number of flybys flown for purposes other than measurement by hot film anemometers and the multitude of variables that could not be controlled during the flight tests and that affect vortex transport and decay.

METEOROLOGY

A wide range of meteorological conditions was observed during the study. Table 4 is a summary of meteorological conditions during the 15 test periods. The air temperature profile indicated that testing was conducted under stable, neutral, and unstable atmospheric conditions. Every test period that began between 0600 and 0800 MDT was conducted, at least initially, under stable atmospheric conditions. Nearly all test periods ended after the atmosphere had become unstable. Most of the flybys were flown under unstable atmospheric conditions. Wind direction was also related to the stability of the atmosphere, as expected from previous experience with the climatology of the test site. Wind direction shifts from the northeast to the

southwest were observed as the atmosphere changed from stable to unstable conditions as the day progressed. Average wind speeds at 200 ft AGL ranged from a low of 2.4 to a high of 14.4 kt. Average air temperatures at 200 ft AGL ranged from a low of 8.2 to a high of 20.6 °C.

Specific meteorological data obtained from the 200-ft tower are given in Appendix B. This appendix contains the average wind speed, wind direction, and air temperature from instruments at the seven instrumented levels of the tower for each flyby. Also included are Ri and air temperature gradient. Appendix C contains the plotted profiles of wind speed, wind direction, and air temperature for each flyby. Meteorological data obtained from the tethersonde are given in Appendix D. Data included in that appendix are wind speed, wind direction, air temperature, wet bulb temperature, dew point temperature, and relative humidity from each sounding. Appendix E contains the plotted profiles of wind speed, wind direction, and air temperature for each atmospheric sounding.

VISUAL AND AUDIO OBSERVATIONS

Several different visual and audio phenomena were observed during the course of the study. The visual phenomenon most often observed was Crow instability, as shown in the photographic series in Figure 37. The photos were taken at 4-s intervals. The vortex system was marked by the smoke from the wing tip smoke generators mounted on the B727-222. The aircraft was in the cruise configuration at 250 knots indicated air speed (KIAS) on approach for flyby number 60. The flyby was made at midday with a tail wind of about 4 kt and under conditions of increasing atmospheric instability. The photographs clearly show the formation, movement caused by Crow instability, and dissipation of the vortex pair. No dissipation from linking of the two vortices was observed. Instead, the starboard wing vortex dissipated by bursting soon after generation. The cause of its demise is not clearly known, although pilot lateral control inputs might have been a contributing factor. The knee-pad data indicated that rough atmospheric turbulence levels were encountered by the flight crew, which would have necessitated manipulation of the wing spoilers. The port wing vortex apparently dissipated through viscous action.

Another visual phenomenon that was not always recorded in the hot film anemometer data relates to vortex persistence. It was visually observed that the vortices often persisted for a much longer period of time than that recorded by the anemometers. For example, Figure 38 shows a time-series of photos of the trailing vortices marked by tower smoke of the B757-200 from flyby 3. These photos were taken 4 s apart near sunrise under conditions of extreme atmospheric stability. The ages of the downwind and upwind vortices as they passed through the tower were 18 and 28 s, respectively. The photos indicate an organized flow field of at least an age of 36 and 64 s, respectively. Had the photographer continued to pan the flow field, the observed ages would very likely have been even older. The FTD frequently directed the pilot to fly the test aircraft farther upwind from the tower in order to obtain hot film anemometer data on older vortices such as those described here. The attempts were often unsuccessful primarily because of Crow instability, which caused the vortices to either loop over the top of the tower

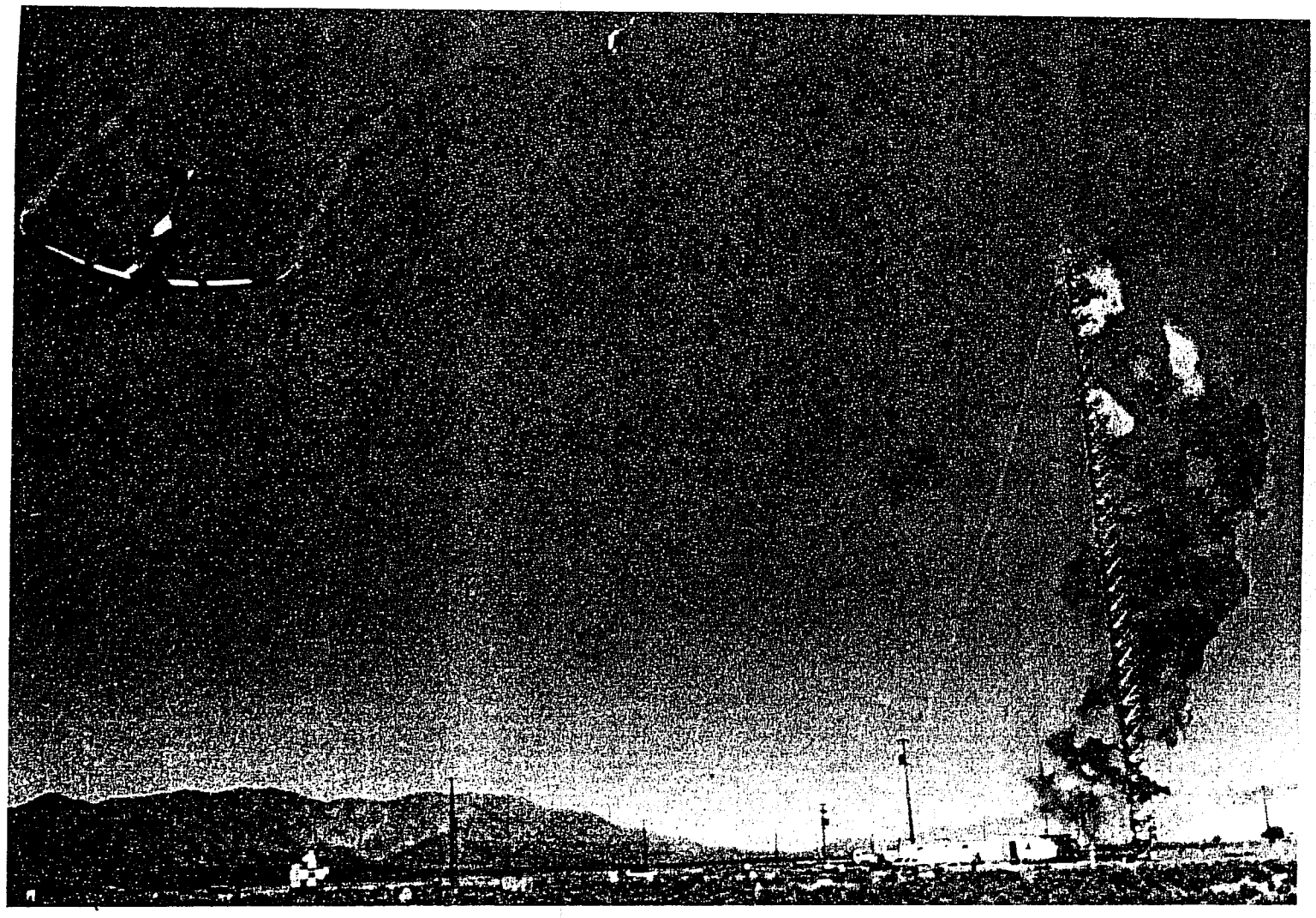

Figure 34. UAL B727-222 with wing tip-mounted smoke generators in operation abeam of the 200-ft tower on a data acquisition flyby.

Figure 35. UAL B757-200 abeam of the 200-ft tower on a data acquisition flyby.

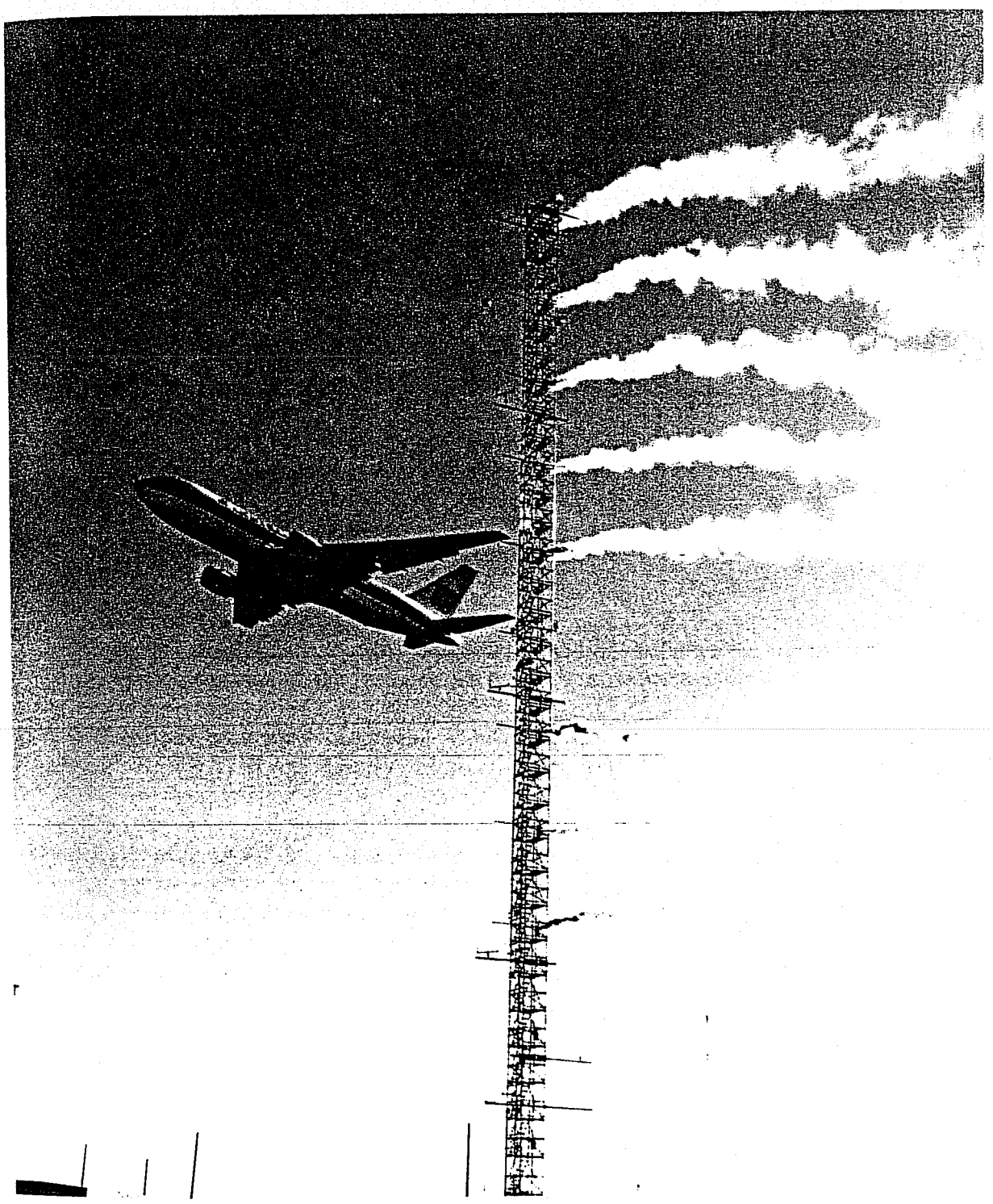

Figure 36. UAL B767-200 abeam of the 200-ft tower on a data acquisition flyby.

Table 3. Summary of the number of tower flybys flown by each test aircraft in each of the four configurations and the percentages of the totals.

Aircraft	Configuration				
	Landing	Takeoff	Holding	Clean	Total
B727-100	28 (54%)	11 (21%)	6 (12%)	7 (13%)	52
B727-222	48 (80%)	6 (10%)	4 (7%)	2 (3%)	60
B757-200	38 (54%)	23 (33%)	4 (6%)	5 (7%)	70
B767-200	28 (47%)	28 (47%)	2 (3%)	1 (3%)	59
Total	142 (59%)	68 (28%)	16 (7%)	15 (6%)	241

or to loop and remain upwind of the tower until they dissipated. Another contributing factor was an occasional low-level wind direction shear, as shown in Figure 39. This caused dissipation of the vortices upwind of the tower or advected them away from the tower.

There has been some discussion about the effect of the tower on a vortex as it passes through the tower. It was visually observed that the basic vortex structure remained intact most of the time after passing through the tower. The primary vortex decay mode for most of the vortices was viscous dissipation. However, the tower occasionally caused vortex dissipation to accelerate as it passed through the tower. Figure 40 shows a vortex partially disrupted by the tower, yet the vortex core appeared to remain intact. Significant bi-directional or uni-directional axial flow in the vortex core was also occasionally observed after the vortex had passed through the tower. Axial flow in the direction of the aircraft flight was considered to be caused by wing profile drag, rather than by the tower. The degree of the tower-induced effect appeared to increase with vortex age at tower passage. A direct relationship could not be defined because of the large variability in the data.

The audio phenomenon most often observed was a vortex "whistle." The loud whistling was most often heard from vortices generated by the UAL B757-200 as the vortices passed overhead. It occurred most often when the aircraft was in the landing configuration with the landing flaps at the 30°. The whistling was similar to the noise generated by an artillery shell passing overhead. The sound was heard by the majority of the personnel underneath the aircraft's flight path after it had passed overhead. The whistle was separate and distinct from the jet engine noise and could often be heard while the aircraft was making its 180° turn to go

Table 4. Test aircraft and flyby number designations with corresponding date, start, and ending time of flight tests. Also given are average wind speed, general wind direction, average air temperature, and range of atmospheric stability as determined by air temperature gradient for the various flyby test periods.

Aircraft	Flybys	Date	Start Time (MDT)	End Time (MDT)	Wind Speed (kt)	General Wind Dir.	Air Temp. (°C)	Atmospheric Stability Category
B727-100	1-8	20 June	0609	0811	2.4	NE	11.7	Stable to Unstable
B727-100	9-18	20 June	1126	1230	13.1	SW	20.5	Always Unstable
B727-100	1-16	21 June	0614	0812	14.4	ENE	15.2	Stable to Unstable
B727-100	1-18	21 Sept.	1056	1318	5.0	NE to SW	15.3	Always Unstable
B727-222	1-26	23 Sept.	0717	1010	8.1	NNE	10.5	Stable to Unstable
B727-222	27-36	23 Sept.	1231	1330	2.9	NE to SW	20.5	Always Unstable
B727-222	37-48	24 Sept.	0715	0840	6.0	SW to NE	12.5	Stable to Neutral
B727-222	49-60	24 Sept.	1120	1237	3.2	SE to SW	18.7	Neutral to Unstable
B757-200	1-21	25 Sept.	0720	0937	7.3	NNE	9.7	Stable to Unstable
B757-200	22-41	25 Sept.	1145	1410	7.4	SW	20.6	Always Unstable
B757-200	42-60	26 Sept.	0705	0928	4.8	ENE	11.7	Stable to Unstable
B757-200	61-70	26 Sept.	1415	1511	5.2	NE to NNW	19.2	Always Unstable
B767-200	1-21	29 Sept.	0716	0921	7.1	NNE	8.2	Stable to Unstable
B767-200	22-41	30 Sept.	0826	1024	4.6	NNE	10.6	Stable to Unstable
B767-200	42-59	30 Sept.	1216	1353	6.5	S	20.6	Always Unstable

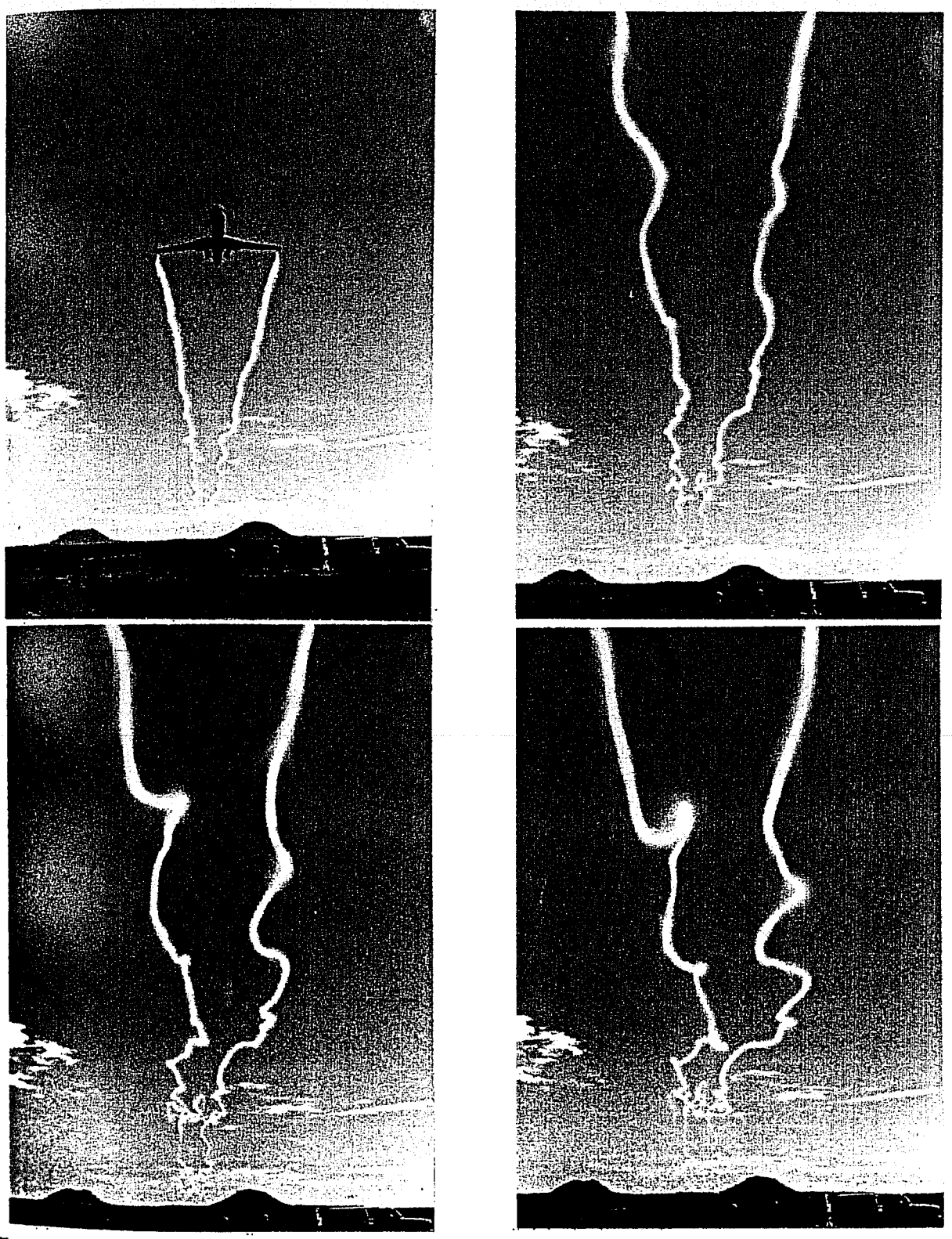

Figure 37. Timed photographic sequence, taken at 4-s intervals, of the UAL B727-222 trailing vortex system exhibiting Crow instability during flyby 60.

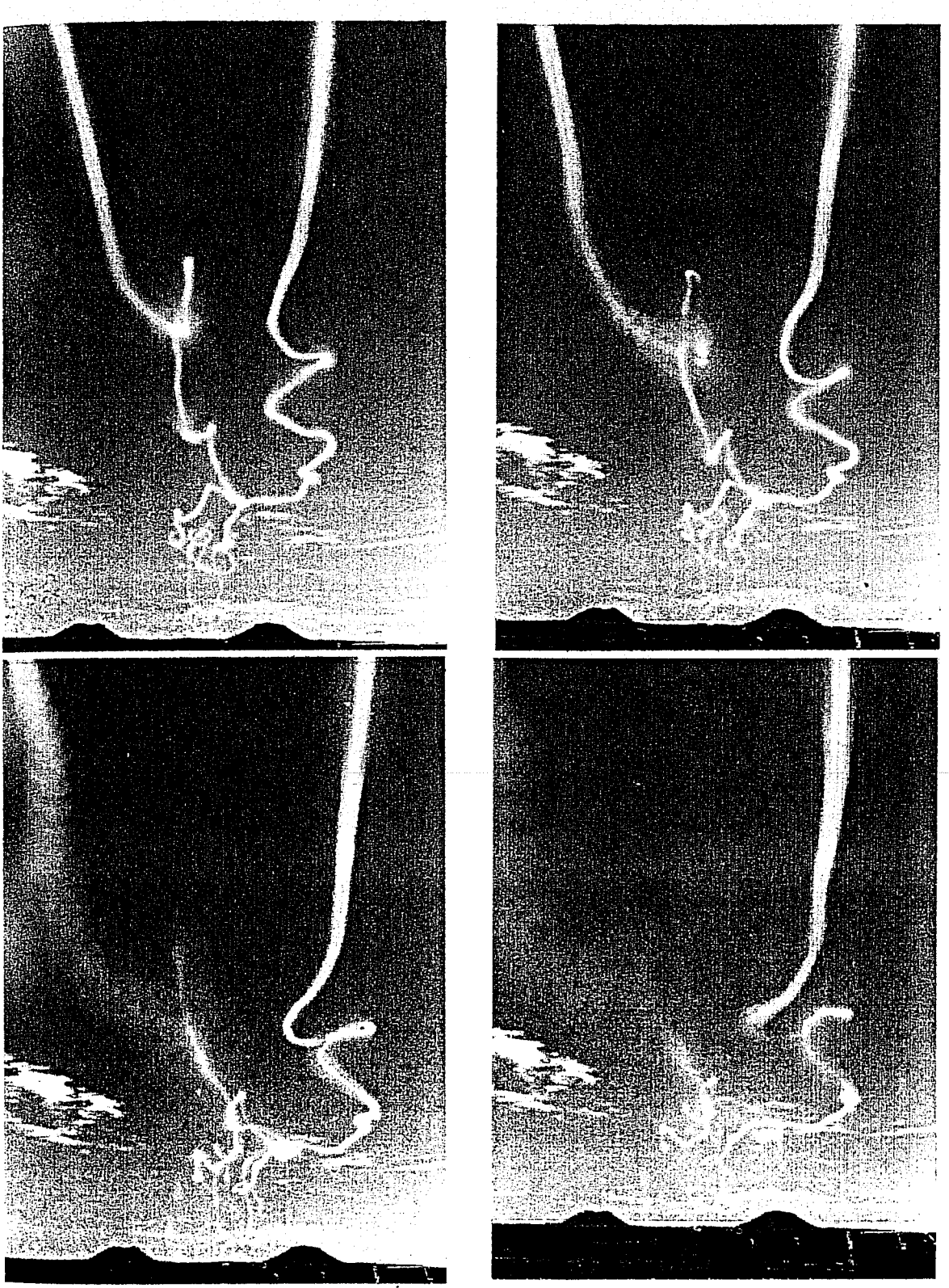

Figure 37. (cont.)

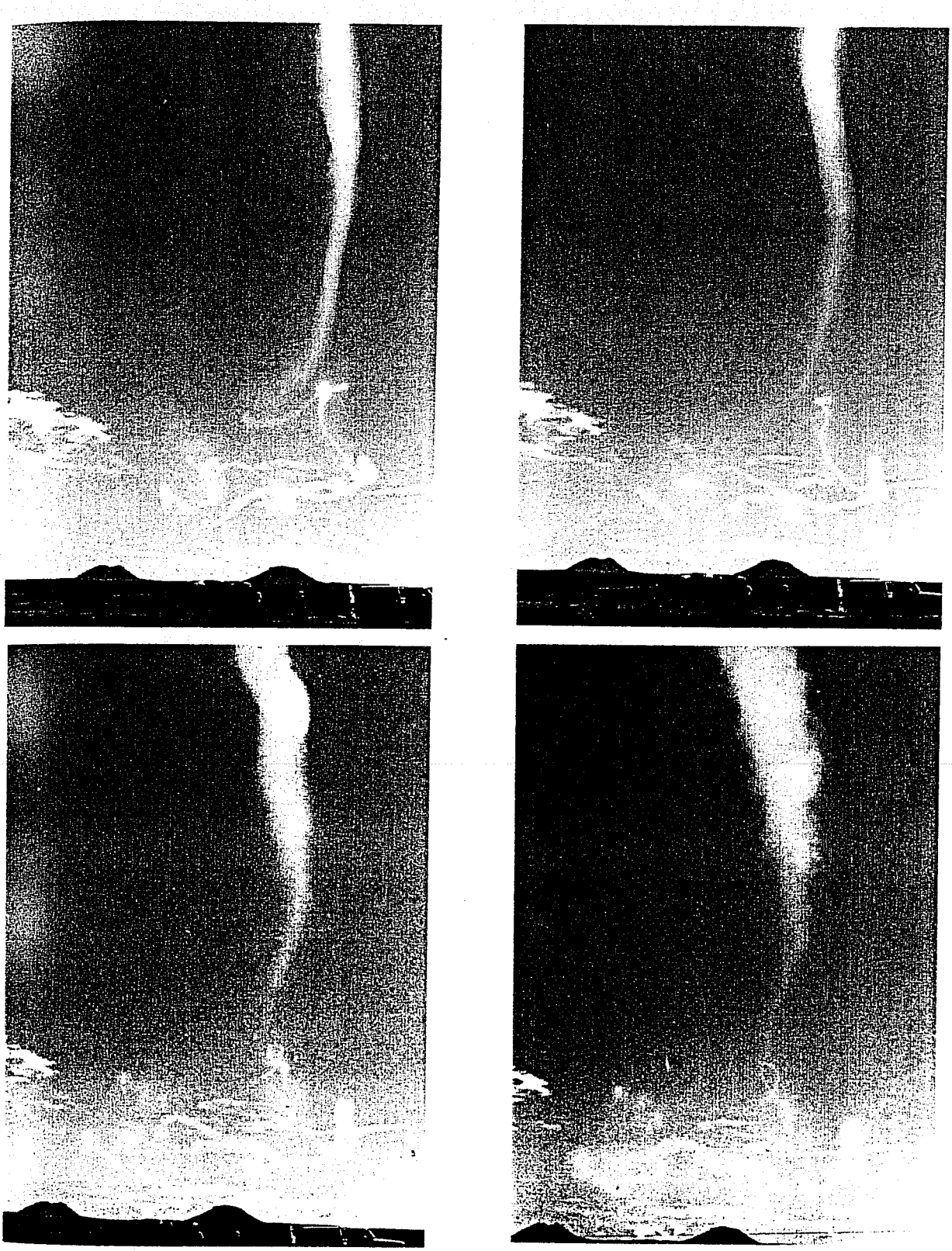

Figure 37. (concluded)

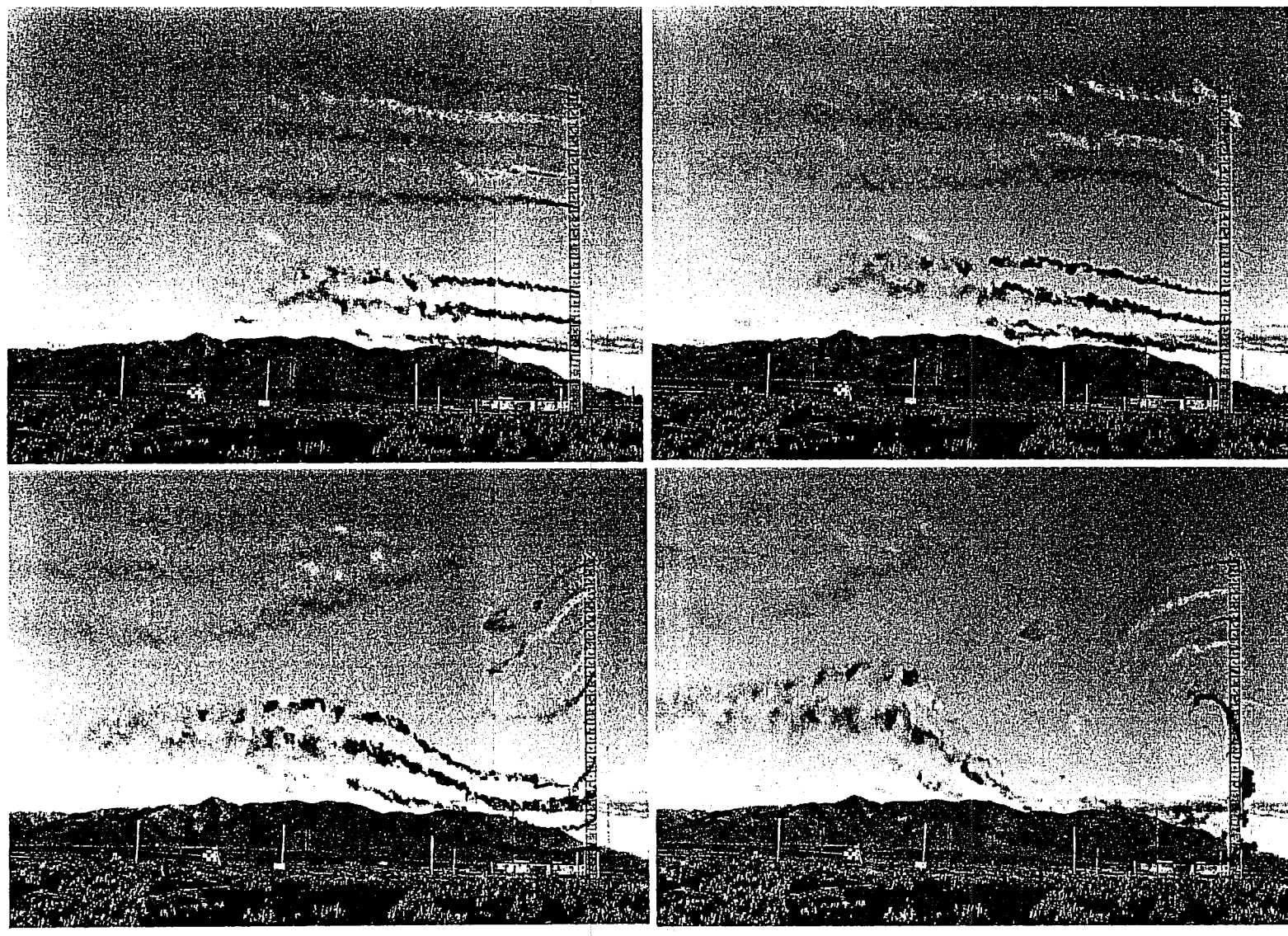

Figure 38. Timed photographic sequence, at 4-s intervals (left to right and top to bottom), of the UAL B757-200 trailing vortex system during flyby 3, exhibiting organized flow at ages of at least 18 and 36 s more than the ages measured at the time of passage through the tower (18 and 28 s, respectively).

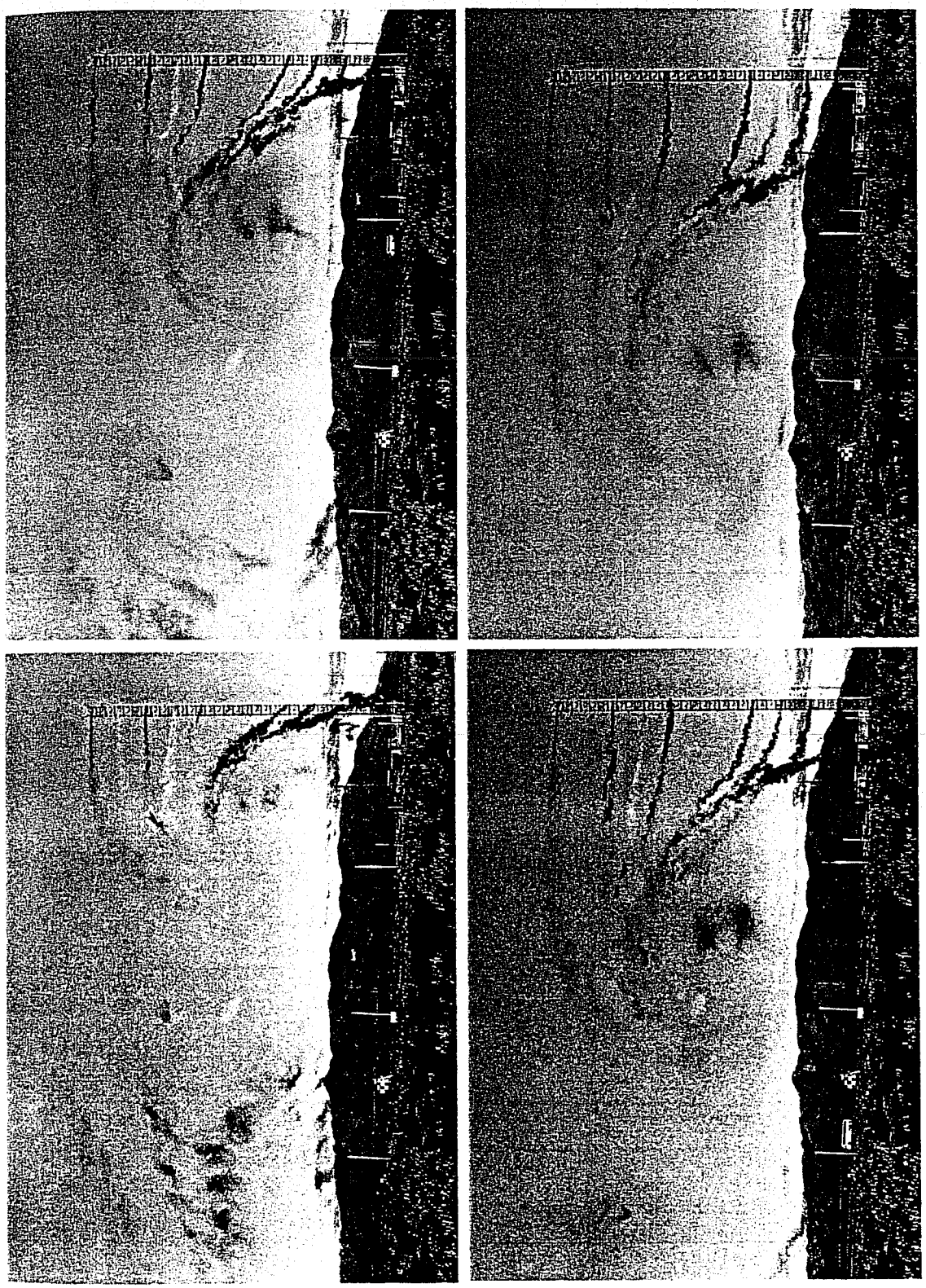

Figure 38. (cont.)

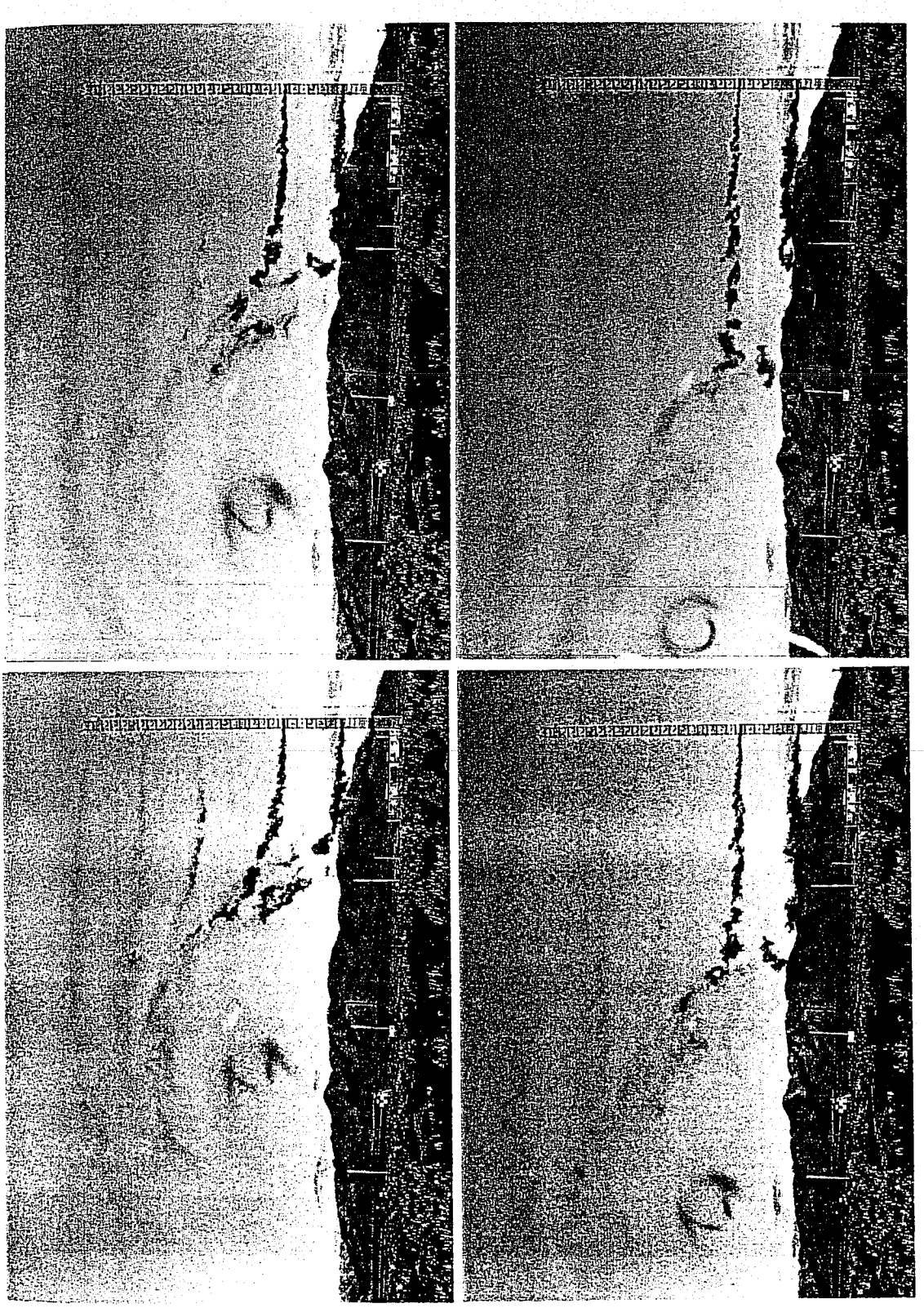

Figure 38. (concluded)

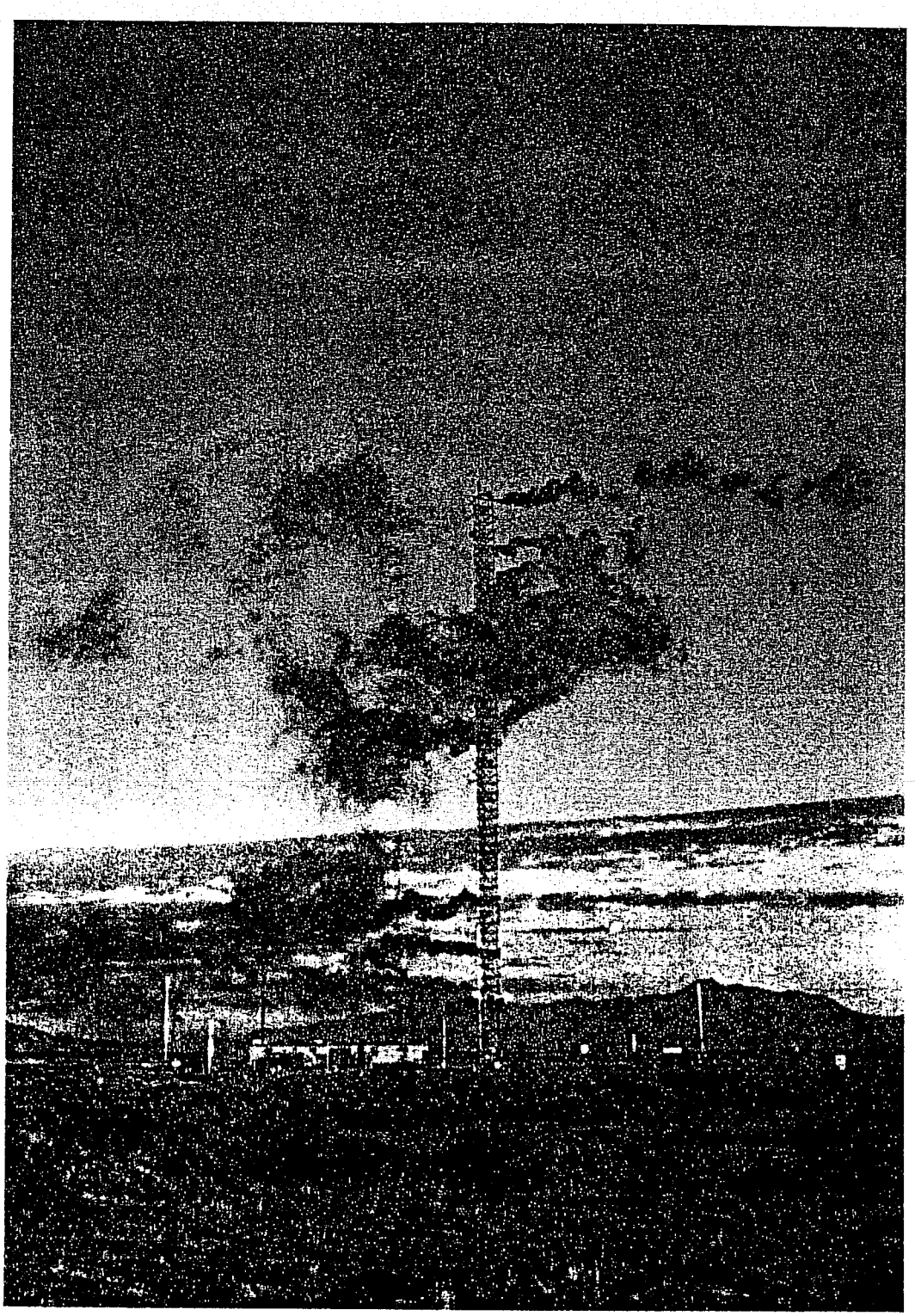

Figure 39. Wind direction shear of 180° over the 200-ft span of the test tower as indicated by tower smoke.

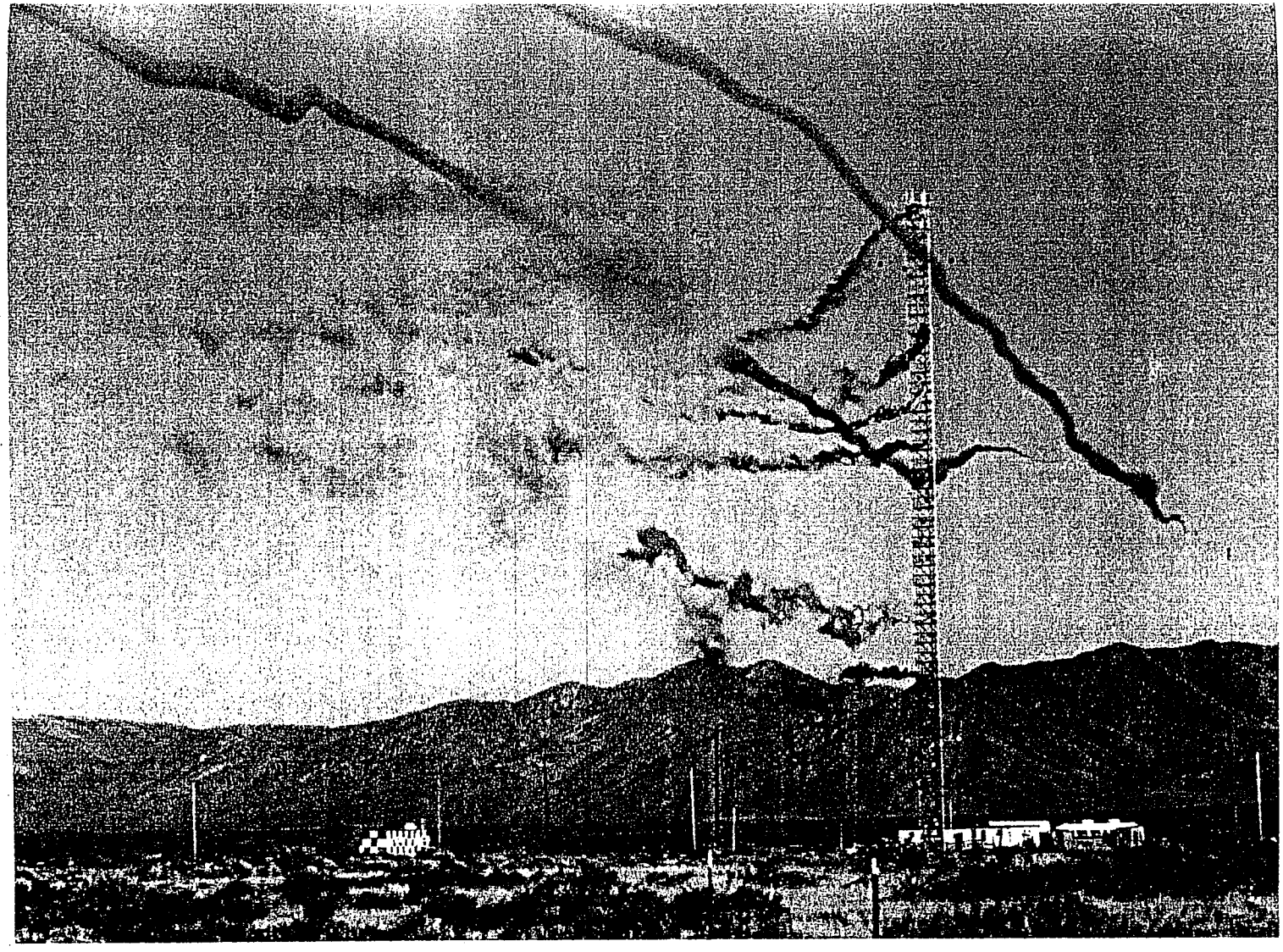

Figure 40. UAL B727-222 downwind vortex flow partially disrupted by the test tower, but with an intact vortex core.

back up-course to commence another flyby. A whistling vortex was previously reported by Garodz (1971a) and Garodz et al. (1974a) with the B727-100. However, the B757-200 vortex-generated whistle was louder.

Vortex whistling was also noticed on the UAL B767-200. However, the whistling became louder as the degree of landing flap was decreased, and evolved into a "roar" when the flaps were completely retracted for two holding configuration flybys. This is just the opposite of what was observed with the UAL B757-200. The most repeatable whistling occurred when the B767-200 was in the takeoff configuration with the flaps set at 1°.

The source of the vortex whistle is not fully known. However, it is probably produced by the shearing action between the tightly rolled-up vortices and the surrounding air mass. Very small vortex cores were calculated for the B757-200, as discussed in detail later in this chapter. The small vortex cores, when combined with high vortex core tangential velocities, could have been a causal factor of the vortex whistle.

It was not known before the flight tests that a vortex whistle would occur. Quantitative measurements of the whistle could have been made by a sound measurement system installed under the aircraft flight path. Such a device would have permitted measurement of intensity levels and frequency characteristics of the whistle, which could have aided in determining the origin of the whistle. The sound recording mechanism in the camcorders used by the video crew were overwhelmed by the jet engine noise, and were unable to discriminate the vortex whistle from all the other noise.

BASELINE AIRCRAFT INTERCOMPARISON

The results of the B727 intercomparison are shown in Figure 41. The $V_{\theta max}$ and age data sets of the FAA B727-100 and UAL B727-222 acquired during this study are indicated by blue and green symbols, respectively. The data set was rather sparse and scatter in the data was large, because of the use of the aircraft for other experimental purposes. The primary use of the FAA B727-100 was to provide an equipment and personnel "shakedown". The primary use of the UAL B727-222 was for cross-calibration of the hot film anemometers with the remote sensing equipment. However, a total of 76 $V_{\theta max}$ data points were recovered from 112 flybys by collecting data points of opportunity. Thus, only general trends in the data could be described.

The observations did not, by themselves, indicate a statistically significant difference between B727 aircraft models. Three noteworthy excursions in the data were observed. The B727-222 indicated a higher overall $V_{\theta max}$ in two downwind vortex data points at an age of approximately 12 s. The B727-100, on the other hand, indicated greater vortex longevity in one upwind vortex at an age of approximately 63 s. If more flybys had been flown for intercomparison purposes, it is assumed that the data scatter would have been smaller, and that the $V_{\theta max}$ values and vortex ages would have been even more similar for both aircraft.

The Garodz et al. (1974a) B727-100 data set is also shown in Figure 41, and is indicated by red symbols. All the new B727 data fell within the envelope delineated by the Garodz et al. data. The new data were obtained at about 5000 ft MSL whereas the old data were obtained near sea level. Overall $V_{\theta max}$ from the new data was 67 fps less than the previously reported B727-100 $V_{\theta max}$ (Table 5). Maximum vortex ages in this study were 51 s less than the maximum B727-100 age previously reported. $V_{\theta max}$ in each 10-s age category was at least 25 fps less than the previously reported value. The systematic bias in the new data toward lower tangential vortex velocities may indicate that lower values are to be expected at higher altitudes. However, the velocity differences are greater than the 15% decline which might be expected from the decrease in air density caused by the difference in altitude. The bias, however, is more likely an artifact of the sparse data set. If more data had been collected, it is probable that vortex tangential velocities would also have been measured at this altitude that would have been similar to those measured at sea level. The same is likely true of vortex ages, since no attempt was made to extend the vortex age envelope of the B727-100/200 beyond about 60 s.

The exponential function given in Equation (6) using coefficients from Garodz et al. (1974a) is indicated by the red line in Figure 41. The fitted exponential equation easily encompassed all the new data. Hence, the data sets from previous B727 studies can be combined with current B727 data to provide a larger vortex characteristics database. Such an operation can be performed without regard to minor variations in the B727 model. This approach was used for much of the analysis presented here. A larger baseline data set was generated for comparison with the B757-200 and B767-200. A similar approach could also be used in the future for comparison with other test aircraft.

VORTEX INTENSITY AND DURATION

A summary of $V_{\theta max}$ for each test aircraft is listed in Table 5. This table gives the highest $V_{\theta max}$ from all flybys made during this study. The highest $V_{\theta max}$ of all aircraft was generated by the B757-200 at 326 fps, followed by the B727-222 at 235 fps, and the B767-200 at 190 fps. The highest $V_{\theta max}$ value for the B767-200 was much lower than expected compared to the B727-100/-222, if only MTOGW is considered. Minimum $V_{\theta max}$ values as low as 10 fps were recorded, and ranged between 10 and 26 fps for all test aircraft.

Table 5 also contains a summary of maximum and minimum vortex ages for each test aircraft. The oldest vortex of the study was produced by the B767-200 at 135 s. The oldest vortex generated by the B757-200 was 84 s, followed by the B727-100 at 62 s. The oldest vortex age of the B767-200 was not as old as the oldest vortex on record, but was 22 s older than any reported for the baseline aircraft. The oldest reported vortex in the tower flyby literature was generated by a C141. The age of that vortex was 176 s (Clawson, 1988).

Figure 42 shows the relationship of $V_{\theta max}$ as a function of age. The graph includes both upwind and downwind vortices obtained from all test aircraft in all five flight configurations. The Garodz et al. (1974a) B727-100 data set is also included in the figure. The combined B727-100/-222 data are indicated by red symbols. The B757-200 data are indicated by blue symbols,

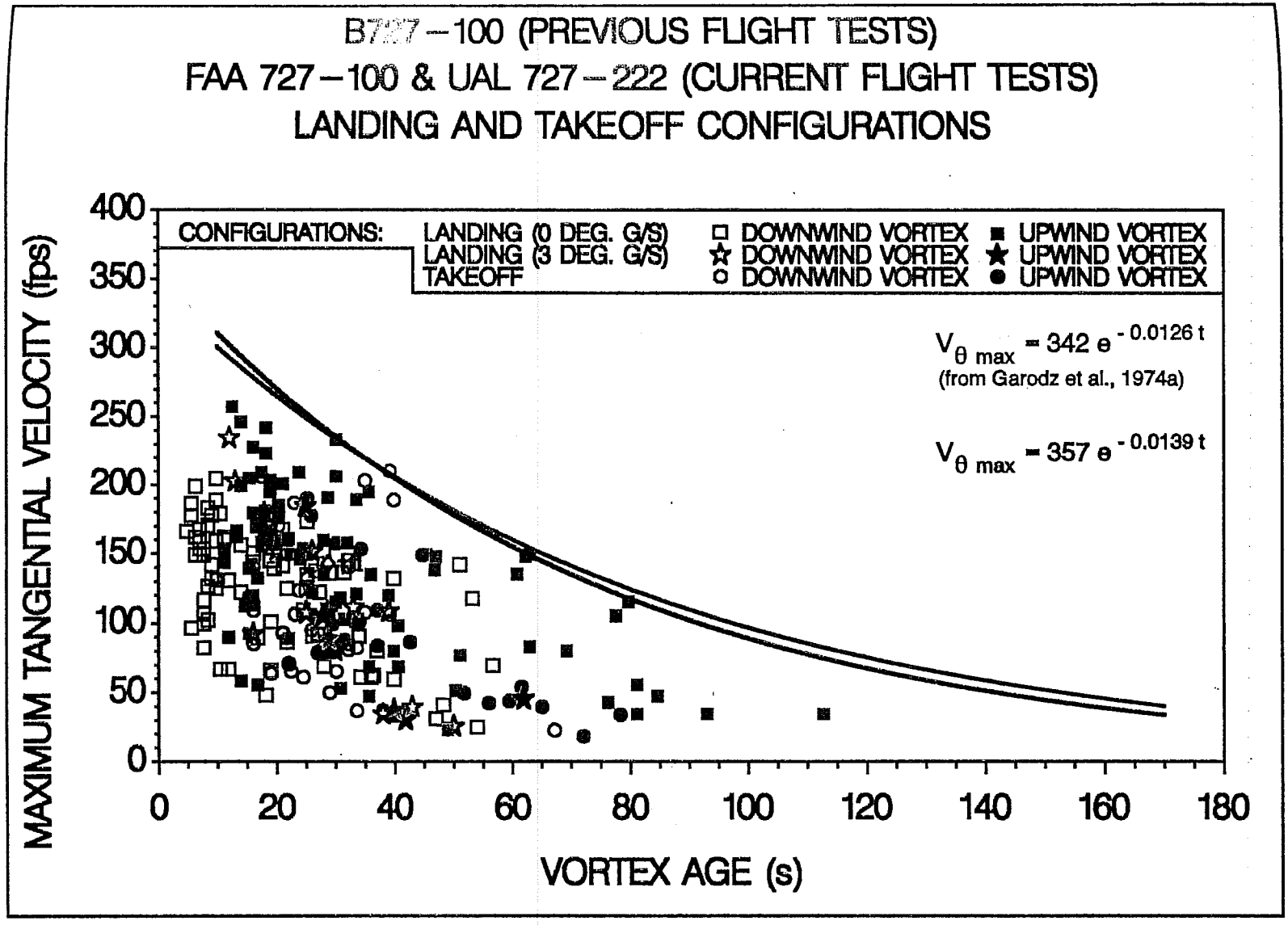

Figure 41. Maximum vortex tangential velocity ($V_{\theta max}$) as a function of age for the FAA B727-100 and UAL B727-222 (blue and green symbols, respectively), and for the FAA B727-100 from previous flight tests (Garodz et al., 1974a), as indicated by the red symbols. The red line represents the Garodz et al. (1974a) vortex decay function as specified by the equation in red. The black line represents the new vortex decay equation that is also in black.

Table 5. Maximum and minimum vortex tangential velocities ($V_{\theta max}$) and ages for the B727-100 and -222, the B757-200, the B767-200, and also for the B727-100 from previous tests (from Garodz et al., 1974a).

Aircraft	$V_{\theta max}$ (fps)		Age (s)	
	Maximum	Minimum	Maximum	Minimum
B727-100 (past)	260	18	113	5
B727-100 (present)	193	26	62	16
B727-222	235	10	54	10
B757-200	326	21	84	11
B767-200	190	16	135	10

and the B767-200 data are indicated by green symbols. The analyses contrasting the B757-200 and B767-200 with the B727-100/-222 data are discussed in detail in the separate aircraft subsections that follow.

Downwind vortices were predominant at vortex ages < 20 s, since downwind vortices are always the first vortices to arrive at the tower. Upwind vortices arrive at the tower after the downwind vortices, making them the predominant vortex at older ages. However, the order of passage through the tower is not the only factor that contributes to the longevity of upwind vortices. The interaction of each vortex with the ambient wind tends to enhance the flow of the upwind vortex and diminish the flow of the downwind vortex in crosswind operations such as those used for the tower flybys. This is illustrated schematically in Figure 43. The wind speed profile is characteristically logarithmic because of frictional drag at the earth's surface. The ambient wind speed is zero at the surface and increases with height. Considering the direction of flow around a given vortex and the resulting velocity vectors when the vortex velocity and ambient wind velocity vectors are added together, it becomes obvious that the ambient wind aids in rotation of the upwind vortex. The ambient wind speed is greater at the top of the vortex than at the bottom, thus aiding the upwind vortex rotation. Momentum is imparted to the upwind vortex as it spins along in the wind. Conceptually, it becomes like a ball, being blown with the wind. The downwind vortex does not roll with the ambient wind, but rather against it. The area of greatest ambient wind velocity, which is at the top of the vortex, directly opposes the vortex flow. This process aids in the demise of the downwind vortex. Hence, the longest-lived vortices are the upwind vortices.

B727-100/-222 Aircraft

Additional analyses were performed on the combined B727-100/-222 $V_{\theta max}$ data. Some interesting features found in the age-stratified data set are summarized in Table 6. The 11 oldest vortices (> 68 s) were all upwind vortices. Furthermore, of the 20 vortices that were ≥ 60 s, 19 or 95% were upwind vortices. On the other hand, the 28 youngest vortices (≤ 10 s) were all downwind vortices.

The majority of the combined B727-100/-222 $V_{\theta max}$ data were obtained when the aircraft was in the landing configuration. Of a total of 257 data points, 72%, 22%, 4%, and 2% were obtained in the landing, takeoff, holding, and clean configurations, respectively. At the younger vortex ages, the landing configuration was the predominant flight mode (Table 6). Indeed, all vortices < 15 s were obtained in this configuration. The remaining vortex age categories were populated with aircraft configurations in approximately the same proportions as the overall experiment. No distinct configuration or vortex type was predominant in the vortex velocity-stratified $V_{\theta max}$ data.

New coefficients for Equation (6) were generated for the combined B727-100/-222 data. The curve is indicated by the black line in Figure 41. The new coefficients were slightly different than those given by Garodz et al. (1974a), and the new curve fits the data somewhat better. Both the initial vortex velocity coefficient (A) and the decay rate coefficient (B) were greater than the previous coefficients. The new curve is also plotted in Figure 42 as a red line. The curve for the combined B727, B757, and B767 data is plotted as a black line in Figure 42.

B757-200 Aircraft

The highest $V_{\theta max}$ value ever recorded during this and all previous studies using the tower flyby technique was generated by the B757-200. The velocity was measured at 326 fps during flyby number 10 on the downwind vortex. Its age was 16 s. The second highest $V_{\theta max}$ for this study (281 fps) was recorded for the upwind vortex of this same flyby with an age of 25 s. The aircraft was in the landing configuration with 30° flaps on a 3° G/S. The previous highest $V_{\theta max}$ reported in the literature was 268 fps with an age of 13 s, reported by Clawson (1988). That value was from a downwind vortex generated by a C5A/B with flaps at 15% on a 0° G/S. Just as significant is the observation that the highest B757-200 $V_{\theta max}$ value was approximately 50% greater than the highest $V_{\theta max}$ value for the B767-200 and the B727-100/-222 (new data) at the younger vortex ages up to about 45 s.

The hot film anemometer, arm, and associated electronics that recorded the 281 fps $V_{\theta max}$ of the upwind vortex of flyby number 10 of the B757-200 was pulled out of its mounting socket by the force of the vortex. The ground crew watched as the components fell to earth. The hot film arm was mounted to the tower with a pressure-fit, snap-in/snap-out mounting, which permitted quick and easy exchange of broken hot films. It is impossible to calculate the force required to remove the arm from its mounting, but the change procedure required both hands for removal. It can be inferred from the direction in which all arms were designed to be

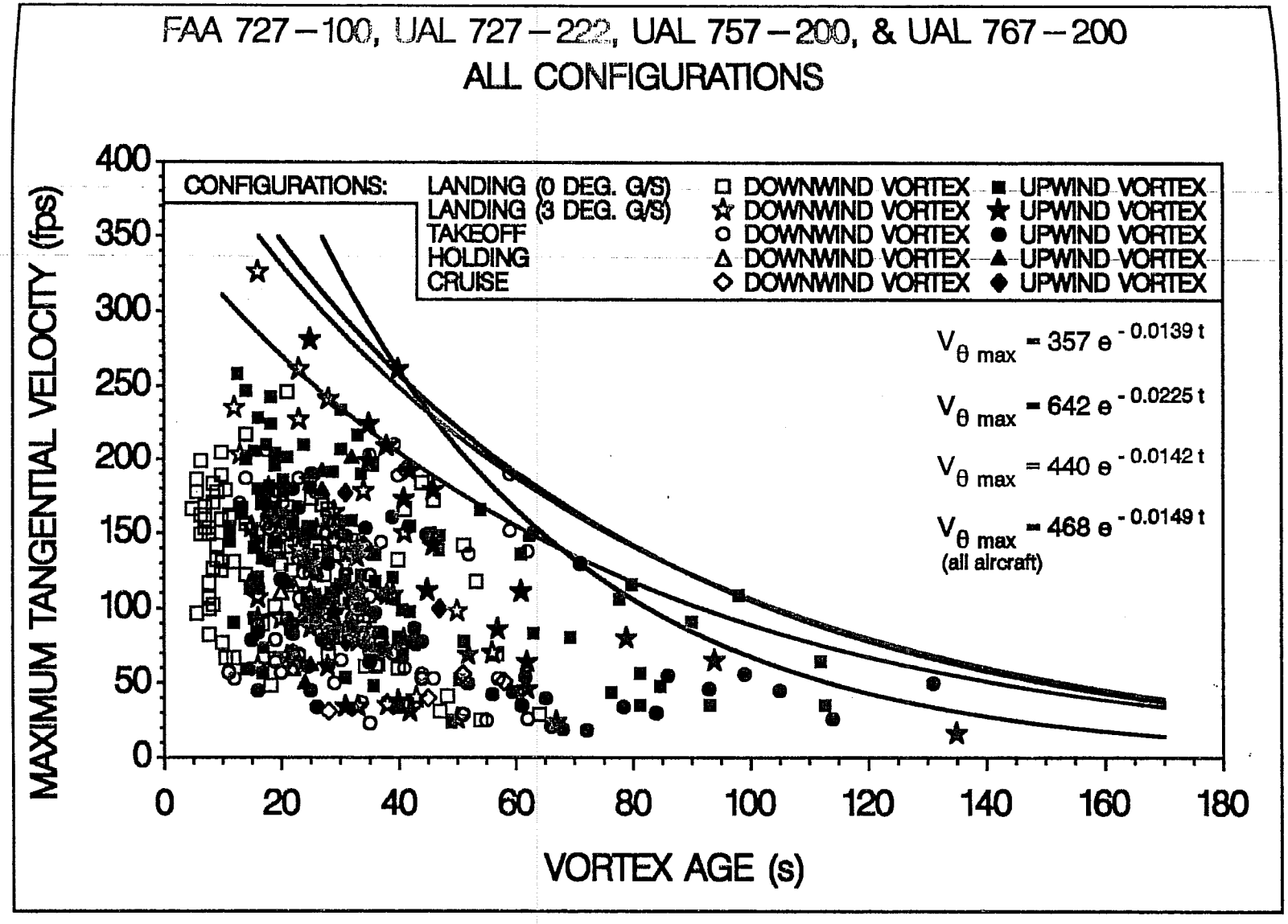

Figure 42. Maximum vortex tangential velocity ($V_{\theta max}$) as a function of age for the B727-100 from previous flight tests (Garodz et al., 1974a), the B727-100 and B727-222 from the current flight tests (all B727 data are shown with red symbols), the B757-200 (blue symbols), and the B767-200 (green symbols). The red, blue, green, and black lines are vortex decay functions specified by the equations with corresponding colors for the B727-100/-222, B757-200, B767-200, and all test aircraft combined, respectively.

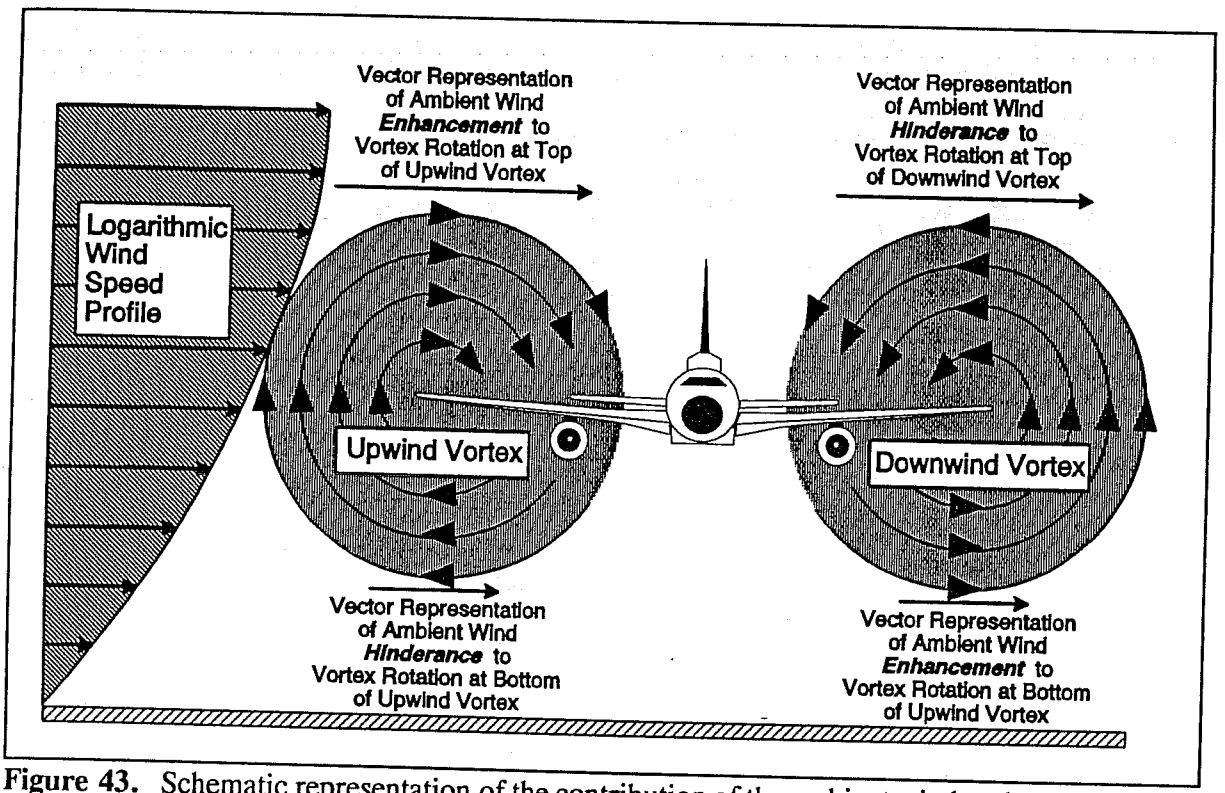

Figure 43. Schematic representation of the contribution of the ambient wind to the enhancement of the upwind vortex flow and to the demise of the downwind vortex.

removed, that the hot film anemometer was probably removed by axial flow within the vortex core. It is therefore conjectured that considerable axial flow accompanied the tangential flow of that particular vortex. The axial flow component may have been formed by disruption of the vortex as it impinged on the tower. It is also possible that a large axial flow normally accompanies vortices generated by this aircraft. Neither hypothesis could be definitively accepted nor discounted because the hot film anemometer data is ambiguous on this account. Axial flow cannot be distinguished from tangential flow by the two-dimensional hot film anemometers used in the study.

The B757-200 produced all the highest $V_{\theta max}$ in the landing configuration. In fact, of the 36 vortices that exhibited a $V_{\theta max} \geq 140$ fps, 33 (91%) were generated in the landing configuration (Table 7) with a flap setting of 25 to 30°. The data in Table 3 indicate that only 54% of all B757-200 flybys were flown in the landing configuration. This, therefore, indicates a disproportionately high concentration of vortices generated in the landing configuration in the ≥ 140 fps range. The three $V_{\theta max}$ exceptions in this velocity band were generated in the other three configurations with flaps ranging from 0 to 5°. Both downwind and upwind vortices were evenly represented in this high-velocity category.

The production of the highest $V_{\theta max}$ by the B757-200 in the landing configuration is contrary to that exhibited by most other aircraft with wing-mounted engines. The majority of

Table 6. Miscellaneous B727-100/-222 vortex characteristics observed in the age-stratified $V_{\theta max}$ data. Italics indicate the aircraft flight configuration and/or vortex type that occurred most frequently in a given age range.

Characteristic of Interest	Vortex Age Range (s)	Aircraft Configuration Frequencies		Downwind/ Upwind Vortex Frequencies	
Vortex Type	> 60	landing	74%		
		takeoff	26%	***upwind***	***95%***
		holding	0%	downwind	5%
		clean	0%		
	≥ 30 and ≤ 60	landing	63%		
		takeoff	31%	downwind	54%
		clean	5%	upwind	46%
		holding	1%		
	< 30	landing	77%		
		takeoff	17%	downwind	58%
		holding	5%	upwind	41%
		clean	1%		
Aircraft Configuration and Vortex Type	< 20	***landing***	***90%***		
		takeoff	10%	***downwind***	***62%***
		holding	0%	upwind	38%
		clean	0%		
Aircraft Configuration and Vortex Type	≤ 15	***landing***	***100%***		
		takeoff	0%	***downwind***	***79%***
		holding	0%	upwind	21%
		clean	0%		

aircraft tested to date showed that $V_{\theta max}$ decreased with an increase in landing flap deflection (Garodz and Miller, 1975; Garodz et al., 1975; Garodz and Clawson, 1991). An investigation into this dichotomy leads to an examination of the B757-200 wing. The B757-200 exhibits a continuous wing flap trailing edge when the flaps are lowered, which is fairly "clean" when compared with other aircraft. There is no cut-out or gap between the inboard and outboard flaps in the jet engine exhaust area. The result is manifested in the relatively smooth wing span load distribution, which is shown in Appendix A. The lack of cut-outs decreases or eliminates the generation of multiple vortices in the landing configuration at the various flap and wing tip edges. Multiple vortices tend to interact and attenuate each other, thus decreasing $V_{\theta max}$ downstream from the airplane. Another factor that may contribute to high $V_{\theta max}$ in the landing configuration is wing geometry. The B757-200 has a low wing sweep angle (Λ) of 25° with a

fairly straight wing trailing edge (Figure 21 and Appendix A). Other commercial jet transports have a Λ of about 35°.

The B757-200 vortex velocity data exhibited other stratifications according to aircraft configuration, as summarized in Table 7. A disproportionately large number of vortices generated by the aircraft in the takeoff configuration were recorded in the $V_{\theta max}$ range < 140 fps. Fifty-three percent of all vortices with a $V_{\theta max}$ less than 140 fps were generated in the takeoff configuration with flaps ranging from 5 to 20°. Only 32% of all flybys were flown in the takeoff configuration. Further, of the 25 vortices that exhibited a $V_{\theta max}$ < 90 fps, 19 (76%) were generated in the takeoff configuration; an additional 4 vortices (16%) in that lower velocity band were generated in the landing configuration with flaps at 30°. Downwind vortices predominated in this velocity category at a ratio of approximately 2:1. In addition, of a total of 11 vortices generated in the holding and clean configurations, five were contained in the $V_{\theta max}$ band between 90-111 fps. This was 63% of all vortices generated in that narrow velocity band. The remainder of the vortices generated in the holding and clean configurations were scattered throughout the data set.

The three oldest vortices generated by the B757-200 were upwind vortices. Indeed, of the seven vortices with ages greater than 60 s, five (71%) were upwind vortices. These and other vortex age data from the B757-200 are summarized in Table 8. On the other hand, downwind vortices were predominant in the ≤ 30 s age group at a ratio of about 2:1. Downwind vortices became even more predominant in the younger vortices, reaching a ratio of nearly 2.5:1 in the ≤ 20 s age group. Vortices measured in the 30-60 s age group were nearly equally divided between upwind and downwind types. These results compare well with the baseline aircraft and expected vortex behavior.

Additional aircraft flight configuration stratifications were noted in the vortex age data. Five (71%) of the seven vortices with ages > 60 s were generated in the takeoff configuration, with flaps ranging from 1 to 20°. Only 29% of the vortices in that age category were generated in the landing configuration with flaps at 30°. Vortices generated in the takeoff configuration were also predominant at ages ≤ 20 s. Of the 14 vortices that fell into this age group, 8 (57%) were generated in the takeoff configuration, 5 (36%) were generated in the landing configuration, and 1 (7%) was generated in the holding configuration. In the 20-60 s age group, the four flight configurations were represented in approximately the same proportions as the overall study statistics specified for the B757-200 in Table 3.

The B757-200 $V_{\theta max}$ envelope decay function as specified in Equation (6) is shown by the blue line in Figure 42. The envelope decay function encompassed all the B757-200 vortex data. The initial velocity coefficient (A) was 642 fps, which was 300 fps greater than the value for the baseline aircraft. The larger value was the result of much larger $V_{\theta max}$ value at ages less than 45 s. The preponderance of B757-200 data lies between the ages of 15 and 65 s. Only two vortices were measured at ages greater than 65 s. Both of those occurrences were upwind vortices generated in the takeoff configuration. The vortex decay rate was also nearly twice as large as for the baseline aircraft because of the relatively short life spans of the B757-200 vortices.

Table 7. Miscellaneous B757-200 vortex characteristics observed in the velocity-stratified $V_{\theta max}$ data. Italics indicate the aircraft flight configuration and/or vortex type that occurred most frequently in a given velocity range.

Characteristic of Interest	Velocity Range (fps)	Aircraft Configuration Frequencies		Downwind/ Upwind Vortex Frequencies	
Aircraft Configuration	$\geq$ 140	***landing***	***91%***		
		takeoff	3%	downwind	56%
		holding	3%	upwind	44%
		clean	3%		
	< 140	***takeoff***	***53%***		
		landing	26%	downwind	53%
		holding	15%	upwind	47%
		clean	6%		
Aircraft Configuration	$90 \leq x < 111$	***holding & clean***	***63%***	downwind	50%
		takeoff	25%	upwind	50%
		landing	12%		
Aircraft Configuration and Vortex Type	< 90	***takeoff***	***76%***		
		landing	16%	***downwind***	***64%***
		clean	8%	upwind	36%
		holding	0%		

It may be concluded, based solely on the vortex data recorded during this study, that the B757-200 generates very strong, short-lived vortices. However, it is highly likely that the data set is incomplete because of the short time the aircraft was available for flight tests. This restricted the range of environmental conditions under which the aircraft could be tested, thereby also restricting the possibility of obtaining older vortices. It is surmised that the vortices were subjected to accelerated dissipation due to vortex-atmospheric interaction as indicated by the large number of tests conducted under unstable atmospheric conditions (Table 4). It is therefore reasonable to assume that the B757-200 aircraft could have generated longer-lived vortices under a different set of environmental conditions. Thus, further flight tests under different atmospheric conditions are recommended.

B767-200 Aircraft

The oldest vortices obtained during this study were produced by the B767-200 (Figure 42). Eleven B767-200 vortices were older than any of the other vortices produced by the other aircraft during this study. Three of the B767-200 vortices were older than any vortices in the combined B727-100/-222 data. These are not the oldest vortices ever obtained during tower

Table 8. Miscellaneous B757-200 vortex characteristics observed in the age-stratified $V_{\theta max}$ data. Italics indicate the aircraft flight configuration and/or vortex type that occurred most frequently in a given age range.

Characteristic of Interest	Vortex Age Range (s)	Aircraft Configuration Frequencies		Downwind/ Upwind Vortex Frequencies	
Aircraft Configuration and Vortex Type	> 60	***takeoff***	***71%***	***upwind***	***71%***
		landing	29%	downwind	29%
		holding	0%		
		clean	0%		
	≥ 30 & ≤ 60	landing	59%	upwind	51%
		takeoff	28%	downwind	49%
		clean	13%		
		holding	0%		
	≤ 30	landing	54%		
		takeoff	30%	***downwind***	***65%***
		holding	11%	upwind	35%
		clean	5%		
Vortex Type	< 25	landing	46%		
		takeoff	41%	***downwind***	***68%***
		holding	13%	upwind	32%
		clean	0%		
Aircraft Configuration and Vortex Type	≤ 20	***takeoff***	***57%***		
		landing	36%	***downwind***	***71%***
		holding	7%	upwind	29%
		clean	0%		

flybys, but they are useful in defining the vortex intensity-duration envelope and the $V_{\theta max}$ envelope decay function.

As was the case with the B727-100/-222 and B757-200 data, the oldest B767-200 vortices were upwind vortices, as indicated in Table 9. Of the 16 vortices that were older than 60 s, 94% were upwind vortices. All 14 vortices > 62 s were upwind vortices. The downwind vortices were predominant in the younger ages and constituted 69% of all vortices < 30 s in age. The disparity was even more dramatic in vortices younger than 20 s, when 77% of all vortices were downwind. For vortex ages between 30 and 60 s, the mix of downwind and upwind vortices was nearly equal. The takeoff configuration was the predominant configuration in the age range. No other age ranges exhibited a predominant flight configuration.

Table 9. Miscellaneous B767-200 vortex characteristics observed in the age-stratified $V_{\theta max}$ data. Italics indicate the aircraft flight configuration and/or vortex type that occurred most frequently in a given age range.

Characteristic of Interest	Vortex Age Range (s)	Aircraft Configuration Frequencies		Downwind/ Upwind Vortex Frequencies	
Aircraft Configuration and Vortex Type	> 60	takeoff	50%		
		landing	50%	***upwind***	***94%***
		clean	0%	downwind	6%
		holding	0%		
	≥ 30 and ≤ 60	***takeoff***	***67%***		
		landing	33%	downwind	57%
		clean	0%	upwind	43%
		holding	0%		
	< 30	landing	53%		
		takeoff	47%	***downwind***	***69%***
		clean	0%	upwind	31%
		holding	0%		
Vortex Type	≤ 20	landing	54%		
		takeoff	46%	***downwind***	***77%***
		clean	0%	upwind	23%
		holding	0%		

Speed-stratified $V_{\theta max}$ data (Table 10) showed that vortex velocities greater than 130 and less than 60 fps were dominated by takeoff configurations at a rate of 72 and 84%, respectively. This is clearly opposite to the results obtained for the B757-200. The velocities obtained between 60 and 130 fps for the B767-200 were dominated by landing configurations. Both the landing and takeoff aircraft configurations were flown in equal proportions by the B767-200 during the study, as indicated in Table 3. The downwind vortex was predominant at velocities greater than 130 fps, whereas the upwind vortex was the predominant vortex at velocities less than 60 fps. This occurred at the ratios of approximately 2:1. However, at $V_{\theta max} \leq 50$ fps, the ratio of upwind to downwind vortices was 9:1. This again contrasts with the B757-200 data, which indicated a predominance of downwind vortices at $V_{\theta max} < 90$ fps.

The $V_{\theta max}$ envelope decay function from Equation (6) is shown as the green line in Figure 42. The coefficients indicate an initial vortex velocity at time zero of 440 fps, and an exponential decay rate of -0.0142. Both the initial velocity and decay rate are slightly higher than that of the B727-100/-222. This was caused by two data points at 59 and 98 s, where notably higher $V_{\theta max}$ values were observed. Although higher B767-200 $V_{\theta max}$ values were observed at older ages than for the baseline aircraft, this was not the case at vortex ages younger

Table 10. Miscellaneous B767-200 vortex characteristics observed in the velocity-stratified $V_{\theta max}$ data. Italics indicate the aircraft flight configuration and/or vortex type that occurred most frequently in a given velocity range.

Characteristic of Interest	Velocity Range (fps)	Aircraft Configuration Frequencies		Downwind/ Upwind Vortex Frequencies	
Aircraft Configuration and Vortex Type	≥ 130	***takeoff***	***72%***	***downwind***	***67%***
		landing	22%	upwind	33%
		clean	6%		
		holding	0%		
	> 60 and < 130	***landing***	***80%***		
		takeoff	20%	downwind	50%
		clean	0%	upwind	50%
		holding	0%		
	≤ 60	***takeoff***	***84%***		
		landing	16%	***upwind***	***63%***
		clean	0%	downwind	37%
		holding	0%		
Vortex Type	≤ 50	***takeoff***	***73%***		
		landing	27%	***upwind***	***91%***
		clean	0%	downwind	9%
		holding	0%		

than about 45 s. In this age range, the B767-200 did not produce any vortices with velocities > 190 fps, whereas the baseline aircraft produced velocities as high as 260 fps.

The B767-200 $V_{\theta max}$-vortex age data lead to the conclusion that vortices from the B767-200 are relatively long-lived, but are of lesser intensity than the baseline B727-100/-222 aircraft. However, as with the dearth of longer-lived vortices for the B757-200, it is surmised that meteorological conditions also contributed to the dearth of high-velocity B767-200 vortices at younger ages. It is also suspected that meteorological conditions conducive to producing long-lived vortices were prevalent at the time of the B767-200 flight tests. The limited aircraft flight time also limited the meteorological conditions under which the aircraft could be flown. The result was a data set that was very likely incomplete, yet is the best assemblage of data on this aircraft to date.

All Aircraft

A $V_{\theta max}$ envelope decay function using Equation (6) for all aircraft including the combined B727-100/-222 data, is indicated by the black line in Figure 42. The curve encompassed the data for all ages out to the data limit of 135 s. The relationship beyond this age limit may

continue to be exponential, but is more likely described by some other function. Because there was no $V_{\theta max}$ data older than 135 s, the relationship could not be determined. Compared with the original B727 function (Figure 41), the value of the initial vortex tangential velocity coefficient increased by 126 fps to 468 fps. The decay rate coefficient also increased from -0.0126 to -0.0149. The curve was affected primarily by three data points, at 40, 59, and 98 s. The youngest data point was from the B757-200, whereas the latter two data points were from the B767-200. Thus, the overall envelope was affected by the two larger aircraft, and not the smaller baseline aircraft.

The trailing vortex systems generated by the B757 and B767 at flight altitudes near the ground did not persist with any significant rotational velocities for longer than 135 s. A vortex with significant rotational velocity is defined in this report to be a vortex with a $V_{\theta max}$ value below the detection limits of the hot film vortex sensing system used in this study. From Table 5, this appears to be about 10 fps. It is left to the discretion of the FAA to determine the "hazard" of any of the vortices reported herein.

The exponential decay function [Equation (6)] can assist in determining expected vortex velocities generated by the three test aircraft at the equivilent aircraft separation times specified by existing aircraft separation standards. The equivilent time delays can be used in the $V_{\theta max}$ envelope decay function to calculate a $V_{\theta max}$. Table 11 contains estimates of $V_{\theta max}$ at the current aircraft separation standards for each test aircraft in this study. From this table of estimates, an aircraft following 3 min behind a B727-100/-222 could conceivably encounter a vortex with a $V_{\theta max}$ up to 29 fps. An encounter at 4 min reduces $V_{\theta max}$ to 13 fps. The 29 fps $V_{\theta max}$ value is greater than the 10 fps detection limit of the vortex sensing system and is considered to have a significant rotational velocity. The 13 fps $V_{\theta max}$ value is near the 10 fps threshold and, therefore is considered to have an insignificant rotational velocity. The B757-200 predicted $V_{\theta max}$ values at 3 and 4 min were considered to exhibit insignificant rotational velocities because of the rapid decline in $V_{\theta max}$ with time for this particular aircraft. The predicted $V_{\theta max}$ of the B767-200 was similar to the B727-100/-222. All $V_{\theta max}$ predictions for all test aircraft were outside of the time domain defined by actual data. The predictions in Table 11 are the best currently available, but must be evaluated with caution because of the prediction equation was used beyond the limited age-range of the observed data.

METEOROLOGY AND VORTEX BEHAVIOR

The effects of atmospheric turbulence on vortex persistence have been the subject of several investigations, e.g., Tombach (1973), Tombach et al. (1977), and Crow (1976). Atmospheric turbulence was also incorporated into the mechanistic vortex decay model proposed by Green (1986). However, the direct relationship between turbulence and vortex persistence has remained ill-defined. Another effort at determining a correlation was attempted using the data from this study.

Atmospheric turbulence is primarily a function of wind shear and buoyancy effects. Direct measurement of atmospheric turbulence is difficult and costly. Hence, several indices of

Table 11. Estimated $V_{\theta max}$ at 2.5, 3, 4, and 5 min ages using Equation (6) and coefficients in Figure 42 for the B727-100/-222, B757-200, B767-200, and all test aircraft combined.

Aircraft	Estimated $V_{\theta max}$ (fps)			
	2.5 min	3 min	4 min	5 min
B727-100/-222	44	29	13	6
B757-200	22	11	3	1
B767-200	52	34	15	6
All Aircraft	50	32	13	5

atmospheric turbulence have been proposed that are derived from easily-measured standard meteorological parameters. Two such indices currently in use are Ri and $\Delta T/\Delta z$. Although these indices are easily determined, they include simplifications and assumptions that are not always valid. Analyses of vortex age as a function of these two indices of atmospheric turbulence as well as horizontal wind speed are discussed. Although atmospheric turbulence was subjectively estimated and recorded in the pilot knee-pad data, an insufficient amount of data were collected for any meaningful vortex decay analysis. The correlations presented are empirical only, since the required experimental design prohibited incorporation of direct turbulence measurements. Future analyses of this type will continue to be empirical until an experiment can be designed by meteorologists and aeronautical engineers to isolate and document the role of atmospheric turbulence in vortex dissipation.

Richardson Number

Vortex behavior as related to Ri is illustrated in Figure 44. The red symbols indicate $V_{\theta max}$ obtained during stable atmospheric conditions while the green symbols indicate $V_{\theta max}$ obtained during unstable atmospheric conditions. Much of the study was conducted under unstable atmospheric conditions, as manifested by the large ratio of green to red symbols.

Although much of the stable $V_{\theta max}$ data was found interspersed with the unstable $V_{\theta max}$ data, a distinctive age-related feature was observed in the data set. All the $V_{\theta max}$ data with ages > 100 s were obtained under stable atmospheric conditions. Indeed, fully 82% of the $V_{\theta max}$ data > 80 s were obtained under stable or near neutral atmospheric conditions. This indicates, in general, that stable or neutral atmospheric conditions were conducive to long-lived vortices.

A more complete investigation was undertaken in an effort to establish a direct cause and effect between Ri and $V_{\theta max}$ and between Ri and vortex age. It was expected that as atmospheric turbulence declined, vortex intensity and persistence would increase. Conversely, it was expected that as atmospheric turbulence increased, vortex intensity and persistence would decrease. However, a direct relationship between Ri and vortex age could not be established

through statistical procedures because of the large scatter in the data. A graph illustrating this attempt is shown in Figure 45. However, some general trends in the vortex age data were observed when Ri indicated unstable atmospheric conditions. The data envelope indicated a decline in age as Ri became increasingly negative. The black line in Figure 45 includes the data envelope, which indicated a decline in maximum vortex age from 99 s at an Ri of -1.05 to a maximum age of about 43 s at an Ri of -1590. No definitive effect of aircraft type on the relationship between vortex age and Ri was observed. The graph shows that most of the data were acquired in an Ri range -1 to -30, which was an unstable atmosphere. In stable atmospheric conditions, most of the data were acquired in the Ri range of 0.4 to 1.

A graph of $V_{\theta max}$ as a function of Ri for all test aircraft is shown in Figure 46. $V_{\theta max}$ was stratified into age categories as follows: < 30 s, from 30 through 60 s, and > 60 s. A direct correlation between Ri and $V_{\theta max}$ was not found in the data because the scatter was too large for any statistically significant relationship to be determined through least-squares regression techniques. General trends were observed in the data envelope, however. Under stable atmospheric conditions, as Ri increased from 0.69 to 9.37, the envelope containing $V_{\theta max}$ actually declined from 246 to 152 fps. Only in the range from about 0.03 to 0.69 did an increase in Ri result in a progressively larger $V_{\theta max}$ from 162 to 246 fps. On the other hand as Ri declined from -1.86 to -151, $V_{\theta max}$ generally declined as well from 261 to 79 fps. A few exceptions were noted at Ri less than -200. It was in this range that Ri became an unreliable parameter because the wind speed gradient was near zero. Because wind speed is the denominator in the Ri equation [Equation (5)], dividing by a wind speed gradient that was near zero with a negative $\Delta T/\Delta z$ in the numerator resulted in very large negative numbers. Ri then became only a qualitative index of atmospheric turbulence.

Further scrutiny of Figure 46 indicated that nearly all $V_{\theta max}$ velocities > 240 fps were obtained under near-neutral conditions. Of the six data points in that speed range, only one was obtained during moderately unstable atmospheric conditions. In addition, 10 of the 14 $V_{\theta max}$ data points with velocities > 200 fps (71%) were obtained under stable or near-neutral conditions. Thus, a stable atmosphere, in general, tended to promote vortices with high $V_{\theta max}$.

The numerical limits for the unstable, neutrally stable, and unstable segments of Ri are not well defined. This leads to some ambiguity in setting the Ri values that distinguish the stability categories. Several references list various limits for these three segments or bands. For example, Rosenberg (1970) stated: "Ri of zero is neutral stability, negative Ri is instability and positive Ri is stability" without providing further resolution as to the degree of atmospheric stability or instability. Lumley and Panofsky (1964) and Hanson (1967) also discussed Ri but did not set strict limits regarding the three stability regimes. For the study reported here, neutral stability was set at an Ri between -1 and 1.

The weak correlations observed in the Ri-$V_{\theta max}$ data set were not observed in a previous flyby test with military transport aircraft (Garodz and Clawson, 1991). Although the Ri correlations of the two studies did not agree, they both exhibited traits regarding Ri that are a result of complex study designs. When multiple primary factors affecting vortex behavior such

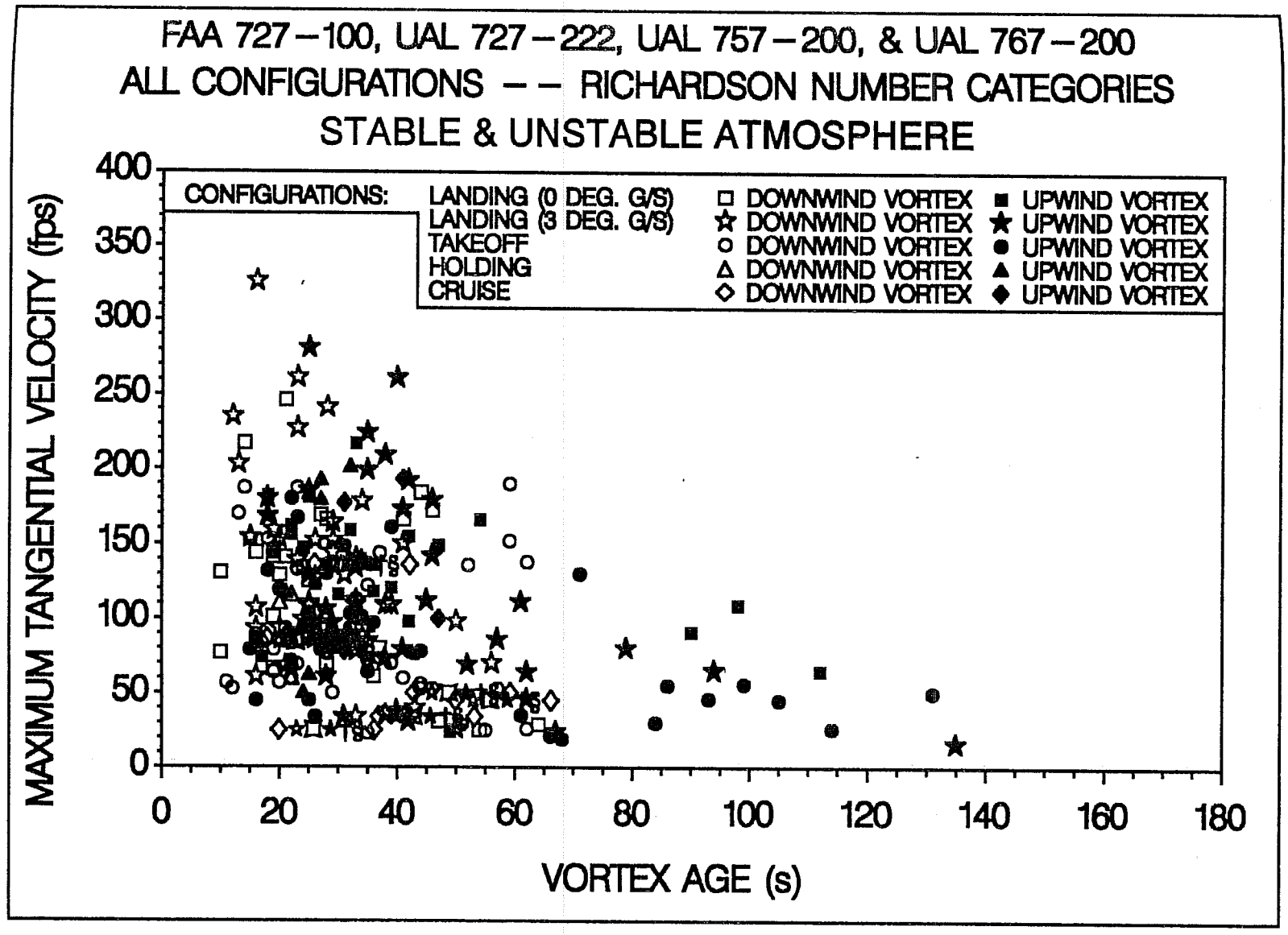

Figure 44. $V_{\theta max}$ as a function of age, stratified for atmospheric stability according to Ri for all test aircraft. Red and green symbols indicate stable and unstable atmospheric conditions, respectively.

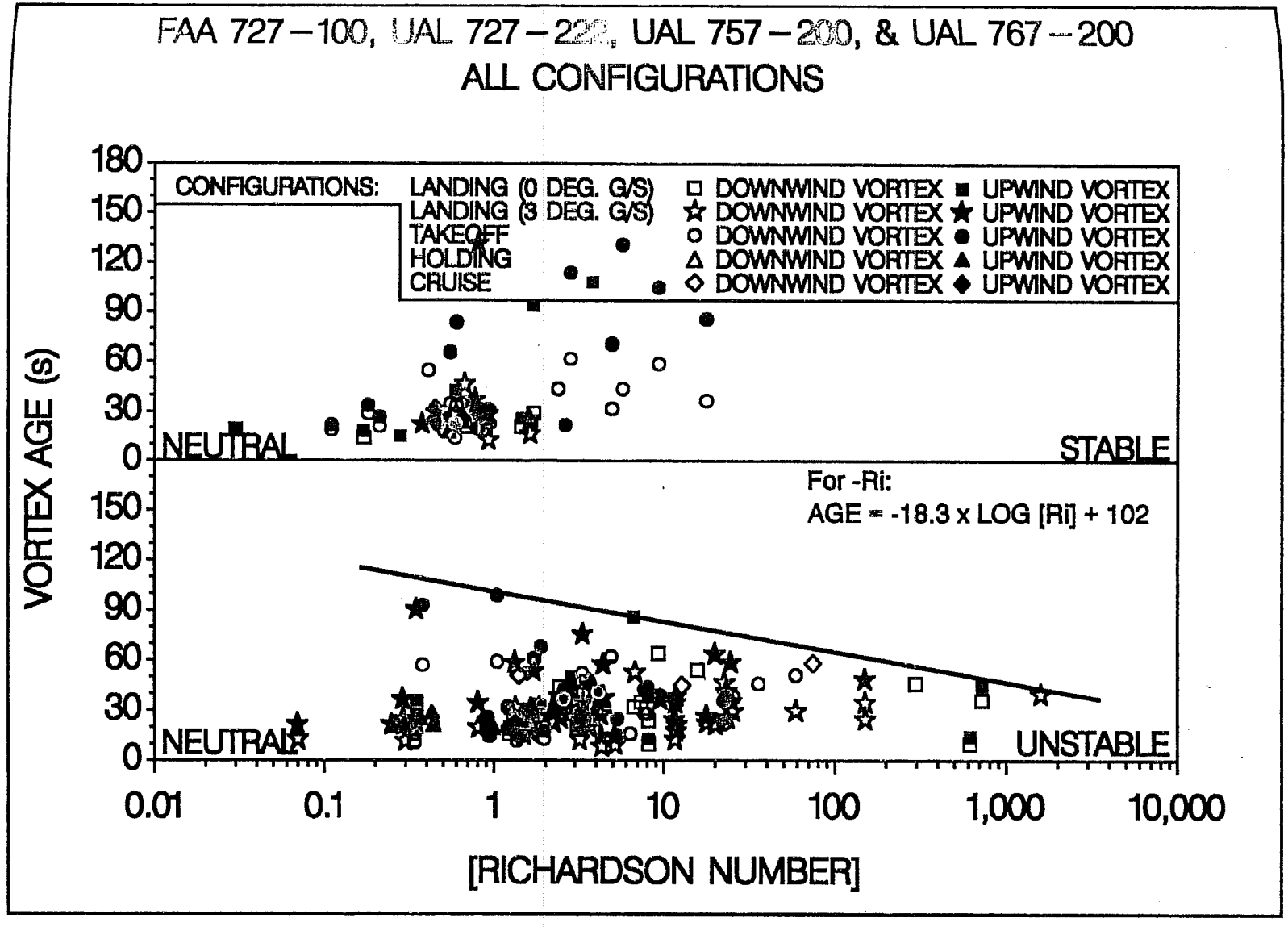

Figure 45. Vortex age as a function of Ri. Red, blue, and green symbols indicate B727-100/-222, B757-200, and B767-200 data, respectively. The data envelope in the unstable region is represented by the black line, as specified by the equation.

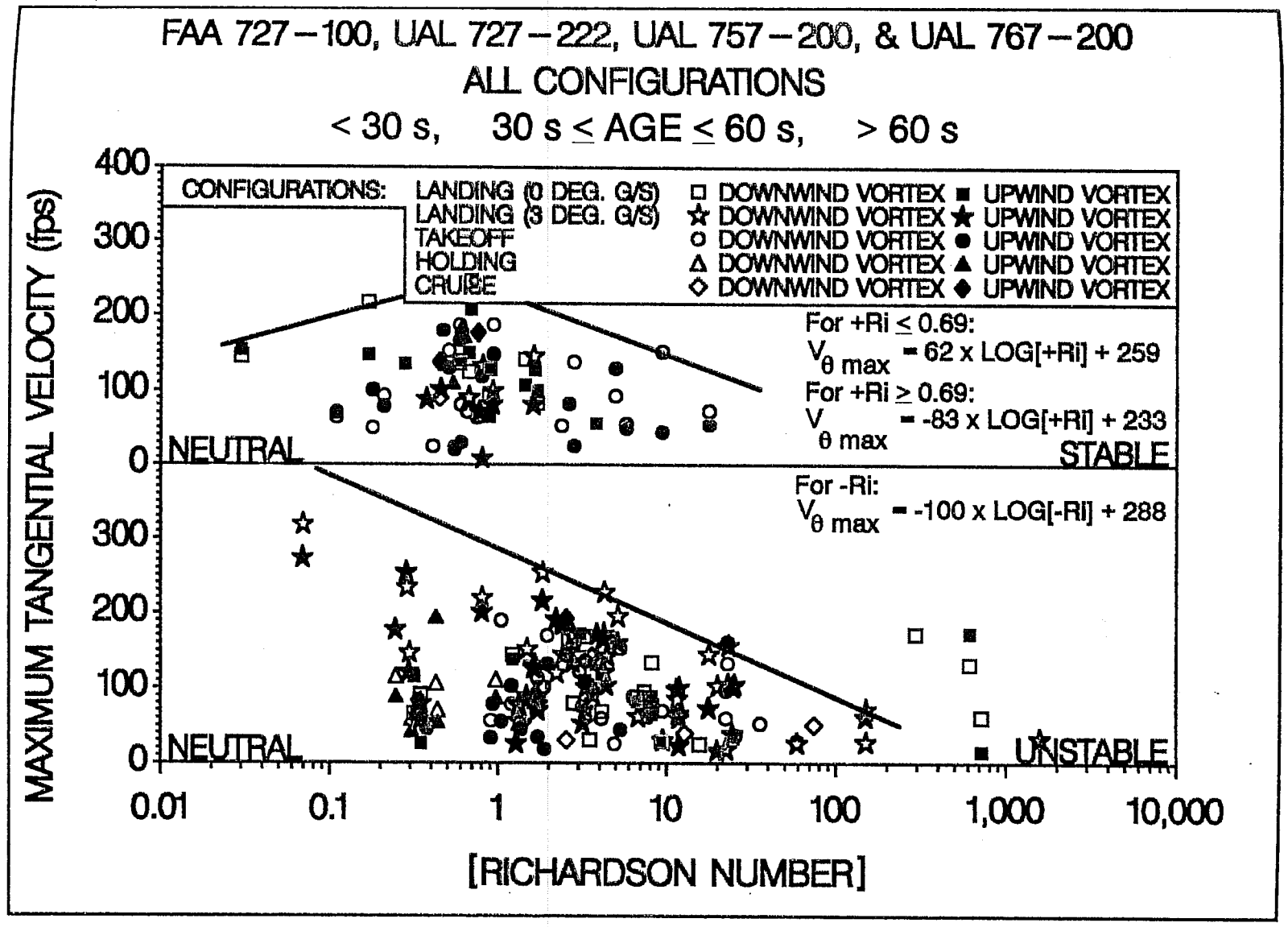

Figure 46. $V_{\theta max}$ as a function of Ri for all test aircraft. Red, blue, and green symbols indicate vortex ages < 30 s, from 30 to 60 s, and > 60 s, respectively. The data envelope is represented by the black lines, as specified by the equations.

as vortex age and aircraft configuration are allowed to vary along with secondary factors such as Ri, as was the case in both studies, a direct cause-and-effect relationship among the secondary factors can be difficult to determine. A better method for determining the direct effect of Ri on vortex persistence would be to obtain measurements of $V_{\theta max}$ at constant ages and aircraft configurations while permitting only Ri to vary. A varying Ri would occur naturally as the study progressed from near dawn through midday. A plan to examine Ri in this manner was considered during the formation of the program plan. However, the urgent need for obtaining an envelope of $V_{\theta max}$ and vortex persistence for the B757-200 and B767-200, together with the short-time availability of the test aircraft, precluded such a flight test operation.

Another factor that may have contributed to the weak correlation between Ri and vortex age may have been the short data averaging time. This constraint was forced by the location and operation of the general meteorological equipment. The tower-mounted sensors were placed to measure the same volume of airspace traversed by the vortices as they passed through the tower. Therefore, the sensors measured the additional disturbances to air temperature and wind speed that were created by the passing vortices. The passing vortices thereby temporarily contaminated the meteorological data. Longer averaging times on the order of 15-30 min would have provided a more reliable data set of undisturbed atmospheric conditions, which is normally required for proper use of Ri. However, this was not possible because only 6-8 min separated each flyby. Placing the sensors on another tower in the vicinity of the test tower would have prevented any vortex-induced meteorological data contamination.

Should Ri be found, after further study, to be a reliable and useful indicator of vortex persistence, an airport installation would most likely preclude the erection of tall meteorological towers. Shorter towers or remote sensing instruments would be required close to the runway Middle Marker (MM) or threshold area because of concern for aircraft obstruction clearance limits. The Low Level Wind Shear Alert System (LLWSAS) meteorological towers, for example, are only 20 ft above the extended runway surface. Forcing a calculation of Ri from data obtained so close to the ground may negate any correlation obtained using tall towers. An indication of atmospheric turbulence provided by Ri is particularly needed at the Outer Marker, normally about 1000 to 1200 ft AGL, where the ATC final approach controller normally establishes aircraft longitudinal separations based on the vortex hazard.

Vertical Air Temperature Gradient

Another index of atmospheric turbulence is $\Delta T/\Delta z$. Unlike Ri, the definitions for stable, unstable, and neutral atmospheric conditions for $\Delta T/\Delta z$ have been strictly defined by the U.S. NRC (1980). This index is also much easier to measure than Ri, and is also less susceptible to averaging errors during the short time periods required by this study. Thus, the ease of use, steadiness of the values, and widespread acceptance are advantages of $\Delta T/\Delta z$ over Ri.

A graph of $V_{\theta max}$ as a function of age and stratified by atmospheric stability as defined by the U.S. NRC (1980) from $\Delta T/\Delta z$ is shown in Figure 47. The plot revealed the same general trends regarding vortex age and $V_{\theta max}$ as was observed for Ri. That is, all long-lived vortices

and all high-intensity $V_{\theta max}$ values were generated under stable or neutral atmospheric conditions. However, more of the longer-lived and higher-velocity vortices were placed in the stable and neutral categories. The similar results obtained with Ri and $\Delta T/\Delta z$ were expected inasmuch as $\Delta T/\Delta z$ is included as one of the controlling variables in Ri [Equation (5)]. $\Delta T/\Delta z$, however, amplified the correlation between atmospheric turbulence and vortex age as well as the correlation between atmospheric turbulence and $V_{\theta max}$. All 13 of the vortices older than 70 s were generated in either stable or neutral atmospheric conditions. In addition, 86% of the vortices with $V_{\theta max} > 200$ fps were generated in either stable or neutral atmospheric conditions.

Vortex age as a function of $\Delta T/\Delta z$ is shown in Figure 48. The large amount of scatter in the data made development of direct statistically significant relationships through least-squares regression techniques impossible. Hence, vortex age was not a direct function of $\Delta T/\Delta z$. Nevertheless, the data envelope indicated a trend toward a maximum vortex age under slightly stable atmospheric conditions. Vortex age increased from 49 s at a $\Delta T/\Delta z$ of -4.99 °C/100 m to a maximum of 135 s at a $\Delta T/\Delta z$ of 0.64 °C/100 m. Vortex age then decreased to 31 s at a $\Delta T/\Delta z$ of 11.72 °C/100 m. No distinct effect of aircraft model was observed in the vortex age-$\Delta T/\Delta z$ data.

$V_{\theta max}$ was not directly related to the quantitative value of $\Delta T/\Delta z$, as illustrated in Figure 49. A statistical relationship through least-squares regression analyses again could not be determined because of the large scatter in the data. The relationship was only qualitative, similar to that observed for Ri. Relatively high $V_{\theta max}$ values were observed at conditions termed only slightly stable. $V_{\theta max}$ did not increase with a decrease in atmospheric turbulence as indicated by $\Delta T/\Delta z$ over the entire range of $\Delta T/\Delta z$. The $V_{\theta max}$ data envelope did, however, indicate that $V_{\theta max}$ increased with decreasing atmospheric turbulence from 182 fps in unstable conditions at a $\Delta T/\Delta z$ of -4.32 °C/100 m to 326 fps in slightly stable conditions at a $\Delta T/\Delta z$ of -0.17 °C/100 m. The $V_{\theta max}$ data envelope then declined in stable conditions to 177 fps at a $\Delta T/\Delta z$ of about 11.72 °C/100 m. Aircraft model did not appear to affect the age-$\Delta T/\Delta z$ relationship.

In general, $\Delta T/\Delta z$ provided a more useful indicator of atmospheric turbulence than did Ri. Its use is, therefore, recommended over that of Ri. $V_{\theta max}$ and vortex age exhibited similar responses to both Ri and $\Delta T/\Delta z$. That is, both $V_{\theta max}$ and vortex age increased in value as the atmosphere became less turbulent, until a maximum was reached under slightly stable atmospheric conditions. $V_{\theta max}$ and age then decreased as the atmosphere became more stable and less turbulent. More research is clearly needed, however, to elucidate the role of either Ri or $\Delta T/\Delta z$ in vortex intensity and persistence. This should be incorporated into a future study designed for only that purpose.

Yet another phenomenon was observed during the test periods in which a stable atmosphere was indicated on the basis of $\Delta T/\Delta z$. Temperature inversion conditions normally existed during the early morning hours before and immediately after sunrise. During these periods it was observed that the vortices descended through the inversion layer during their descent. A strong inversion did not appear to hinder their descent.

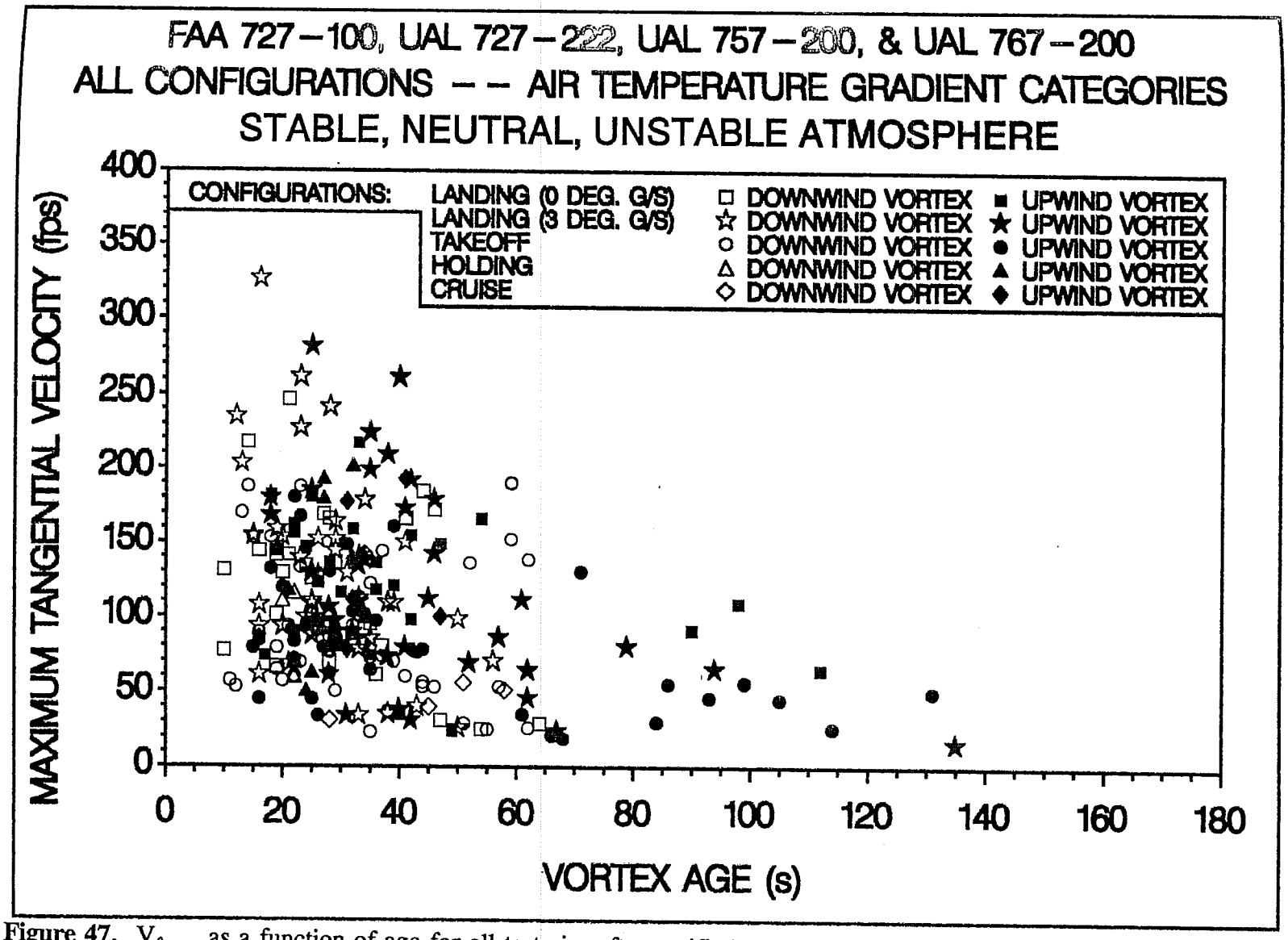

Figure 47. $V_{\theta max}$ as a function of age for all test aircraft, stratified by atmospheric stability as determined by $\Delta T/\Delta z$. Red, blue, and green symbols indicate stable, neutral, and unstable atmospheric conditions, respectively.

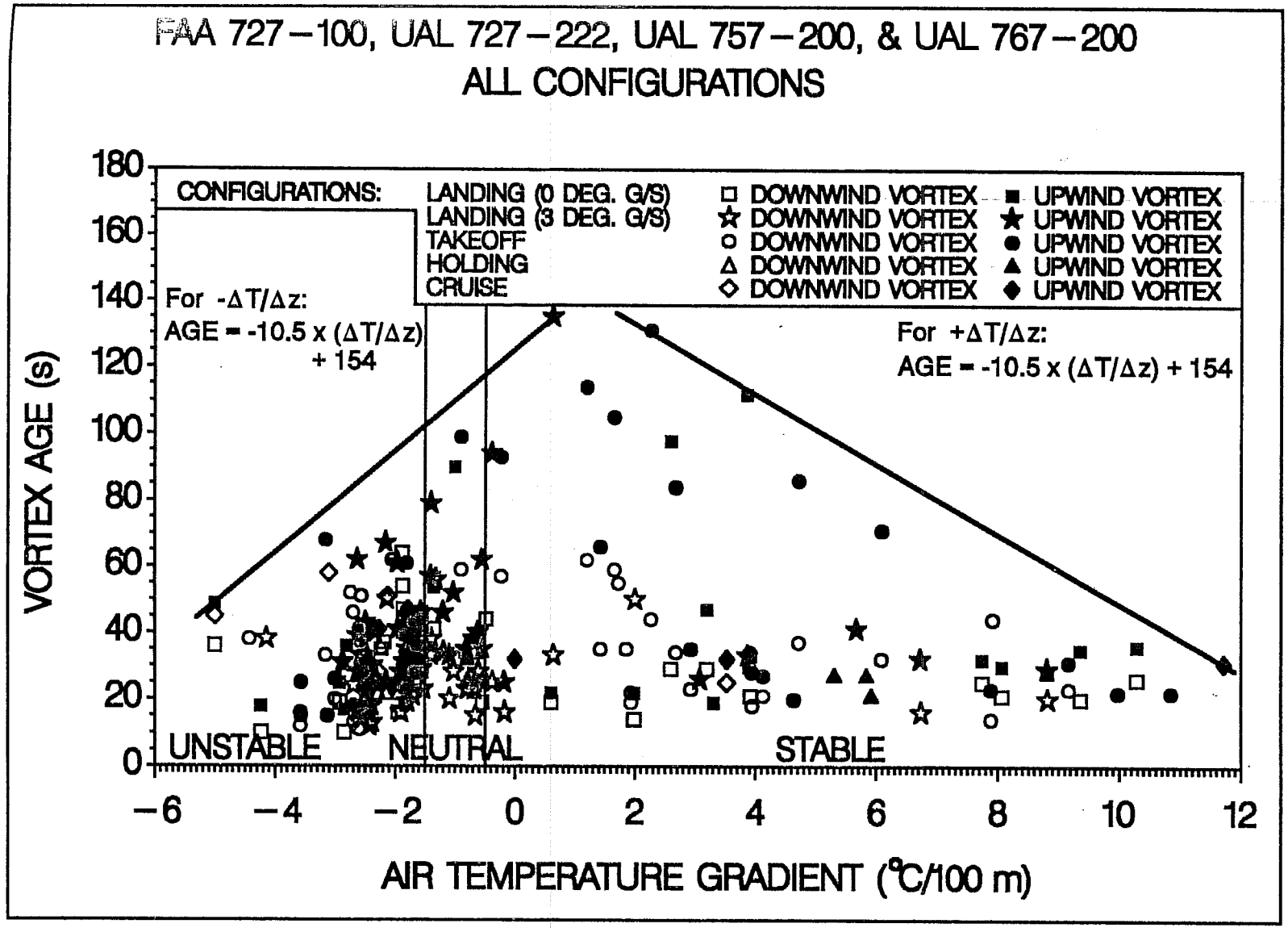

Figure 48. Vortex age as a function of air temperature gradient (ΔT/Δz). Red, blue, and green symbols indicate B727-100/-222, B757-200, and B767-200 data, respectively. The data envelope is represented by the two black lines, as specified by the equations.

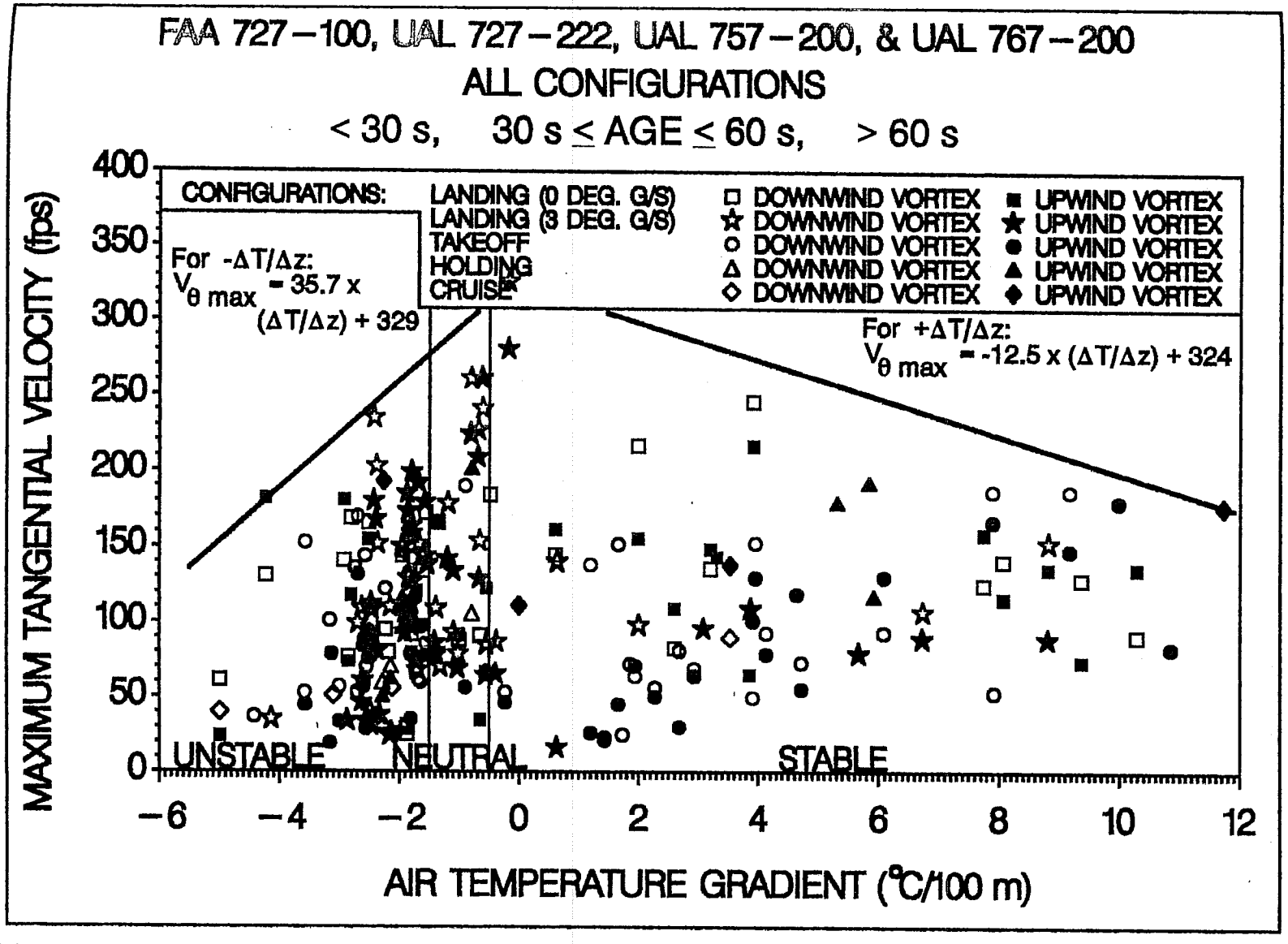

Figure 49. $V_{\theta max}$ as a function of $\Delta T/\Delta z$. Red, blue, and green symbols indicate vortex ages < 30 s, from 30 to 60 s, and > 60 s, respectively. The data envelope is represented by the two black lines, as specified by the equations.

Ambient Wind Speed

Another part of the Ri equation is the wind speed gradient with height. It appears in the denominator of Equation (5) and is an important contributor to atmospheric turbulence. Because wind speed is related to wind speed gradient (a correlation coefficient of 0.77 was obtained for this study), a simple wind speed measurement can be used as an indicator of atmospheric turbulence. Ambient wind speed has been correlated with vortex age in previous experiments with moderate success. Garodz (1970) and Garodz and Clawson (1991) are examples. The wind speed from the sensor placed at 200 ft was selected for the correlations presented here.

$V_{\theta max}$ as a function of vortex age and stratified according to three wind speed categories is shown in Figure 50. Red symbols indicate $V_{\theta max}$ values from flybys when the wind speed was less than 5 kt, green symbols indicate wind speeds greater than 10 kt, while blue symbols represent wind speeds between and including 5-10 kt. All vortices older than 85 s were generated when the wind speed was less than 5 kt. In addition, all vortices older than 35 s were generated when the ambient wind speed was less than or equal to 10 kt. A wind speed relationship was also observed for $V_{\theta max}$. All vortices with $V_{\theta max} > 200$ fps except one were generated in the wind speed range of 5-10 kt. A higher ambient wind speed and accompanying greater wind shear tended to promote vortex decay. This was indicated by the preponderance of green symbols ($V_{\theta max}$ data collected with the ambient wind speed > 10 kt) at ages below 40 s. However, low wind speeds indicated less atmospheric turbulence and tended to promote vortex longevity. This was indicated by the preponderance of red symbols ($V_{\theta max}$ data collected with the ambient wind speed < 5 kt) at ages above 25 s. $V_{\theta max}$ data collected with moderate ambient wind speeds between 5 and 10 kt (blue symbols) were spread between vortex ages of 10 and 85 s.

The relationship between vortex age and ambient wind speed is more clearly seen in Figure 51. The most persistent vortices were generated in the 3-5 kt ambient wind speed band. An attempt to determine a direct statistically significant relationship through least-squares regression techniques was again made futile because of the large scatter in the data. No distinct aircraft model effect was observed either. However, the data envelope was rather well defined, and was similar in shape to that observed for the $V_{\theta max}$-age envelope illustrated in Figure 42. Since the age-wind speed envelope exhibited the same shape, an exponential decay curve was fitted to those data as well. The equation [an appropriately modified Equation (6)] indicated a maximum vortex age of 210 s and a decay rate of -0.123. The line specified by that equation is shown in solid black in Figure 51. All the data fell either on the line or below it. Thus, at a given ambient wind speed, a vortex age is expected to be the same or less than that specified by the equation. This relationship could provide a fairly reliable indication of vortex hazard.

Also shown in Figure 51 is the data envelope presented by McGowan (1971), which is indicated by the stippled area. That envelope was constructed from both flyby data and vortex probe data. The envelope indicated much larger vortex ages at most wind speeds except those in the range of 3-5 kt. The new data also showed that the McGowan envelope did not extend

to very low wind speeds, i.e., less than 2 kt, or to young vortex ages in ambient wind speeds of 5-10 kt.

The upper limit of vortex ages as proposed by McGowan (1971) is indicated by the dashed line in Figure 51. That curve was much more conservative than the one specified by the data obtained during this study. Thus, the McGowan envelope and upper limit provided overestimates of actual vortex ages. The difference was as large as 55 s at an ambient wind speed of 10 kt.

$V_{\theta max}$ as a function of ambient wind speed is shown in Figure 52. No definitive and direct statistically significant effect of ambient wind speed on $V_{\theta max}$ could be determined through least-squares regression techniques because of the large scatter in the data. The data did lend themselves to the determination of a data envelope, as indicated by the black lines in Figure 52. The envelope increased from a $V_{\theta max}$ of 193 fps at an ambient wind speed of 0.8 kt, to a maximum of 326 fps at an ambient wind speed of 8.2 kt. $V_{\theta max}$ then declined to 162 fps at an ambient wind speed of 17.8 kt. No distinct airplane model effect was observed.

GLIDE SLOPE AND VORTEX BEHAVIOR

The results of the t-tests that were performed to determine the effect of glide slope on $V_{\theta max}$ are summarized in Table 12. The first set of tests were conducted on $V_{\theta max}$ from adjoining 0 and 3° G/S flybys. Not enough data were collected to permit testing aircraft model effects. Therefore, only vortex position (either downwind or upwind) data were subjected to the statistical tests along with the combined data set. Table 12 lists the average test differences in $V_{\theta max}$ that were calculated by subtracting $V_{\theta max}$ in the 3° G/S flyby from $V_{\theta max}$ in the 0° G/S flyby. Thus, a negative difference indicates a smaller $V_{\theta max}$ from the 0° flybys than $V_{\theta max}$ from the 3° flybys. Also given in Table 12 in parentheses are the number of paired data points used in each analysis. Maximum and minimum differences are also provided in brackets.

The downwind vortex and the combined vortex differences for flyby pairs indicated that, on the average, the vortices obtained from the 3° G/S were slightly more intense than those obtained during level flight. However, the differences were small and statistically insignificant, even at α=0.10. The range from minimum to maximum was large, which indicated that the scatter in the data was large as well. On the other hand, the average difference for the upwind vortex indicated that $V_{\theta max}$ obtained in level flight was more intense than in a 3° G/S. The difference was also small, the scatter in the data was large, and was statistically insignificant.

The large scatter in the data was mainly caused by diverse vortex ages. Some of the flyby-paired $V_{\theta max}$ data were as much as 79 s apart in age. The effect of age on $V_{\theta max}$ is well known. It was discussed in a previous section and illustrated in Figures 41 and 42. Hence, a t-test was designed to measure the effect of the 3° G/S by accounting for the effect of vortex age. This was accomplished by averaging $V_{\theta max}$ values in 5-s age blocks and comparing the resulting differences. This comparison is given in Table 12 under the t-test type labeled "Age Pairs."

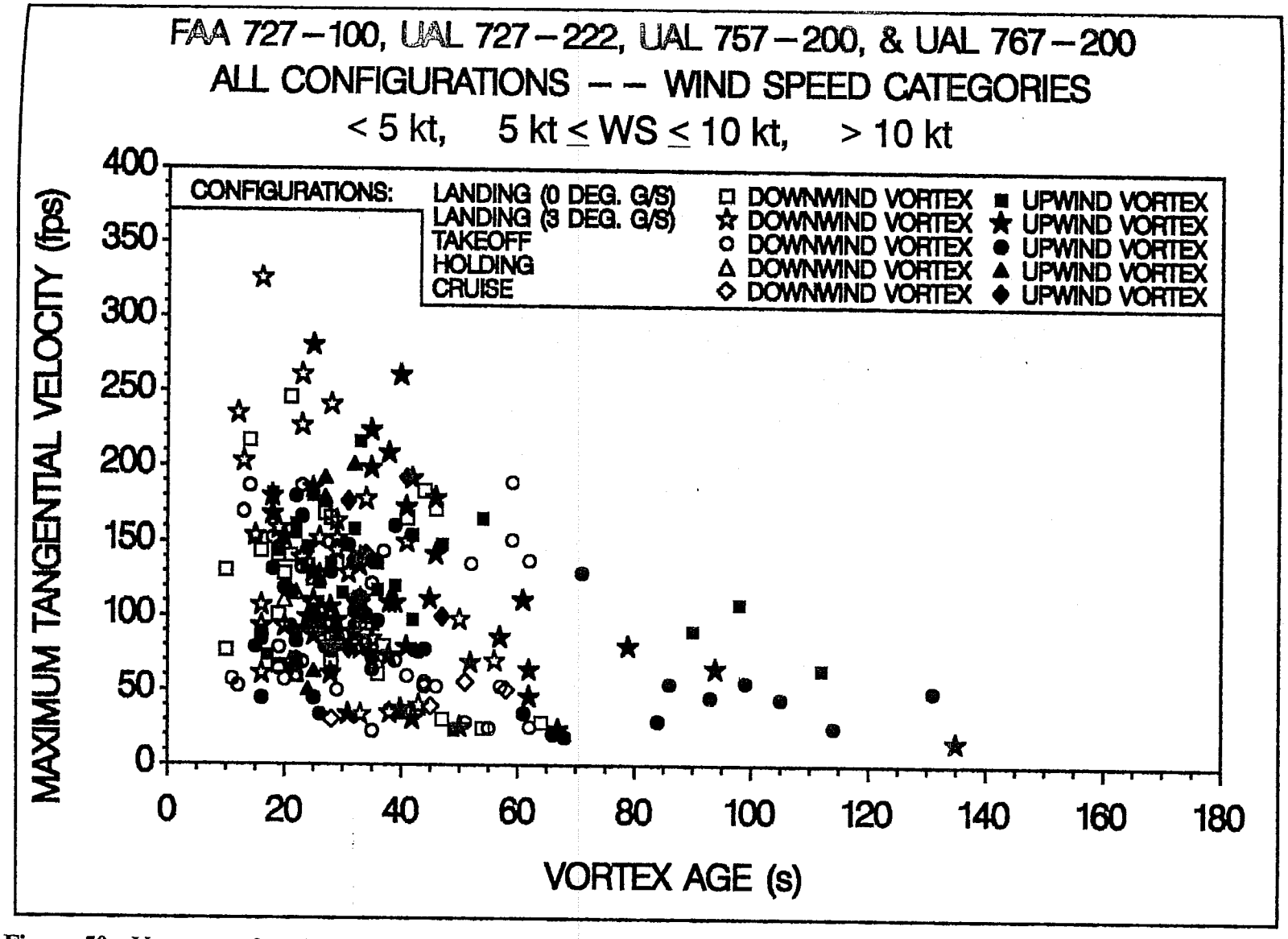

Figure 50. $V_{\theta max}$ as a function of age for all test aircraft, stratified by ambient wind speed ranges. Red, blue, and green symbols indicate wind speeds < 5 kt, between and including 5-10 kt, and > 10 kt, respectively.

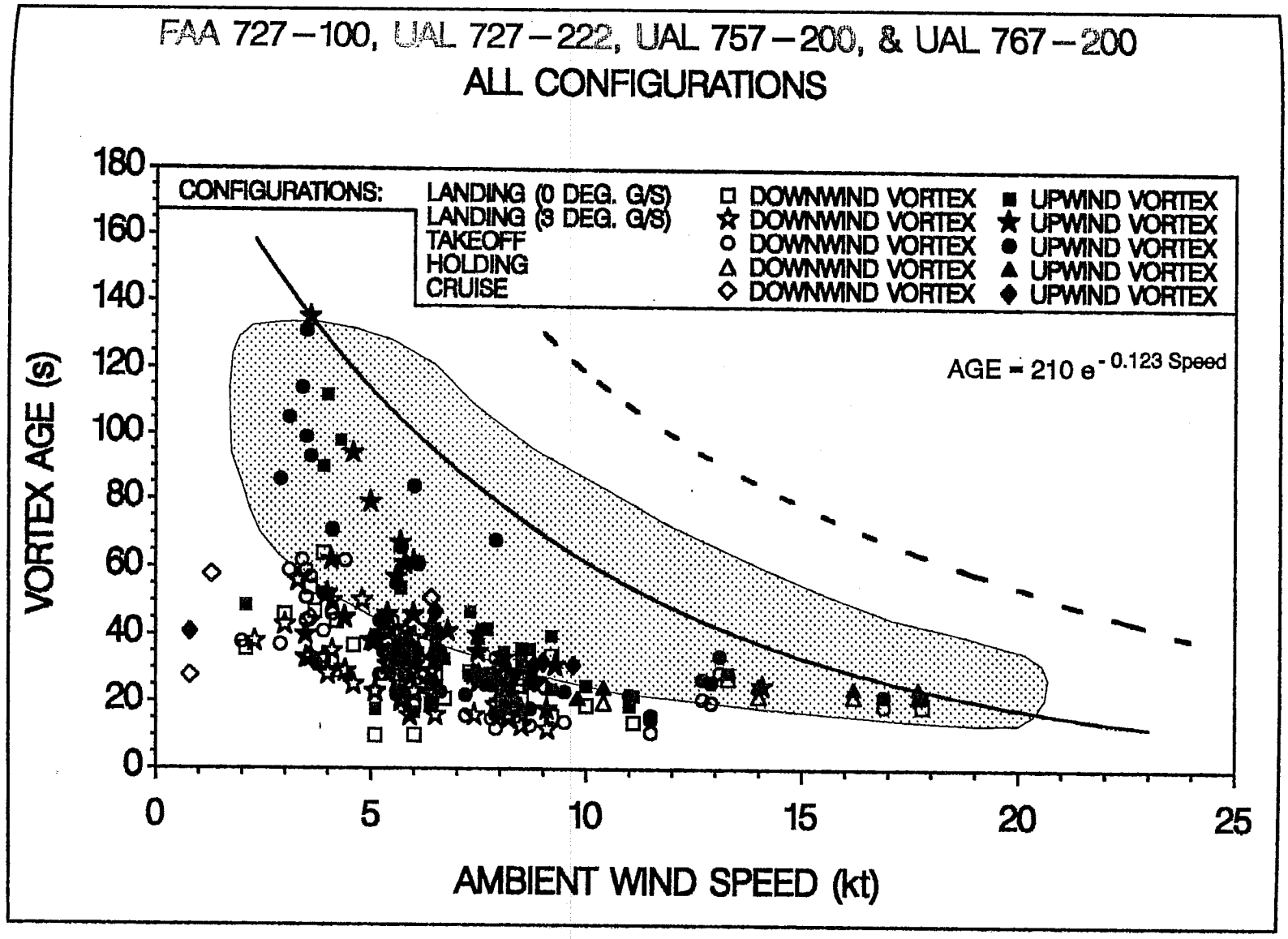

Figure 51. Vortex age as a function of ambient wind speed. Red, blue, and green symbols indicate B727-100/-222, B757-200, and B767-200 data, respectively. The solid line indicates the exponential equation encompassing all the data as given by the equation. The stippled area represents the data scatter from McGowan (1971). The dashed line, also from McGowan (1971), represents his expected maximum data envelope from future flight tests.

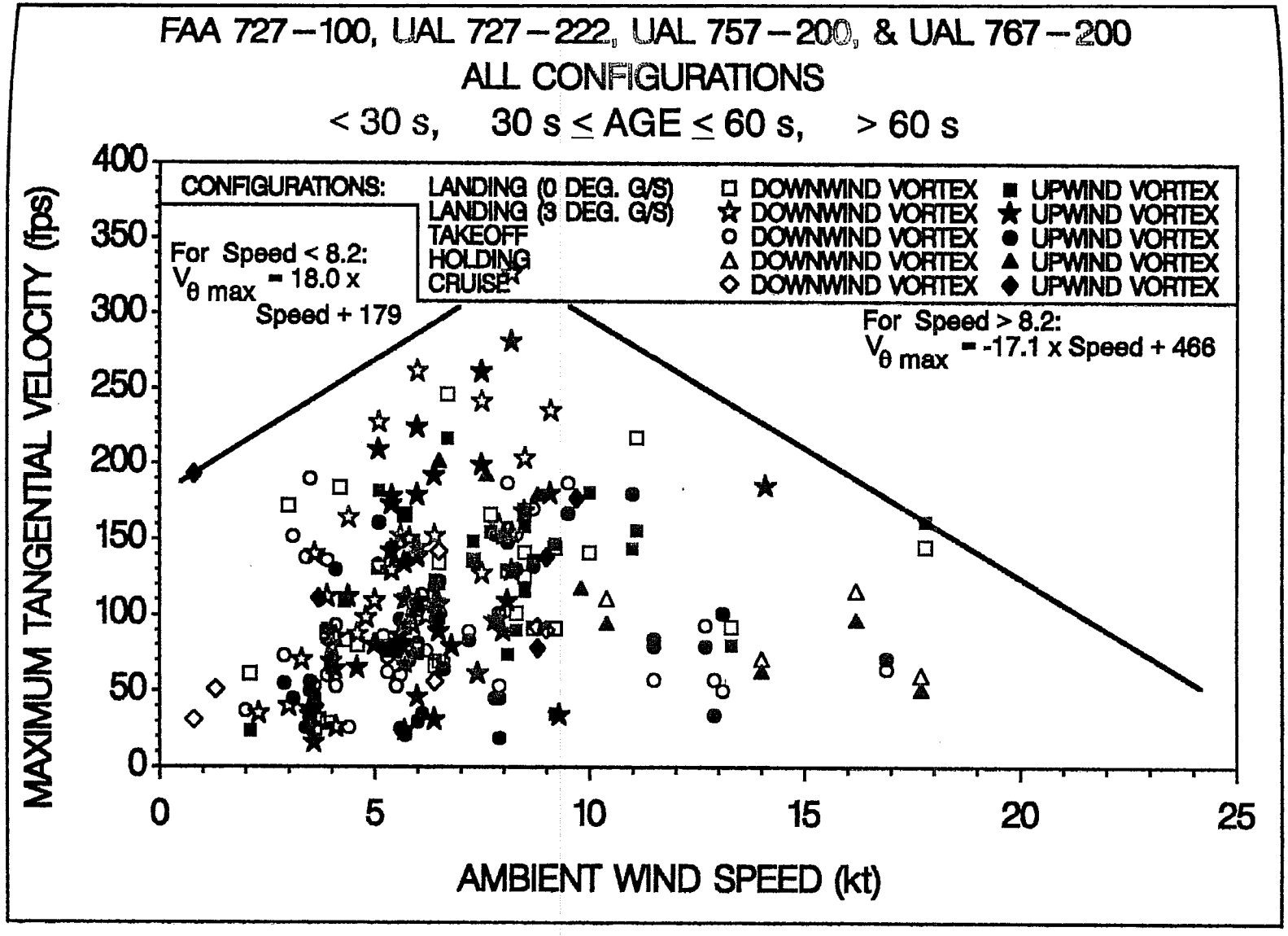

Figure 52. $V_{\theta max}$ as a function of ambient wind speed. Red, blue, and green symbols indicate vortex ages < 30 s, from 30 to 60 s, and > 60 s, respectively. The data envelope is represented by the black lines, as specified by the equations.

Table 12. Average $V_{\theta max}$ difference of 0° minus 3° G/S data paired according to flyby or vortex age criteria. Numbers in parentheses and brackets are the number of data points in the analysis and the minimum and maximum $V_{\theta max}$ in each category, respectively.

t-Test Type	Downwind Vortex Difference (fps)	Upwind Vortex Difference (fps)	Combined Data Difference (fps)
Flyby Pairs	-13.4 (20) [-135 to 107]	5.63 (16) [-125 to 147]	-4.9 (36) [-135 to 147]
Age Pairs	-7.7 (68) [-45.0 to 59.8]	-10.3 (57) [-40.7 to 88.5]	5.1 (125) [-26.7 to 44.0]

The age-averaged $V_{\theta max}$ data obviously overcame the age factor, as exemplified in the distinct $V_{\theta max}$ change observed for the upwind vortices. Both the upwind and downwind age-averaged $V_{\theta max}$ data indicated that the 3° G/S produced slightly stronger vortices than did level flight. The differences were again small and statistically insignificant. On the other hand, the overall age-averaged $V_{\theta max}$ data indicated that level flight produced stronger $V_{\theta max}$, although not significantly so. Thus, the data did not conclusively show that either level flight or a 3° G/S produced statistically stronger vortices. It must, therefore, be concluded that there is no significant difference in vortex intensity between 3° G/S and level flight at identical aircraft speeds and altitudes.

A similar statistical test was conducted on vortex age with nearest-neighbor flybys. Although the ages were widely divergent, no significant differences were found due to G/S flight. The average vortex age differences (level flight minus 3° G/S) for the downwind, upwind, and combined data were, in order: -0.7, -1.1, and -0.8 s.

These results can be substantiated by manipulating the vortex circulation (2). Lift (L) is equal to the normal load factor (n) multiplied by aircraft weight (W), which is part of the numerator of Equation (2). L is part of the coefficient of lift (C_L):

$$C_L = \frac{L}{\frac{1}{2}\rho V^2 S}, \tag{13}$$

where S is aircraft wing area and all other variables are as previously defined. An appropriate substitution yields

$$\Gamma = \frac{4}{\pi}\frac{cC_L V}{2}, \tag{14}$$

where c is the mean wing aerodynamic chord. C_L is also a function of aircraft angle of attack (α):

$$C_L = \frac{\delta C_L}{\delta \alpha}(\alpha - \alpha_o). \tag{15}$$

The test aircraft were flown at identical approach speeds and at nearly the same angles of attack during both level and 3° G/S approaches. Therefore, according to Equation (14), C_L remains nearly constant with small change in α. Thus, circulation or $V_{\theta max}$ should not be affected by minor changes in G/S.

These results contradict a previous investigation by Kurkowski et al. (1976). They analyzed test pilot reports of vortex-probing aircraft following a B727-222. The vortex wakes appeared to be more intense when the generating aircraft was in descending flight rather than in climbing flight for similar gross weights, aircraft configurations, and air speeds. It was assumed that the contributing force was jet engine thrust. However, a previous tower flyby study using a Convair 880 (Garodz, 1970) showed that engine thrust did not affect vortex intensity. This conclusion was based on test procedures that required two engines on one wing to be at approximately idle thrust while the two engines on the opposite wing had the thrust increased to maintain air speed and altitude. Furthermore, Smith (1975), Barber et al. (1977), and Patterson and Jordan (1977) showed experimentally that when engine thrust and flap vortex wakes are directly in line, engine thrust can attenuate vortex intensity.

MISCELLANEOUS VORTEX CHARACTERISTICS

Two other vortex characteristics can be easily computed from the flyby data set, namely vortex advection rate and vortex descent rate. Vortex advection rate is the time required for a vortex to arrive at the tower after it has been produced. Vortex descent rate is the speed at which the vortex descends vertically along the path from the generating aircraft until it arrives at the tower.

Vortex Advection Rate

Vortex advection rate as a function of ambient wind speed is shown in Figure 53. The graph includes a 1:1 line for reference together with a line representing a linear least-squares regression equation for the data. The analysis of variance specified that 68% of the scatter in the vortex advection rate was explained by the ambient wind speed. The equation specified that the vortex advection rate was approximately one-half that of the ambient wind speed. No differences in the advection rate were observed either for aircraft model or for vortex position, i.e., downwind or upwind. A larger scatter in the data was observed at wind speeds less than 8 kt. This is consistent with a greater meander of the vortices under light wind speed conditions.

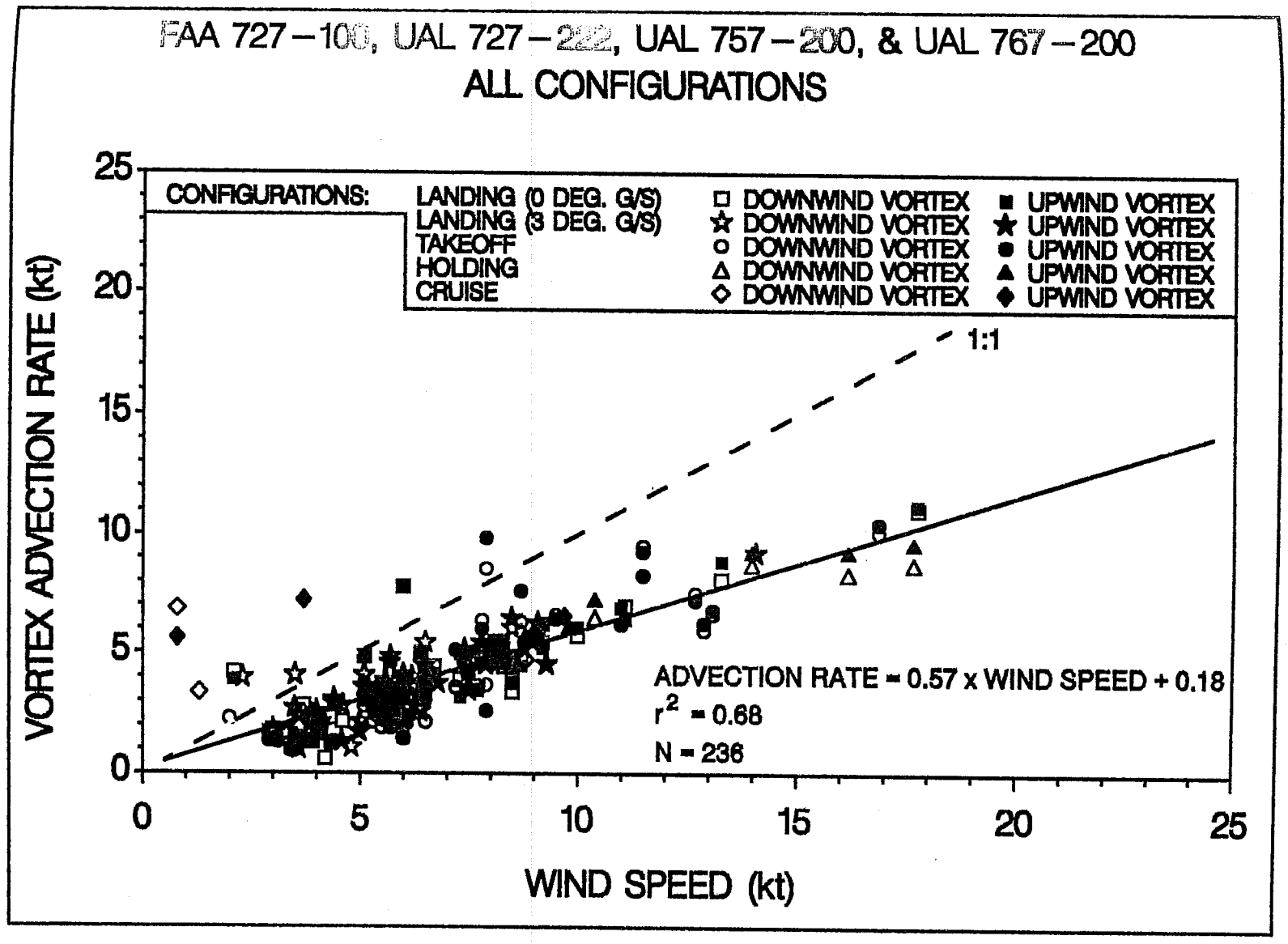

Figure 53. Vortex advection rate as a function of ambient wind speed. Red, blue, and green symbols indicate B727-100/-222, B757-200, and B767-200 data, respectively. The 1:1 line is indicated by the dashed line, while the least-squares linear fit is given by the solid line as specified by the accompanying equation.

The vortex advection rate can be used in conjunction with the vortex decay rate to evaluate current or proposed runway separation standards. The FAA has mandated that independent adjoining runway operations can only be conducted when the runways are laterally separated by a distance of at least 2500 ft. Table 13 lists the advection times for a distance of 2500 ft calculated from the vortex advection rate equation for all test aircraft given in Figure 53 for a range of crosswind speeds. Advection times ranged from 489 s for a 5 kt crosswind to 103 s for a 25 kt crosswind, which is the maximum allowable crosswind speed. Advection times were then equated to vortex ages, assuming that a vortex was generated at the threshold of a runway some 2500 ft upwind. The vortex ages were then used to determine $V_{\theta max}$ for the various crosswinds. The calculated values are also given in Table 13. $V_{\theta max}$ was calculated from the $V_{\theta max}$ envelope decay equation for all vortex data given in Figure 42 ($V_{\theta max} = 468\ e^{-0.0149\ t}$). Estimated $V_{\theta max}$ ranged from 0 fps for a 5 kt crosswind to 102 fps for a 25 kt crosswind.

The calculated $V_{\theta max}$ values indicate that for crosswinds of 10 kt or less, a vortex advected for a distance of 2500 ft would have no significant rotational velocity. For crosswinds of 15 kt or more, a vortex advected for the same 2500 ft distance would exhibit a $V_{\theta max}$ with significant rotational velocity on the parallel runway. However, the $V_{\theta max}$ values predicted for 20- and 25-kt crosswinds are outside of the measured wind speed range. Furthermore, the $V_{\theta max}$ values predicted for 5, 10, and 15 kt crosswinds are based on calculated vortex ages older than the vortex ages actually observed during the study. Therefore, the predicted $V_{\theta max}$ values must be evaluated with caution. The values in Table 13 also do not account for the decay caused by increased turbulence under high wind conditions. Figure 52 illustrated the $V_{\theta max}$ envelope as a function of ambient wind. It is possible that vortices advected for 2500 ft may exhibit no significant rotational velocity once $V_{\theta max}$ decay is accounted for at the higher crosswind speeds. This is only a supposition, since the estimated values reported here were not designed to directly investigate this particular aspect of vortex decay.

Vortex Descent Rate

Calculated vortex descent rates ($\dot{z}_v$), which invoked Equation (4), were used to determine the initial test aircraft flyby height such that a vortex pair would advect into the 200-ft test tower at an appropriate height. Actual descent rates are shown in Figure 54. The vertical lines in Figure 54 show the expected descent rates for each aircraft in the clean (flaps retracted) and dirty (flaps extended) configurations, as given in Table 2 and calculated from Equation (4). The values in Table 2 are considered to be indicative of vortex descent rates that occur immediately after initial vortex formation. The horizontal lines show the estimated altitude of the onset of ground effect for the test aircraft in the clean or dirty configurations as calculated from Equation (4).

The data exhibited a large amount of scatter. This was probably caused by the action of ambient air turbulent activity or Crow-instability. However, the calculated $\dot{z}_v$ values provided a good estimate of the maximum $\dot{z}_v$ for each test aircraft. The calculated values accurately described the data envelope. For each aircraft, whether in the clean or dirty configuration, the observed $\dot{z}_v$ never exceeded the corresponding calculated $\dot{z}_v$. Thus, Equation (4) can be used as a good predictor of maximum $\dot{z}_v$.

Table 13. Estimated vortex advection time and associated vortex intensity as a function of ambient wind speed for a 2500-ft advection distance.

Wind Speed (kt)	Estimated Advection Time (s)	Estimated $V_{\theta max}$ (fps)
5	489	0
10	252	11
15	170	37
20	128	69
25	103	102

The observed $\dot{z}_v$ values in the dirty configuration generally indicated an increase over those obtained in the clean configuration. Average observed $\dot{z}_v$ values for each test aircraft are given in Table 14. Equation (4) predicted the increase to be a maximum of 2.5, 2.5, and 3.1 fps, respectively, for the B727-100/-222, B757-200, and B767-200. The average observed increase in $\dot{z}_v$ caused by flap extension for the entire study was 1 fps. However, average observed increases in $\dot{z}_v$ caused by flap extension were recorded only for the B727-100/-222 and B757-200, with values of 2.5 and 1.1 fps, respectively. For the B767-200, average $\dot{z}_v$ actually decreased by 0.4 fps with extended flaps.

Apparently, the decreased distance between vortex pairs with flaps extended facilitated vortex downward movement to a large degree in the B727-100/-222 and only slightly in the B757-200. Perhaps the vortices are so far apart in the larger B767-200 that they cannot interact sufficiently to enhance vortex descent. Further research is needed to fully elucidate the factors involved in decreasing $\dot{z}_v$ in the larger aircraft.

The estimated height of the onset of ground effect also provided a good estimate for the lowest altitude to which the observed vortices descended. Two, three, and 10 vortices of the B727-100/-222, B757-200, and B767-200, respectively, descended below the value calculated by Equation (3). One, two, and six of those 15 vortices were downwind vortices. Thirteen of those vortices were generated by the aircraft in the dirty configuration. The two vortices that were generated in the clean configuration were produced by the B767-200 and were in the downwind position.

Table 14 contains the average tower intercept height (h_v) for each test aircraft in both the clean and dirty configurations. It also contains the average h_v for the entire study. The reduction in h_v with extended flaps was predicted to be 9, 11, and 20 ft for the B727-100/-222, B757-200, and B767-200, respectively. The overall average observed reduction in h_v for the entire study was only 3 ft. The average actual reductions were 19 and 5 for the B727-100/-222 and B757-200. The B767-200 average h_v actually increased in the dirty configuration by 14 ft.

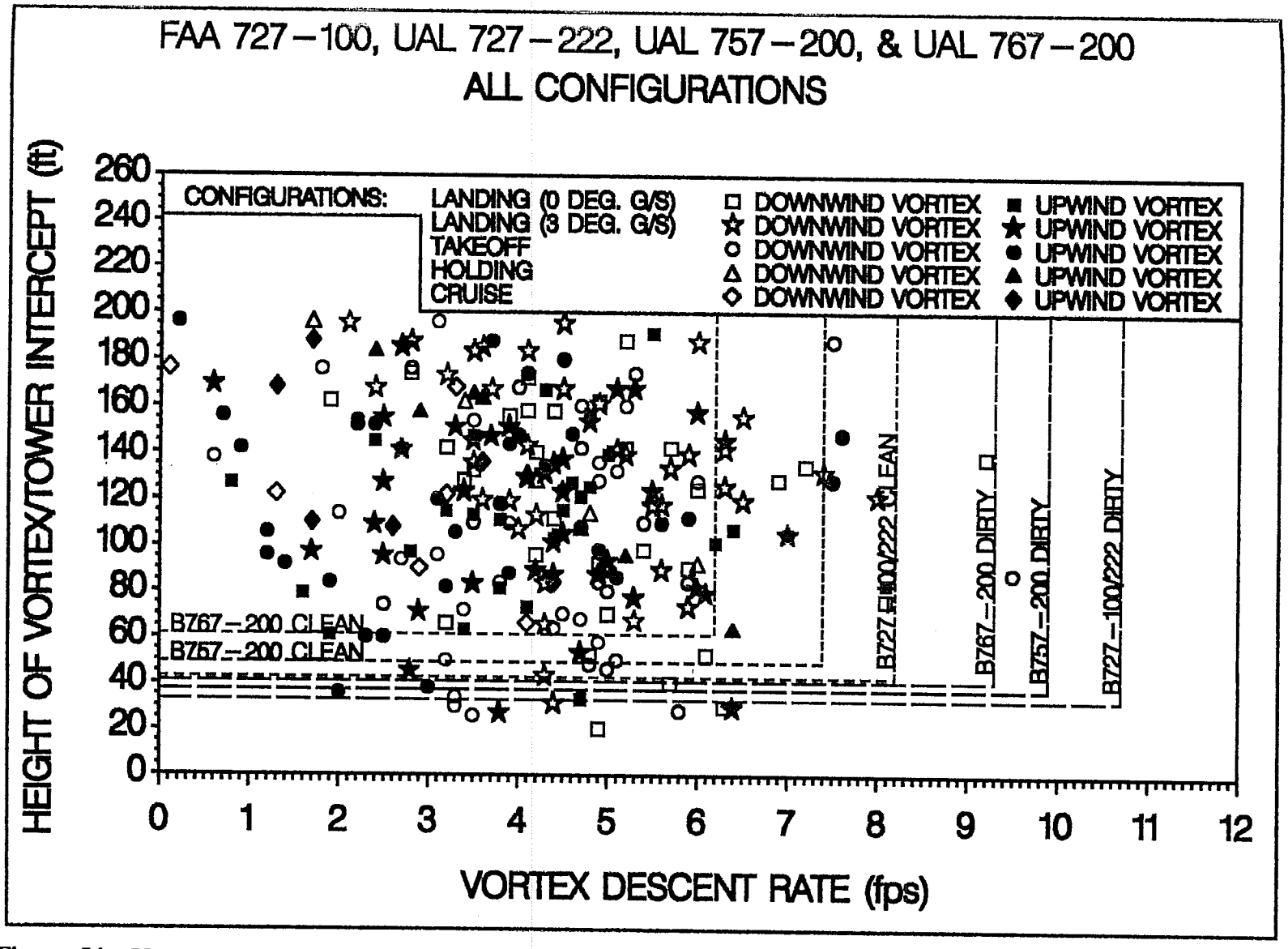

Figure 54. Vortex descent rate ($\dot{z}_v$) as a function of the height of interception with the tower. Red, blue, and green symbols and lines indicate B727-100/-222, B757-200, and B767-200 data, respectively. Horizontal dashed lines represent the calculated h_{vge} for each test aircraft as calculated from Equation (3). Vertical dashed lines represent the initial $\dot{z}_v$ calculated from Equation (4). Clean and dirty descriptors indicate aircraft with retracted and extended flaps, respectively.

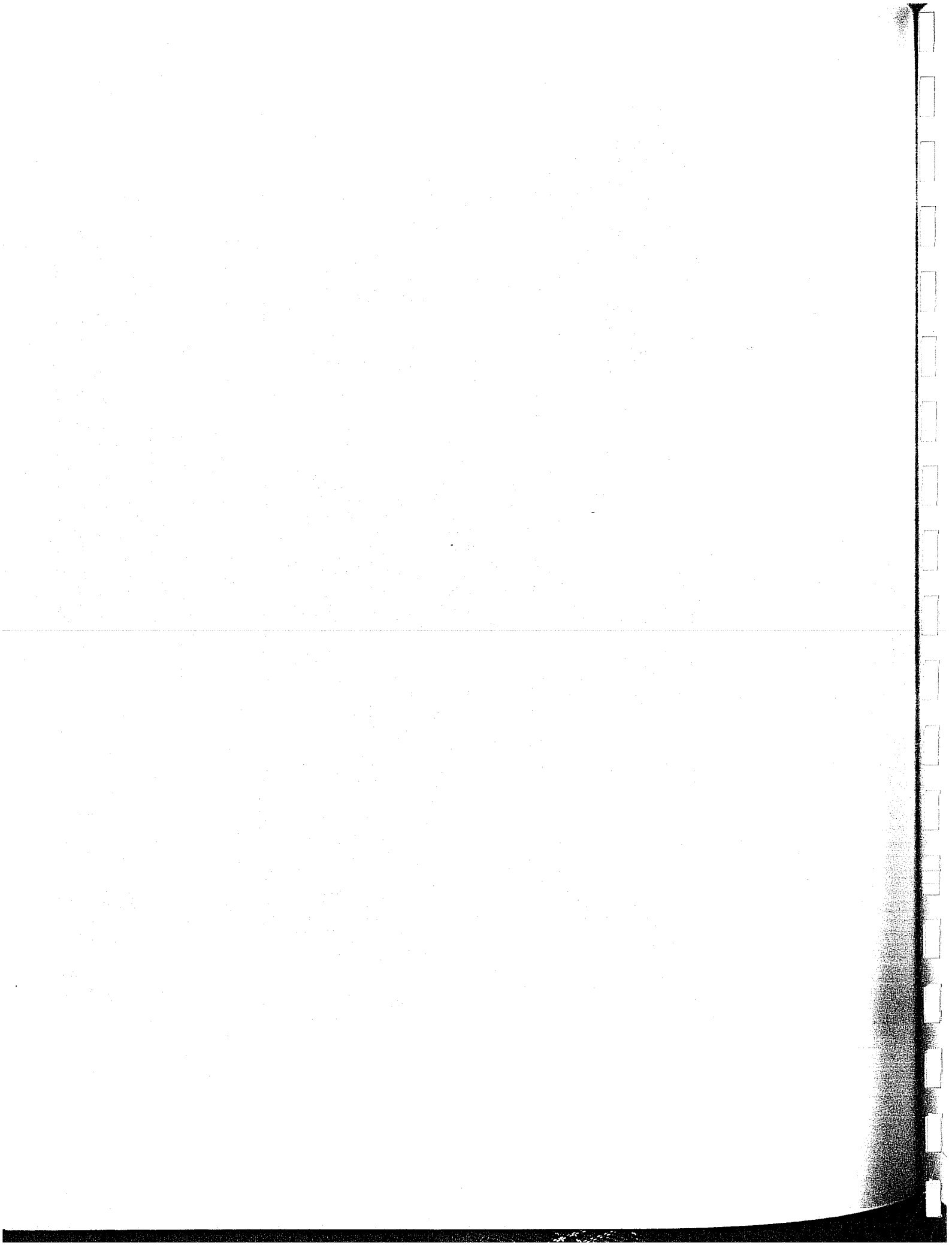

Table 14. Average observed vortex descent velocities ($\dot{z}_v$) and tower intercept heights (h_v) for the B727-100/-222, B757-200, and B767-200 with flaps retracted (clean) or extended (dirty).

Aircraft	$\dot{z}_{v\ clean}$ (fps)	$\dot{z}_{v\ dirty}$ (fps)	$h_{v\ clean}$ (ft AGL)	$h_{v\ dirty}$ (ft AGL)
B727-100/-222	2.6	5.1	138	119
B757-200	3.5	4.6	122	117
B767-200	3.7	3.3	104	118
All Aircraft	3.3	4.3	121	118

The observed h_v were, of course, largely dependent on advection rate, aircraft altitude, and aircraft distance from the tower.

VORTEX VELOCITY PROFILE MODELING

Vortex velocity profiles were modeled with the Hoffman-Joubert model specified in Equation (8). Figure 55 illustrates a vortex velocity profile together with the curve calculated from Equation (8) for flyby 10 of the B757-200. The data for this flyby and all other flybys are summarized in Appendix F. Graphs of each vortex velocity profile and associated curve, as represented by Figure 55, are given in Appendix G. The data always exhibited a logarithmic velocity distribution about the vortex core. The model fit vortex profiles with $V_{\theta max}$ values of $\geq$ 50 fps well, as indicated in Figure 55. The fit was not a good for vortex profiles with $V_{\theta max}$ values $<$ 50 fps.

Vortex Core Size

Vortex core radii were easily determined using the iterative approach. Core radii as small as 0.1 ft and as large as 3.0 ft were calculated, with the average core size at 0.6 ft. A summary of average vortex core sizes (r_c) is given in Table 15. Vortex cores from the downwind vortices were, on the average, only slightly larger than upwind vortices. However, the average difference of 0.5 inches was insignificant compared to the standard deviation of 5 inches.

Small vortex cores were consistently calculated for all test aircraft, even in configurations that involved landing flap deflection. Average r_c values generated in the landing configuration (both 0 and 3° G/S) were smaller than those generated in the takeoff configuration. However, mean r_c differences were small and statistically insignificant when compared with to standard deviation of the r_c averages. Not enough vortices were measured in the holding and cruise configurations for a statistical comparison. The average sizes of the vortex cores were the same for the B727-100/-222 and B757-200, while they were slightly larger for the B767-200.

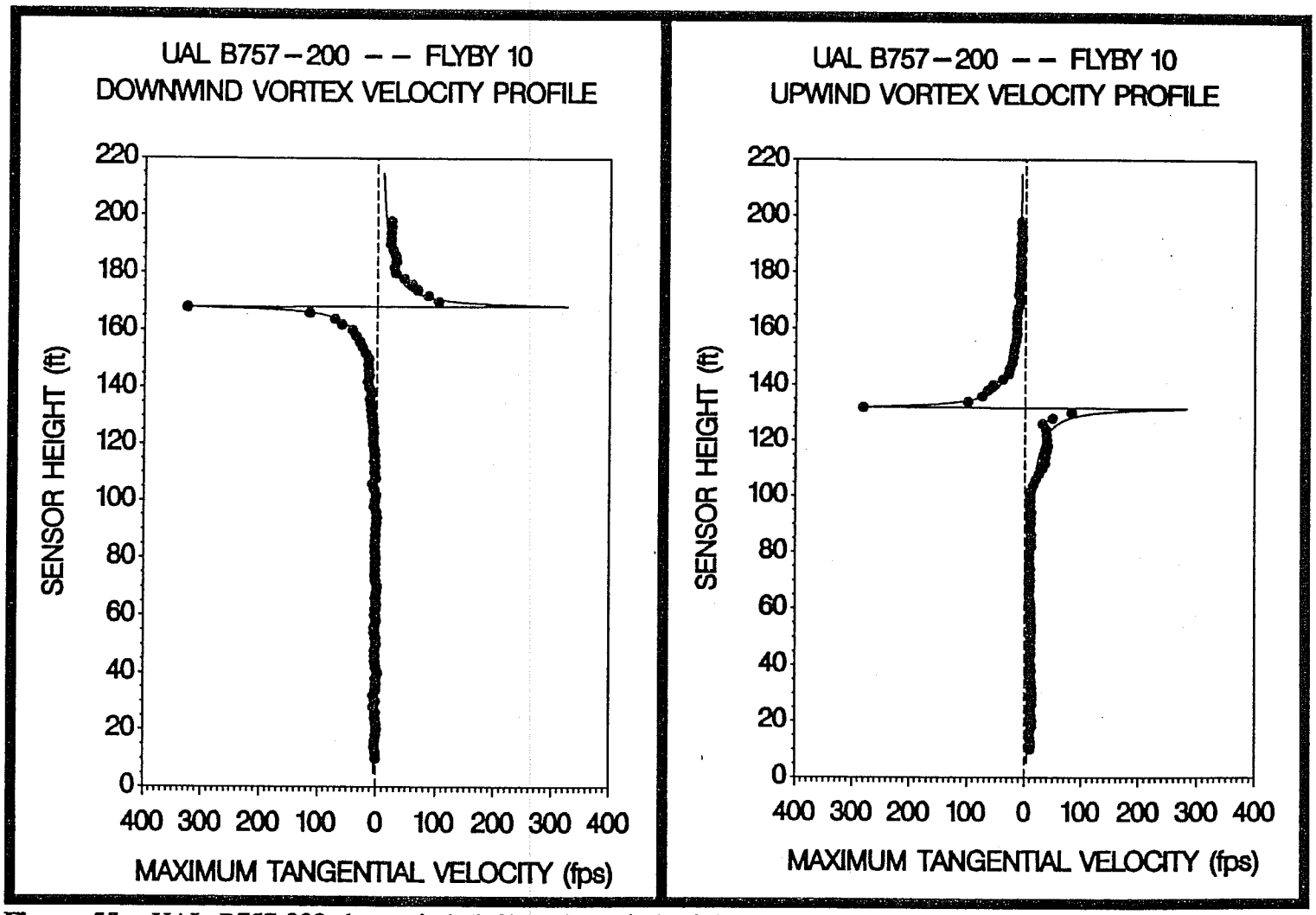

Figure 55. UAL B757-200 downwind (left) and upwind (right) vortex tangential velocity profiles at maximum intensity from Day of Year 268, Flyby 10, ambient wind speed=8.2 kt, δ_F=30°, IAS=134 kt, GW=191,000 lb. Ages, radii, and velocities of the vortex cores are 16 and 25 s, 0.2 and 0.3 ft, and 325.8 and 281.7 fps, respectively.

Table 15. Summary of average vortex core radii (r_c) calculated by iteration of Equation (8) for the B727-100/-222, B757-200, B767-200, and all test aircraft combined in the various flight configurations. Numbers in parentheses are the number of vortices included in the average.

Aircraft	Landing on 0° G/S (ft)	Landing on 3° G/S (ft)	Takeoff (ft)	Holding (ft)	Cruise (ft)	All Configurations (ft)
B727-100/-222	0.6 (30)	0.5 (20)	0.8 (9)	0.6 (9)	0.6 (5)	0.6 (73)
B757-200	0.4 (16)	0.4 (29)	0.9 (27)	0.4 (4)	0.3 (7)	0.6 (83)
B767-200	0.7 (12)	0.9 (29)	0.7 (37)	-- (0)	0.2 (1)	0.8 (79)
All Aircraft	0.5 (58)	0.6 (78)	0.8 (73)	0.5 (13)	0.4 (13)	0.6 (235)

Vortex core size was not directly related to vortex age, which is contrary to what might be expected. Analyses of variance associated with least-squares regressions on vortex size as a function of vortex age indicated that the two parameters were unrelated. A graph of vortex core size and vortex age is shown in Figure 56. Comparatively large r_c were calculated for the B757-200 on separate flybys at ages between 10 and 35 s. These were the largest r_c calculated, yet the B757-200 generated the smallest average r_c. The B727-100/-222 and B767-200 also exhibited relatively large r_c at young vortex ages compared with those at older vortex ages.

Vortex core size was not directly related to $V_{\theta max}$, as indicated by least-squares linear regression. However, the data envelope was described by an exponential curve of the form given in Equation (6), as shown in Figure 57. The curve followed the data envelope, which indicated relatively large r_c at small $V_{\theta max}$ and small r_c at large $V_{\theta max}$. Thus, a more intense vortex was accompanied by a small vortex core, regardless of aircraft model.

Vortex Circulation

Calculated average vortex circulation (Γ') at a vortex radius of 15 ft using Equation (12) ranged from a low of 140 ft^2/s to a high of 2336 ft^2/s. Minimum Γ' for the B727-100/-222, B757-200, and B767-200 were 157, 140, and 264 ft^2/s, respectively. Maximum Γ' were 1944, 2077, and 2336, in order. A summary of Γ' is contained in Table 16. The B757-200 exhibited the highest average Γ' of all aircraft at 1173 ft^2/s. This was attributable to high average Γ' in the two landing configurations in which Γ' from the B757-200 was approximately 10% larger than Γ' from the B767-200. In addition, the landing configurations produced the highest Γ' when averaged over all aircraft, as compared with the takeoff, holding, and cruise configurations.

A graph of Γ' as a function of vortex age is shown in Figure 58. Although no direct relationship could be determined, the data envelope exhibited a decrease in Γ' with an increase

in age. The B767-200 showed the slowest decline in Γ', followed by the B727-100/-222 and the B757-200. However, the data envelopes behaved according to expectation; i.e., the largest envelope was observed for the B767-200, followed by the B757-200 and then the B727-100/-222. Similar relationships were observed for Γ' at 30 and 45 ft radii. More detailed investigations could also have been conducted for Γ' similar to those conducted for $V_{\theta max}$, but they were outside of the scope of work.

Table 16. Summary of average circulation (Γ') for a vortex radius of 15 ft calculated using Equation (12) for the B727-100/-222, B757-200, and B767-200, and all test aircraft combined in the various flight configurations.

Aircraft	Landing on 0° G/S (ft^2/s)	Landing on 3° G/S (ft^2/s)	Takeoff (ft^2/s)	Holding (ft^2/s)	Cruise (ft^2/s)	All Configurations (ft^2/s)
B727-100/-222	1095	1010	1149	901	740	1030
B757-200	1282	1433	978	934	738	1173
B767-200	1140	1305	1028	--	884	1145
All Aircraft	1156	1277	1024	911	750	1119

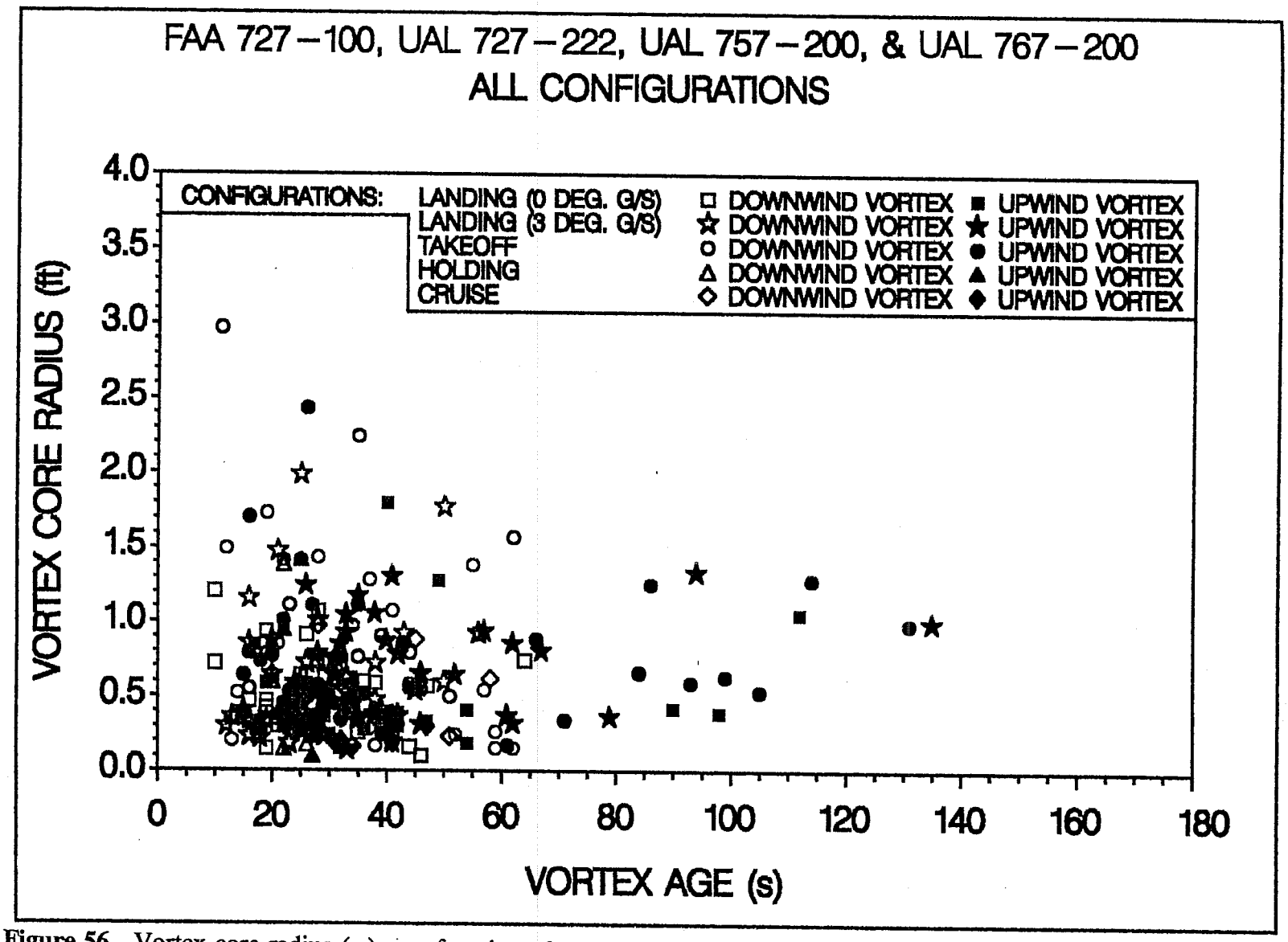

Figure 56. Vortex core radius (r_c) as a function of vortex age. Red, blue, and green symbols indicate B727-100/-222, B757-200, and B767-200 data, respectively.

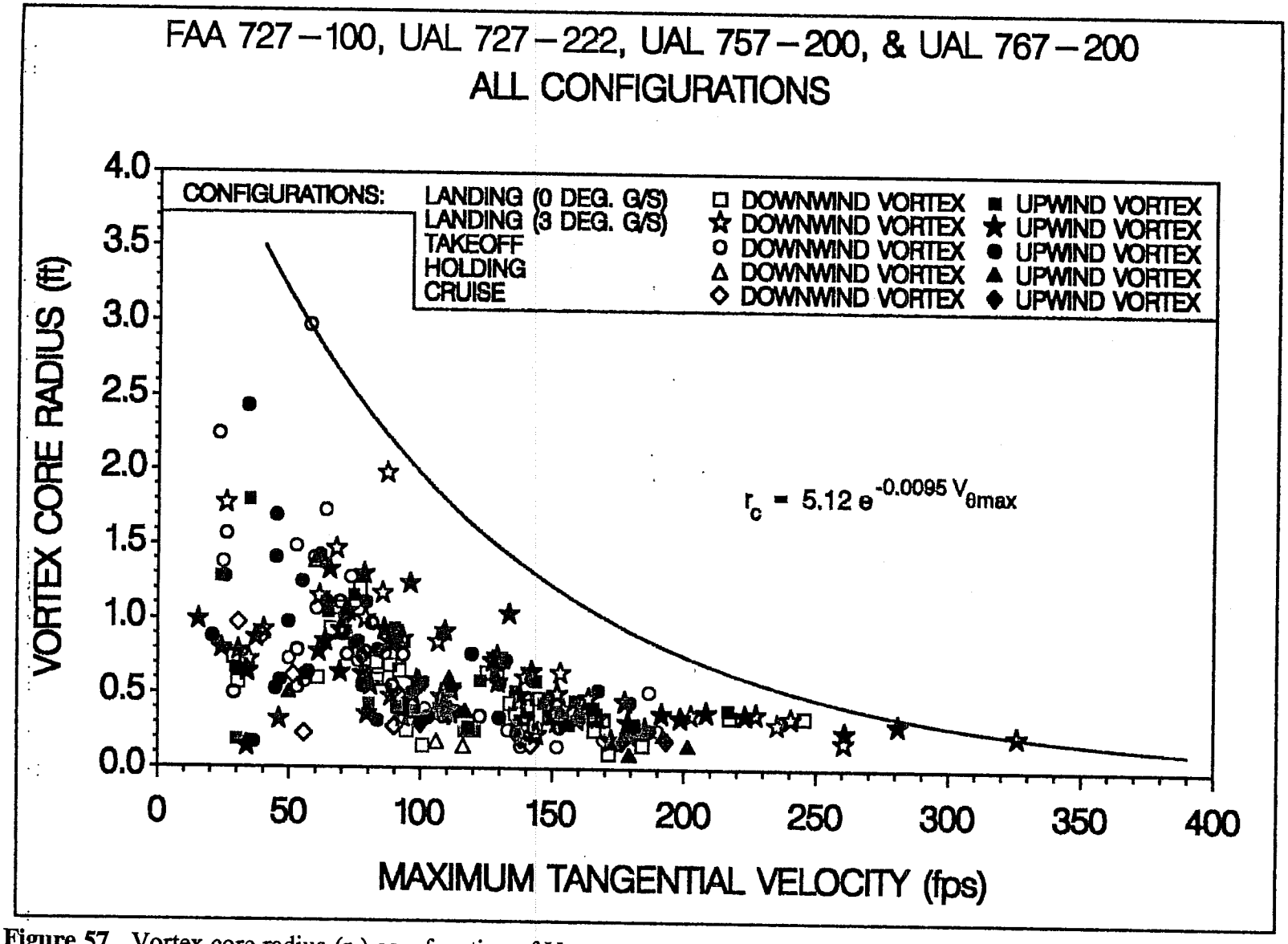

Figure 57. Vortex core radius (r_c) as a function of $V_{\theta max}$. Red, blue, and green symbols indicate B727-100/-222, B757-200, and B767-200 data, respectively. The line indicates an exponential curve drawn according to the associated equation for the data envelope.

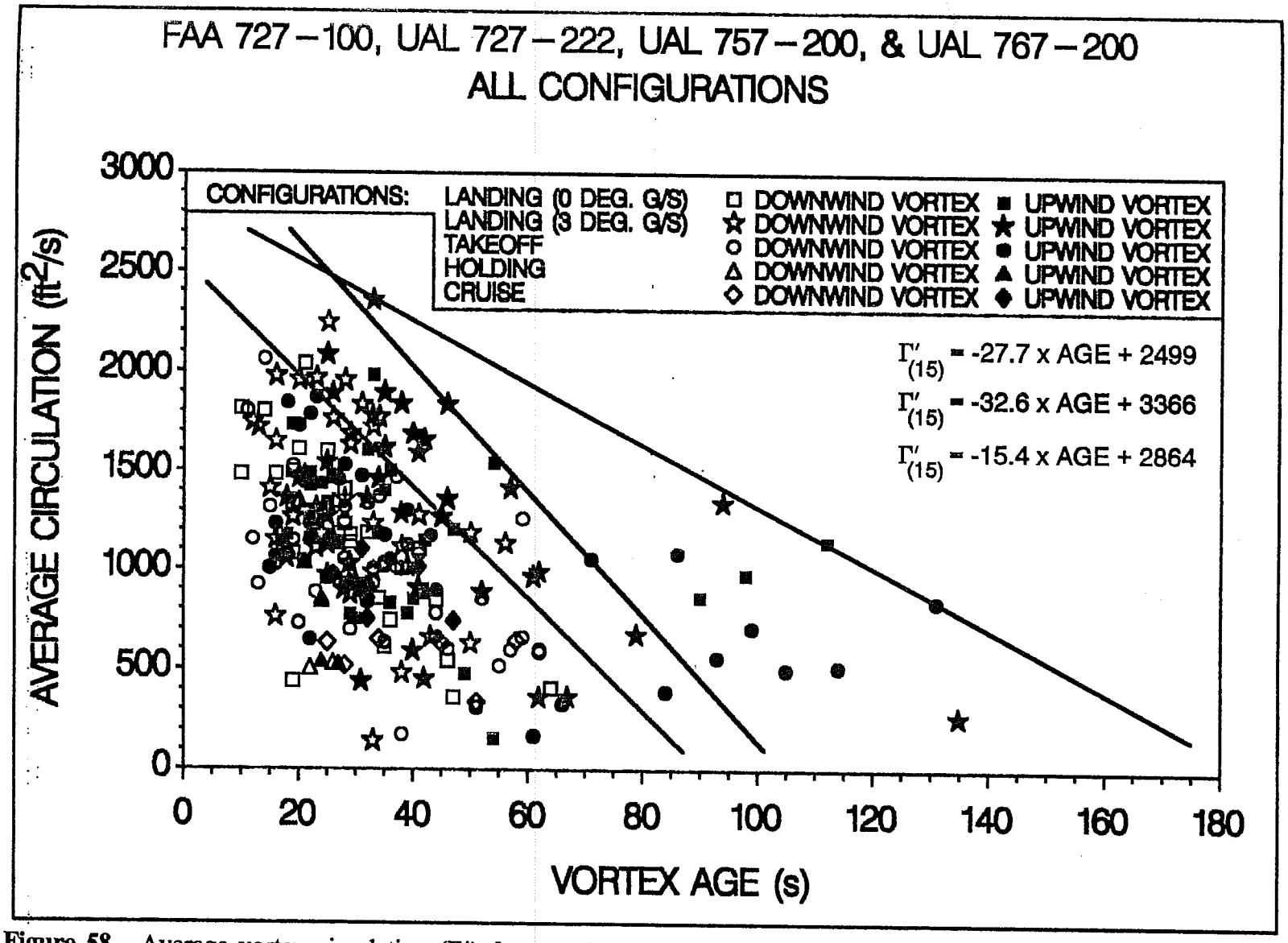

Figure 58. Average vortex circulation (Γ') for a radius of 15 ft as a function of vortex age. Red, blue, and green symbols and lines indicate B727-100/-222, B757-200, and B767-200 data, respectively. The lines indicate the outer bounds of the data envelopes as specified by the corresponding colored equations.

SUMMARY AND CONCLUSIONS

This chapter assembles the important observations and conclusions from the previous chapters. It concludes with comments about the determination of the wake vortex hazard.

- The highest vortex maximum velocity ($V_{\theta max}$) of the study was generated by the B757-200 at 326 fps. The B727-100/-222 highest $V_{\theta max}$ was 235 fps. The B767-200 highest $V_{\theta max}$ was 190 fps. Minimum $V_{\theta max}$ as low as 10 fps were recorded and ranged between 10 and 26 fps for all test aircraft.

- The oldest vortex of the study was produced by the B767-200 at 135 s. The oldest vortex generated by the B757-200 was 84 s, followed by the B727-100/-222 at 62 s.

- The highest $V_{\theta max}$ ever recorded during this and all previous studies using the tower flyby technique was generated by the B757-200. The velocity was measured at 326 fps during flyby number 10 on the downwind vortex at an age of 16 s. The second highest $V_{\theta max}$ for this study (281 fps) was recorded for the upwind vortex of this same flyby with an age of 25 s.

- The B757-200 produced 91% of its vortices with a $V_{\theta max} \geq 140$ fps in the landing configuration. The results were contrary to those reported for most other aircraft in which $V_{\theta max}$ usually decreases with an increase in landing flap deflection. The B757-200 exhibits a continuous wing flap trailing edge when the flaps are lowered, i.e., there are no engine cutouts. The wing in this configuration is fairly "clean" when compared with other aircraft.

- The preponderance of B757-200 data was between the ages of 15 and 65 s. Only two vortices were measured at ages greater than 65 s, leading to the conclusion that the B757-200 generates very strong, short-lived vortices. It is highly probable that longer-lived vortices are produced by the B757-200 than were recorded during this study. The two-day test period did not permit further testing of this hypothesis.

- The B767-200 did not produce any vortices with $V_{\theta max} > 190$ fps, whereas the baseline B727-100/-222 aircraft produced velocities as high as 260 fps. However, 11 B767-200 vortices were older than any of the other vortices produced by the other aircraft during this study. It was concluded that the B767-200 vortices are relatively long-lived, but are of lesser intensity than the baseline B727-100/-222 aircraft. It is highly probable that more intense vortices are produced by the B767-200 than were recorded during this study. This hypothesis could not be tested because of the limited availability of the aircraft.

- The B727-100 and -222 models produced similar $V_{\theta max}$-age data, indicating no differences between B727 models. All the new B727-100/-222 data fell within the envelope delineated

by the Garodz et al. (1974) B727-100 data. The data collection methods used during this study (e.g., instrument calibrations and data acquisition performance) were comparable with those used previously. The data sets from the Garodz test were combined with current B727 data to provide a larger vortex characteristics database for baseline comparison with the B757-200 and B767-200.

- The 3° glide slope (G/S) produced slightly stronger vortices than did level flight, but the differences were small and statistically insignificant. Vortex ages were widely divergent, but no significant differences were found due to G/S flight. Thus, glide slope did not affect either vortex intensity or duration.

- An exponential equation was fitted to the outer envelope encompassing the $V_{\theta max}$ and vortex age data. Coefficients were determined for each aircraft and for the combined data set. The B757-200 initial velocity coefficient was 300 fps greater than the value for the baseline aircraft but the decay coefficient indicated a more rapid decline of $V_{\theta max}$ with age. The B767-200 coefficients were similar to the baseline aircraft, but indicated a slightly higher initial velocity and greater vortex longevity.

- Several visual phenomena were observed during the study. The visual phenomenon most often observed was Crow instability. It was also visually observed that the vortices often persisted for a much longer period of time than that recorded by the hot film anemometers.

- A loud "whistle" was frequently heard from vortices generated by the UAL B757-200 as they passed overhead. The whistling was similar to the noise generated by an artillery shell passing overhead. The cause of the vortex whistle was not determined.

- The study was conducted under stable, neutral, and unstable atmospheric conditions, as determined by Ri and $\Delta T/\Delta z$ measurements. Most flybys, however, were flown under unstable atmospheric conditions.

- Stable or near-neutral atmospheric conditions, as determined by Ri or $\Delta T/\Delta z$, were conducive to long-lived vortices. A direct relationship between Ri or $\Delta T/\Delta z$ and vortex persistence could not be established through statistical procedures because of the large scatter in the data.

- In general, $\Delta T/\Delta z$ provided a more useful indicator of atmospheric turbulence than did Ri. $\Delta T/\Delta z$ amplified the general correlation between atmospheric turbulence and vortex persistence as well as the correlation between atmospheric turbulence and vortex intensity. $\Delta T/\Delta z$ was much easier to measure than Ri, and was also affected by averaging time effects.

- All vortices older than 85 s were generated when the wind speed was less than 5 kt. In addition, all vortices older than 35 s were generated when the ambient wind speed was less than 10 kt. A higher ambient wind speed and accompanying greater wind shear tended to

promote vortex decay. Low wind speeds indicated less atmospheric turbulence and tended to promote vortex longevity.

- A comparison of ambient wind speed-vortex age data with similar data from McGowan (1971) showed that data from the current study fell within measured and expected maximum values.

- A linear least-squares regression equation for the data indicated that 68% of the scatter in the vortex advection rate was explained by the ambient wind speed. The equation specified that the vortex advection rate was approximately one-half that of the ambient wind speed.

- The vortex advection rate was used in conjunction with the exponential equation fitted to the $V_{\theta max}$-vortex age data to evaluate current runway separation standards. Advection times ranged from 489 s for a 5-kt crosswind to 103 s for a 25-kt crosswind. For crosswinds of 15 kt or more, a vortex advected over a 2500 ft distance may still exhibit a significant rotational velocity.

- For each aircraft, whether in the clean or dirty configuration, the observed vortex descent velocity ($\dot{z}_v$) never exceeded the corresponding calculated initial $\dot{z}_v$. The calculated height of the onset of ground effect (h_{vge}) also provided a reasonable estimate for the lowest altitude to which the observed vortices descended, although an occasional vortex descended below the estimate.

- The Hoffman-Joubert vortex velocity profile model provided a good fit to measured velocity profiles when the $V_{\theta max}$ value of the vortex was $\geq$ 50 fps. Calculated vortex core radii ranged in size from about 0.1 to 3.0 ft and averaged 0.6 ft. Vortex core size was not related to vortex age, but maximum core size was described as a function of vortex intensity.

- Average calculated vortex circulation ranged from 140 to 1336 ft^2/s at a radius of 15 ft. Each test aircraft exhibited a unique maximum vortex strength as a function of age, with the largest generated by the B767-200, and followed in descending order by the B757-200 and the B727-100/-222.

- The basic vortex structure remained intact most of the time after passing through the tower, as determined by visual observations. The tower occasionally caused vortex dissipation to accelerate. The tower-induced effect, when observed, appeared to increase with vortex age at tower passage.

- The tower flyby technique proved to be a reliable method to obtain good, useful, full-scale vortex intensity data.

This page intentionally left blank.

RECOMMENDATIONS

- On the basis of the extremely high vortex intensities observed for the B757-200, the FAA should recommend, for an interim period of time, that pilots maintain the same separation distances behind the B757 during Visual Flight Rules (VFR) operations as they do during Instrument Flight Rules (IFR) operations on final approach to landing. During this period, additional full-scale flight tests should be conducted on the B757-200 using the tower flyby technique with the B757-200 to gather additional characteristics of longer-age vortices (if they exist). Vortex probing should also be conducted behind the B757-200 with a suitably instrumented, high-g-load-capable aircraft to determine vortex effects on following aircraft. This extensive data set should then be used for reconsideration of the B757-200 aircraft classification and associated separation standards.

- The B767-200 should remain in the "heavy" category as presently defined in the FAA ATC Handbook. However, another full-scale flight test is recommended for this aircraft in order to complete the vortex intensity-vortex age relationship, particularly at ages less than 30 s.

- Vortex wake characteristics of the Airbus 300 series aircraft should be investigated using the tower flyby technique to ensure proper classification and separation standards of these aircraft. The vortex wake characteristics of the B747-400 should also be investigated.

- Future full-scale flight testing should incorporate independent investigations into the role of atmospheric turbulence in vortex dissipation. Newly developed and highly sophisticated instrumentation now exists for such a study. Flight tests should always be conducted under the three general categories of atmospheric stability, namely, stable, neutral, and unstable.

- Future full-scale flight tests should require the installation of a wing tip vortex flow visualization system on each test aircraft, similar to that used in this study on the B727-222. This would greatly aid in determining various vortex characteristics, particularly vortex transport and mode of dissipation. Future tests should also include the installation of a ground-based sound recording system underneath the general flight path to measure vortex whistles. The information has potential use in the design of a vortex advisory or warning systems, as well as noise-abatement programs.

This page intentionally left blank.

ACKNOWLEDGMENTS

The successful completion of a project of this magnitude demands extraordinary cooperation and unflagging attention to detail. All who participated in this study exhibited these fine qualities, often under extreme physical fatigue. To the following dedicated participants (and others too numerous to mention) we are indebted: Rick Page, who served as the project supervisor from the FAA Technical Center; Al Bazer, Jess Terry, Kenny Johnson, and the entire B727-100 flight and ground crews from the FAA Technical Center; United Air Lines technical representatives Mel Schwartz and Joe Zamuda; the flight and ground crews of the United Air Lines B757-200 and B767-200; Joe Tymczyszyn and Keith Biehl, who assisted with pilot briefings and the onboard data collection; the camcorder and still-camera operators from the Video Lab at the FAA Technical Center; Dan Thompson and others from Galaxy Scientific, who, among other things, operated the Precision Approach Path Indicators; Dianne Hoover, Ray Dickson, G. E. Start, Jerry Sagendorf, Russ Ackermann, Randy Johnson, Dave Dahl, Neil Hukari, Joyce Silvester, Lloyd Peterson, Cliff Spencer, and Harvey Killian, among others from NOAA, who assisted with the field operations; Jim Bruun, David George, and Darin Barron from NOAA, who assisted with data analysis; and Natalie Robison who assisted with the report preparation. We are also grateful to the U.S. Department of Energy for their cooperation and for the use of the facilities at Idaho National Engineering Laboratory.

This page intentionally left blank.

REFERENCES

Bailey, W.H., Jr., T.A. Durham, and G.E. Start. 1979. B-52 tower flyby; final report. AFWL-TR-78-162. U.S. Air Force, Air Force Systems Command, Air Force Weapons Laboratory, Kirtland AFB, NM.

Barber, M.R., E.C. Hastings Jr., R.A. Champine, and J.J. Tymczyszyn. 1977. Vortex attenuation flight experiments. Proceedings Vortex Wake Minimization Symposium, Washington, DC. 25-26 Feb. 1976. SP-409. National Aeronautics and Space Administration, Washington, DC.

Clawson, K.L. 1988. Measurement of wingtip vortex characteristics from C-130, C-141, and C-5A/B aircraft. U.S. Dept. of Commerce, National Oceanic and Atmospheric Administration, Environmental Research Laboratories, Air Resources Laboratory Field Research Division, Idaho Falls, ID.

Crow, S.C. 1970. Stability theory for a pair of trailing vortices. AIAA J. 8:2172-2179.

Crow. S.C. 1976. Lifespan of trailing vortices in a turbulent atmosphere. J. Aircraft 13:476-482.

Donaldson, C. duP., R.S. Snedeker, and R.D. Sullivan. 1973. Calculation of the wakes of three transport aircraft in holding, takeoff, and landing configurations and comparison with experimental measurements. FAA-RD-73-42. Aeronautical Research Association of Princeton, Princeton, NJ.

Eisenhuth, J.J., B.W. McCormick, R.C. Nelson, and L.J. Garodz. 1971. Analysis of experimental measurements of trailing vortex systems of large jet transport aircraft. p. 28-35. *In* Proc. National Aerospace Electronics Conference, 1971, Dayton, OH. Institute of Electrical and Electronics Engineers, New York, NY.

Federal Aviation Administration. 1971. FAA symposium on turbulence, final report. 22-24 Mar. 1971, Washington, DC. U.S. Department of Transportation, Federal Aviation Administration, Washington, DC.

Federal Aviation Administration. 1972. Aircraft wake turbulence. FAA Advisory Circular 90-23D, 15 Dec. 1972. U.S. Department of Transportation, Federal Aviation Administration, Washington, DC.

Garodz, L.J. 1970. Investigation of the relatively long time-history vortex wake characteristics of the CV-880 airplane in terminal area-type flight operation. FAA Data Report, Project No. 504-303-03X. U.S. Department of Transportation, Federal Aviation Administration, National Aviation Facilities Experimental Center, Atlantic City, NJ.

Garodz, L.J. 1971a. Federal Aviation Administration full-scale aircraft vortex wake turbulence flight test investigations: Past, present, future. AIAA Paper 71-97. 9th Aerospace Sciences Meeting, New York, NY. 25-27 Jan. 1971. American Institute of Aeronautics and Astronautics, Washington, DC.

Garodz, L.J. 1971b. Measurements of Boeing 747, Lockheed C5A and other aircraft vortex wake characteristics by tower fly-by techniques. p. 265-285. *In* J. Olsen, A. Goldberg, and M. Rogers (ed.) Aircraft wake turbulence and its detection. Plenum Press, New York, NY.

Garodz, L.J. 1976. Abbreviated full-scale flight test investigation of the Lockheed L1011 trailing vortex system using the tower fly-by technique. FAA-AFS-1-76-2. U.S. Department of Transportation, Federal Aviation Administration, National Aviation Facilities Experimental Center, Atlantic City, NJ.

Garodz, L.J., and K.L. Clawson. 1991. Vortex characteristics of C5A/B, C141B and C130E aircraft applicable to ATC terminal flight operations. NOAA Tech. Mem. ERL ARL-190. U.S. Department of Commerce, National Oceanic and Atmospheric Administration, Environmental Research Laboratories, Air Resources Laboratory Field Research Division, Idaho Falls, ID.

Garodz, L.J., D.M. Lawrence, and N.J. Miller. 1974a. The measurement of the Boeing 727 trailing vortex system using the tower fly-by technique. FAA-RD-74-90. U.S. Department of Transportation, Federal Aviation Administration, Systems Research and Development Service, Washington, DC.

Garodz, L.J., D.M. Lawrence, and N.J. Miller. 1974b. The measurement of the McDonnell-Douglas DC-9 trailing vortex system using the tower fly-by technique. FAA-RD-74-173. U.S. Department of Transportation, Federal Aviation Administration, National Aviation Facilities Experimental Center, Atlantic City, NJ.

Garodz, L.J., D.M. Lawrence, and N.J. Miller. 1975. Measurement of the trailing vortex systems of large transport aircraft, using tower fly-by and flow visualization: Summary, comparison, and application. FAA-RD-75-127. U.S. Department of Transportation, Federal Aviation Administration, National Aviation Facilities Experimental Center, Atlantic City, NJ.

Garodz, L.J., and N.J. Miller. 1975. Investigation of the vortex wake characteristics of jet transports during climbout and turning flight. FAA-AEQ-75-1. U.S. Department of Transportation, Federal Aviation Administration, Washington, DC.

Green, G.C. 1986. An approximate model of vortex decay in the atmosphere. J. Aircraft 23:566-573.

Hanson, F.V. 1967. Spatial and temporal distribution of the gradient Richardson Number in the surface and planetary layers. ECOM-5123. Atmospheric Sciences Laboratory, White Sands Missile Range, NM.

Hoffman, E.R. and P.N. Joubert. 1963. Turbulent line vortices. J. Fluid Mech. 16:395-411.

Kurkowski, R.L., M.R. Barber, and L.J. Garodz. 1976. Characteristics of vortex wake generated by a Boeing 727 jet transport during two-segment and normal ILS approach flight paths. NASA TN D-8222. National Aeronautics and Space Administration, Ames Research Center, Moffett Field, CA.

Lumley, J.L., and H.A. Panofsky. 1964. The structure of atmospheric turbulence. John Wiley and Sons, New York, NY.

McGowan, W.A. 1971. Aircraft wake turbulence avoidance. 12th Anglo-American Aeronautical Conference, Calgary, Alberta, 7-9 Jul. 1971. Paper 72/6. Canadian Aeronautics and Space Institute, Ottawa, Canada.

Nelson, R.C. 1974. The response of aircraft encountering aircraft wake turbulence. AFFDL-TR-74-29. Air Force Flight Dynamics Laboratory, Wright-Patterson Air Force Base, OH.

Page, R.D., K.L. Clawson, L.J. Garodz, and R.P. Rudis. 1992. Panel discussion on tower fly-by testing -- 1990 fall testing. *In* J.N. Hallock (ed.) FAA Wake Vortex Symposium Proceedings, Washington, DC. 29-31 Oct. 1991. VNTSC, Boston, MA.

Patterson, J.C., Jr., and F.L. Jordan, Jr. 1977. Thrust augmented vortex attenuation. p. 251-270. Proceedings Vortex Wake Minimization Symposium, Washington, DC. 25-26 Feb. 1976. SP-409. National Aeronautics and Space Administration, Washington, DC.

Rosenberg, N.J. 1970. Microclimate: The biological environment. John Wiley and Sons, New York, NY.

Smith, H.J. 1975. A flight test investigation of the rolling moments induced on a T-37B airplane in the wake of a B-747 airplane. NASA TM X-56031. National Aeronautics and Space Administration, Flight Research Center, Edwards, CA.

Start, G.E., and C.R. Dickson. 1970. Wingtip vortex diameters, tangential speeds, and horizontal transport withing the first 100 feet above the ground; final report. DOT-FA70NA-AP-73. U.S. Department of Transportation, Federal Aviation Administration, National Aviation Facilities Experimental Center, Atlantic City, NJ.

Taylor, W.R.T. (ed.). 1970. Jane's all the world aircraft, 1969-1970. Vol. 60. McGraw-Hill, New York, NY.

Taylor, W.R.T. (ed.). 1983. Jane's all the world aircraft, 1982-1983. Vol. 73. Jane's Publishing Co., London, England.

Tombach, I.H. 1973. Observations of atmospheric effects on vortex wake behavior. J. Aircraft 10:215-221.

Tombach, I.H., P.B.S. Lissaman, and J.B. Mullen. 1977. Aircraft vortex wake behavior and decay near the ground. p. 297-309. *In* J.N. Hallock (ed.) Proc. Aircraft Vortex Wake Conf., Cambridge, MA, 15-17 Mar 1977. FAA-RD-77-68. U.S. Department of Transportation, Research and Development Service, Washington, DC.

TSI, Inc. No date. Temperature compensation of thermal sensors. Tech. Bull. 16. TSI, Inc., St. Paul, MN.

TSI, Inc. No date. Procedure for temperature correction on velocity measurements. Tech. Bull. 18. TSI, Inc., St. Paul, MN.

U.S. NRC (Nuclear Regulatory Commission). 1980. Meteorological programs in support of nuclear power plants. Reg. Guide 1.23 (Rev.1). U.S. Nuclear Regulatory Commission, Washington, DC.